Validation of Soot Modelling in the CFD code FLACS

Master's Thesis in Process Technology
by
Dhaval Madhusudan Panchal

Department of Physics and Technology
University of Bergen (UiB)

JUNE 2019

Abstract

In a fire scenario, the role of soot is important from different standpoints. It has a significant contribution to heat transfer by radiation and it proves to be a hindrance in evacuation activities as it reduces visibility. As a pollutant from combustion, it is an environmental hazard and it contributes to climate change by causing a very localised warming effect in the atmosphere. A predictive and practical soot model will be extremely helpful to all the design engineers who are working towards solving these problems.

The computational fluid dynamics (CFD) codes, compiled on advanced computing machines of this generation are more than capable of predicting soot concentration and its contribution to radiation. However, these CFD tools need to be validated against experiments. This involves recreating the experimental setup in the CFD environment and comparison of the results from the simulation with the experimental results. The focus of this thesis is to validate the soot models used in FLACS Fire, a CFD code developed by Gexcon AS.

Four fire scenarios from experiments, ranging from small scale such as ethylene jet flame to full scale such as underventilated compartment fire, are selected here. The Formation-Oxidation model (FOX) and Conversion Factor Model (CFM) are the two options used in FLACS to predict soot fractions. The validation is done for result parameters, such as time-averaged temperatures and mass or volume fractions of soot. Soot is a good radiator and it transfers a substantial amount of energy to the surroundings by thermal radiation. This transfer of energy will change the temperature field of the flame. This impact of soot fraction on radiative power is also studied and discussed. Sensitivity study with respect to certain modelling parameters is also included.

The results of average temperature and average soot mass or volume fraction predicted by CFM are in good agreement with the measurements from experiments. However, the predictions of soot fractions using the FOX model are very low compared to experimental values, and a need for code improvement and further validation is identified. The results of temperature are strongly influenced by soot fractions predicted accordingly by the soot models.

Apart from experiments, results from another CFD code Fire Dynamic Simulator (FDS), are used for comparison in a compartment fire case. The importance of soot formation is tested by using no soot model for the compartment fire scenario and demonstrated that the temperatures are over-predicted, and using an appropriate soot model for the given fire scenario is essential.

Preface

This thesis is the final work related to my Master of Science degree in Process Technology at the Department of Physics and Technology of the University of Bergen. It is the result of the thesis work done at Gexcon AS.

I would like to express my most sincere gratitude for my supervisor Professor Bjørn J. Arntzen, for his continuous enthusiasm and interest in my work. I would like to thank Gexcon and especially my supervisor at Gexcon, Deiveegan Muthusamy for providing me with the opportunity to work on this assignment with them. Most importantly the trust they showed in my abilities and helped me through frequent roadblocks was the reason I was able to finish this project successfully.

I am grateful to Gexcon, for providing the office space and access to valuable hardware and simulation software. Employees at Gexcon especially Lorenzo Mauri and Djurre Siccama were swift in helping and encouraging in my thesis work. It has been a great learning experience.

I am pleased to express my gratitude to my employer Aker Solutions AS, my colleague Bård Malstenbråten and department manager Britt Elin Salt for showing the belief in me and helping me manage my work schedule at Aker Solutions with my thesis work.

Finally, I would like to give special thanks to my father Madhusudan Panchal, mother Bharti Panchal and my dear wife Lajja Vyas for her reassuring words, patience and encouragement to take up this course.

Bergen, 3 June 2019

Dhaval Madhusudan Panchal

Contents

List of tables and figures

Tables

Figures

Nomenclature

Latin letters

a	Constant for model proposed by Tesner (EDC soot model)
a_0	Constant for model proposed by Tesner and Magnussen
b	Constant for model proposed by Tesner (EDC soot model)
C_f	Constant for model proposed by Khan and Greeves
C_R	Constant for model proposed by Magnussen and Hjertager
d_p	Soot particle diameter [Å]
D_s^{th}	Diffusion of soot that occurs exclusively by thermophoresis
E_a	Activation energy [J/mol]
f	Linear branching coefficient
f_c	Mass fraction of carbon in fuel
g	Linear termination coefficient
g_0	Coefficient of linear termination on soot particles
k	Turbulent kinetic energy [m^2/s^2]
$\dot{m}$	Mass rate [kg/s]
m_p	Mass of a soot particle [kg]
n	Concentration of active particles involved in the process [particles/m^3.s]
n_0	Spontaneous origination rate of active particles [particles/m^3.s]
p	Total pressure [Pa]
$\overline{P}_{fu}$	Mean partial pressure of fuel [Pa]
r_s	Stoichiometric amount of oxidant for soot combustion
R_u	Universal gas constant [J/K.mol]
S	Concentration of soot particles [particles/m^3]
Sc_T	Turbulent Schmidt number
t	Time [s]
T	Temperature [K]

u_j	Cartesian velocity component in x_j direction [m/s]
X	Mole fraction
x_j	Cartesian coordinate
Y_{fu}	Mean concentration of fuel [particles/m^3.s]
$\tilde{Y}_{min}$	The maximum amount of fuel that can be converted into products in the one-step infinitely fast combustion reaction
Y_n	Mass fraction of radical nuclei
Y_s	Mass fraction of soot

Greek letters

$\emptyset$	Local unburnt equivalence ratio
α	Exponent in model proposed by Khan and Greeves
γ^*	Mass fraction of the fine structures
ε	Dissipation of turbulent kinetic energy [m^2/s^3]
μ_T	Turbulent viscosity [Pa.s]
ρ	Average density [kg/m^3]
χ	Progress variable indicating the potential fuel that has burnt
$\omega_{n/s,}$	Total rate for radical nuclei and soot [kg/kg.s] or [particles/kg.s]
$\overline{\omega}_{s,f}$, $\overline{\omega}_{s,ox}$	Mean reaction rate for soot formation and oxidation [kg/kg.s] or [particles/kg.s]

Subscripts

f	Formation
fu	Fuel
n	Radical nuclei
o	Oxygen
ox	Oxidation
s	Soot

Superscripts

$\overline{\ }$	Mean
~	Mass averaged mean
th	Thermophoresis

Abbreviations

CFD	computational Fluid Dynamics
CFM	Conversion Factor Method
CPU	Central Processing Unit
DTM	Discrete Transfer Method
EDC	Eddy Dissipation Concept
ER	Equivalence Ratio
FDS	Fire Dynamic Simulator
FOX	Formation – Oxidation Model
HACA	H-Abstraction and C_2H_2 Addition
NIST	National Institute of Standards and Technology
PAH	Polycyclic Aromatic Hydrocarbons
RAM	Random Access Memory
RTI	Relative Turbulence Intensity

1 Introduction

In the early days of industrialisation, smoke[a 1] from factory chimney was a sign of prosperity. Soon it was realised to be a nuisance and a health concern. The remedy for the generation of soot and smoke was proposed to be three t's of combustion: time, temperature and turbulence [1]. Which meant allowing for higher residence time at elevated temperatures and ensuring good mixing, which usually assured of oxidizing soot and other hydrocarbons. However, this led to producing larger amounts of NO_x.

In terms of climate change, of all the pollutant particles, black carbon is the most important contributor to warming. Black carbon absorbs light at all wavelengths and converts it to heat, causing a highly efficient and very localised warming effect on the atmosphere [2]. Further understanding of its creation will help develop more accurate climate models in the future. Thus, there is an urgent need to apply knowledge of the subtle science of soot formation and subsequent oxidation to help to predict their occurrence.

Figure 1.1: Soot in air pollution (phys.org [2])

In most fires, the soot is produced in the form of fine carbonaceous particles in the flame zone and dispersed in the smoke layer. These luminous particles significantly contribute to the radiative heat loss and the total heat release rate. Soot mass or volume fraction is a key parameter in fire safety, and also useful for evaluating visibility [3].

In combustion, soot may be an undesirable product, but it is used in many industrial processes. Often known as carbon black it is used in the production of printing ink or as a filling material in rubber tyres which can be as high as 60% of its mass [1]. Soot is also much

[1] For alphabetical superscripts see Appendix D for general concepts and definitions

desired in furnaces, as it contributes largely to heat transfer through radiation. However, the strategy there is to generate soot early in the flame, allow it to radiate, and then oxidise it before it leaves the furnace. So accurate prediction of soot formation is of interest for various reasons.

To predict the distribution of soot particles it is essential to understand the physical and chemical mechanisms associated with soot formation, propagation and oxidation. A computational fluid dynamics (CFD) tool provides the potential to study this kind of complicated problems. Detailed analysis quantifying the modelling and numerical uncertainties in simulations is an important step for the development of CFD code. FLACS is one such CFD tool. This is discussed in chapter 2 and 3 of this thesis.

1.1 Objective

Validation for the available options for soot modelling in the CFD code FLACS Fire is one of the knowledge gaps identified at Gexcon AS who are responsible for the development for this code. At present FLACS provides three alternatives for predicting soot: Formation-Oxidation model (FOX) which is the default option, Conversion Factor Model (CFM) and no soot model. All three options are discussed here with the focus on the FOX model, CFM and their ability to predict soot concentration. The main motivation for performing this validation work is:

- To get an overview of the accuracy and performance of the two soot models, so that the efforts can be prioritised in the continued development
- To develop an understanding of its validity and limitations so that suitable guidelines can be developed
- To assure and demonstrate the validity and performance to the user group, customers and scientific community

1.2 Scope of the study

In this thesis, several fire experiments involving soot production are simulated in FLACS. The objective was to evaluate different scenarios starting from small or lab scale to full-scale experiments. This might help in understanding the effect of different simulation grid conditions, modelling parameters irrespective of scale. Simulation of jet or pool fire is performed with reference to experiments compiled or carried out as below:

1. Turbulent sooty ethylene jet flame by Tessé et al. (2003) [4]
2. Heptane pool fire on a hollow square pan by Wang et al. (2015) [5]
3. Heptane and Toluene pool fire by Chen et al. (2014) [6]
4. NIST full-scale enclosure experiments by Lock et al. (2008) [7]

Predicted results of temperature, soot mass or volume fractions and some other parameters were compared to experimental measurements and numerical results of these research groups. The main objective of this work is to clarify how adequately the soot models correlate

with the experiments and identify a further course of improvement. The scope of the study includes,

- Identifying and model relevant pool or jet fire scenarios
- Testing of experiment case with different soot models and variation in other combustion parameters
- Report validation status
- Present a summary and conclusion

An attempt is made to understand the influence of soot production on the temperature due to radiation heat transfer with respect to different soot modelling alternatives in FLACS Fire.

The work is limited to validation of the CFD models towards experimental work. This means that weaknesses and improvement suggestions are only described. Models are not modified and tested. The outcome of validation is presented with discussion on the results in chapter 4 and with conclusion and recommendation for further work in chapter 5 of this thesis.

1.3 CFD and FLACS

Early in 1920s Lewis Richardson first showed that it was feasible to solve the governing equations of fluid flow using numerical methods [8]. In the next fifty years, CFD emerged as a sophisticated but general analysis tool in the branch of fluid flow. Although the mathematical framework for the subject is almost a hundred years old, it is only in the past thirty years that computers have become fast enough to make the calculations practical.

With the evolutions of modern-day computers, CFD has flourished as a branch of fluid dynamics which used numerical methods and algorithms to solve and analyse practical engineering problems. On the other hand, many hazards encountered in society and especially process industries required explanations and solutions for preventing their future occurrences.

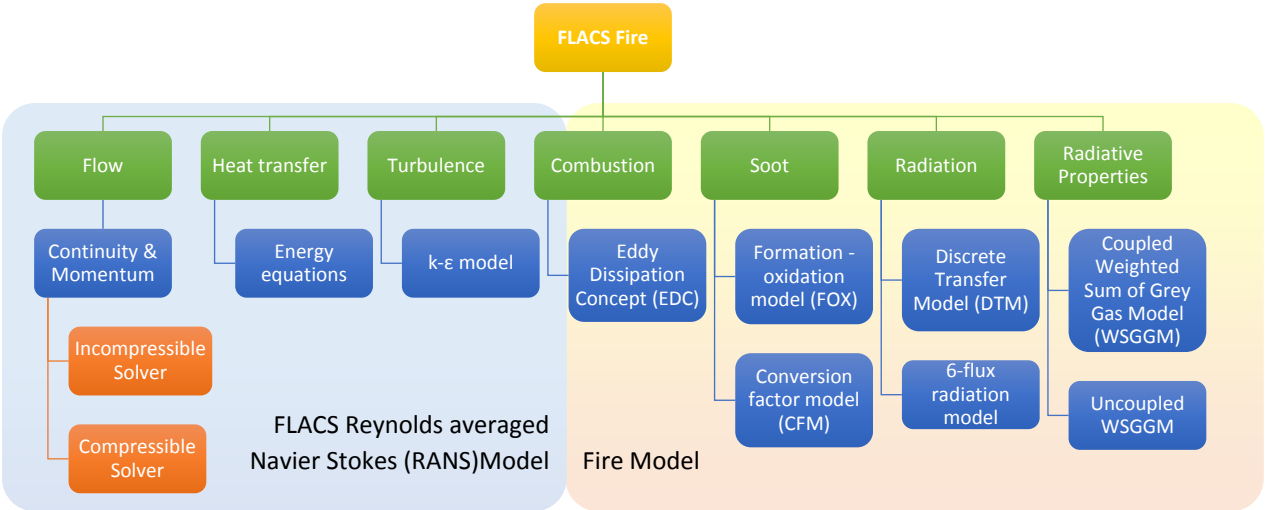

Figure 1.2: Key building blocks of FLACS Fire (FLACS manual [9])

This involved large scale fluid flow problems in complex scenarios in three-dimensional geometries [9]. FLACS is one such comprehensive CFD tool developed to address process safety applications such as:

- Dispersion of flammable or toxic gas
- Gas and dust explosion
- Pool and jet fires
- Propagation of blast and shock waves
- Probabilistic risk analysis

The development of FLACS started in the 1980s at Christian Michelsen Institute (CMI) under the establishment of Gexcon. As of today, Gexcon AS is a wholly owned subsidiary of the newly formed NORCE research group, and they own the proprietary rights to the CFD code FLACS. NORCE is a conglomerate of several research institutions in Norway and Norwegian Research Centre AS is the company's legal name.

FLACS solves the compressible conservation equations for mass, momentum, enthalpy, mass fraction of species and mixture fraction on a 3D Cartesian grid using a finite volume method (control-volume-based technique) to convert the governing equations to algebraic equations. An overview of models included in FLACS is presented in Figure 1.2. More information on FLACS is provided in Appendix C.

Several other CFD software packages are developed for numerical simulation of fire such as Fire Dynamic Simulator (FDS), SmartFire, Kameleon FireEX which are examples of special purpose software. Whereas CFX, FLUENT and PHOENICS are examples of general-purpose software used for fire simulation.

This study is limited to validation of soot modelling for FLACS Fire. For all the simulations FLACS version 10.9 or the latest available FLACS nightly build is used.

1.4 Hardware system

Majority of the simulations performed during this thesis work used the computer hardware configuration given in Table 1.1. Some of the initial simulations were also performed using sim cluster of computers.

Table 1.1: Hardware systems utilised for simulations

Operating System	Hardware configuration
Linux (openSUSE Leap 42.2, 64 bit)	CPU - 4 x Intel® Xeon® CPU (E5630 @2.53 GHz) RAM - 23.5 GB
Linux (openSUSE Leap 42.2, 64 bit)	CPU - 8 x Intel® Xeon® CPU (E5-1620 @3.70 GHz) RAM - 31.3 GB
Windows (Windows 7 professional, 64 bit)	CPU – Intel® Core™ i7-4900MQ CPU (@2.80 GHz) RAM – 16.0 GB

2 Soot formation and oxidation

Particulate smoke or soot is formed in the gas phase in almost all types of fires due to incomplete combustion and high-temperature pyrolysis reaction with low oxygen concentrations. Soot is generated irrespective of the fuel phase: gas, liquid or solid.

The simplest example given by Yeoh and Yuen [10] is a buoyant laminar burning candle in air, which has a non-premixed flame. Its characteristic yellow flame is formed due to the presence of luminous soot particles. More soot can be produced if the flame height is increased due to higher residence time. A sooty yellow diffusion flame radiates much more energy than a blue premixed flame.

As the soot travels through the flame it radiates heat and cools the combustion products, which is the principle of radiative heat loss. At the smoke point[b] flame height, this radiative heat loss can account for 30% of the total heat release rate [10]. In the upper part of the flame, if sufficient time is provided, the soot particles may get oxidised. The cooler combustion products prevent further oxidation of the soot particles, which are dispersed into the surrounding environment.

Even though the primary soot particles are frequently observed to be spherical, smoke generally consists of agglomerations of minute soot particles that come together to form complex chains and clusters, which may have an overall size in excess of 1 µm [10]. However, many experiments suggest that there is a substantial variation in aggregate sizes and shapes indicating poly-disperse[c] characteristic with complex soot structure [10, 11]. So, it is interesting to know how they are generated and why they are not consumed by the flame.

Soot from different flames may be very different in terms of size, structure and composition. It can vary from having almost spherical particles containing few atoms to large aggregate structures containing millions of atoms. Freshly formed soot may contain an almost equal amount of hydrogen and carbon and with heating and ageing, compounds with higher carbon content are produced similar to graphite [1].

However, there is a consensus that irrespective of fuel or type of the flame the basic physical and chemical processes taking place in soot formation are similar in nature. Soot formation is a complex process involving a large number of homogeneous and heterogeneous chemical reactions and other physical processes such as coagulation and agglomeration. The details of these steps are discussed further in this chapter.

2.1 Nucleation and growth

The transition of gas phase combustion products into solid soot particles is still probably the least understood part of the soot formation process. This particle inception takes place at a molecular mass between 500 – 2000 AMU (atomic mass unit)[d] [1]. The widely accepted

mechanism is based on the assumption that polycyclic aromatic hydrocarbons (PAH) are the most important precursors in soot formation [12, 13]. These compounds are usually formed under fuel-rich conditions, which are always present in non-premixed and often in rich premixed flames.

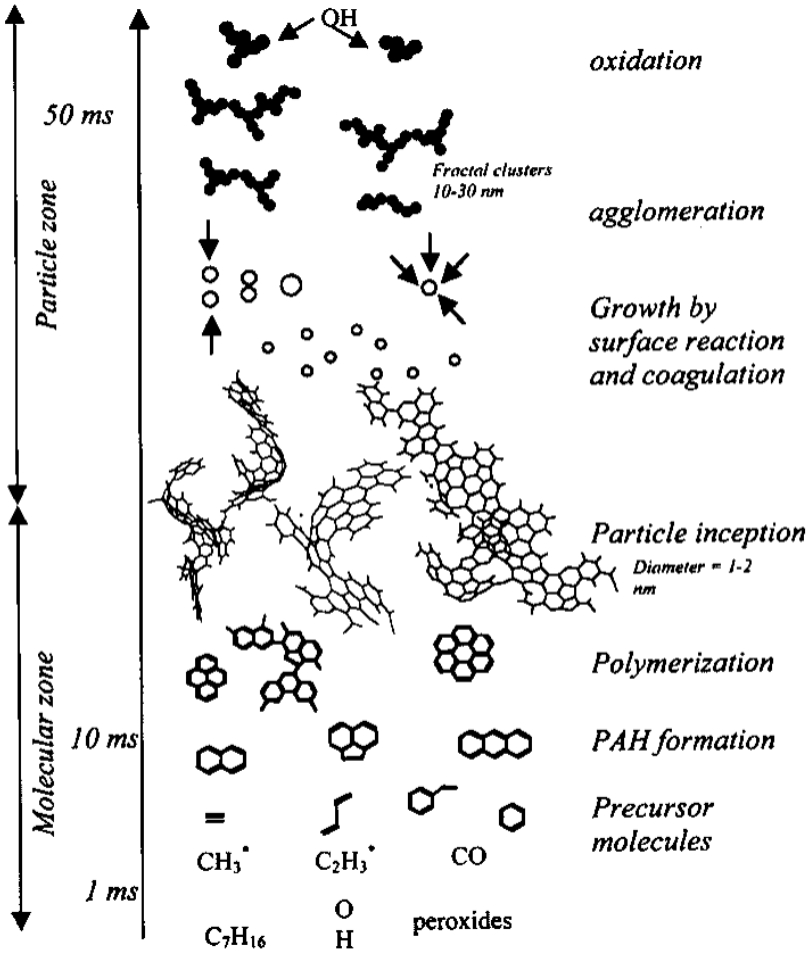

Figure 2.1: PAH transformation pathways to soot (Pugmire et al. [14])

Here, the primary focus is on the formation of the first aromatic ring, which is probably benzene, from small straight-chained molecules, as shown in Figure 2.1. It is perceived that this is the rate-limiting step in the reaction sequence to larger aromatics and the kinetics describing it is the subject of many studies [12, 13, 15]. The following reactions are found to be important in these studies.

$$nC_4H_3 + C_2H_2 \longrightarrow C_6H_5\ (phenyl) \quad 2.1$$

$$nC_4H_5 + C_2H_2 \longrightarrow C_6H_6\ (benzene) + H \quad 2.2$$

$$C_3H_3 + C_3H_3 \longrightarrow benzene \quad 2.3$$

$$C_3H_3 + C_2H_2 \longrightarrow benzene \quad 2.4$$

The first step is the formation of the aromatic species such as benzene C_6H_6 and phenyl C_6H_5 in the gas phase by either C_3H_4 decomposition or reaction of CH- or CH_2 with C_2H_2 to C_3H_3. A

probable cause for this is the oxidation reaction for C_3H_3 which is very slow [1]. As shown here acetylene (C_2H_2) is the key species in the formation of PAH, which is formed in high amounts under fuel rich conditions.

The further growth of PAH is complex and requires a large reaction scheme for describing it in detail. Addition of acetylene to the ring leads to the growth of the molecule, which is a kind of simplification [1, 10, 12]. Example reactions for the growth of the molecules by alternating radical formation by H- atom attack and acetylene addition, presented by Frenklach and Wang [12] are shown in Figure 2.2. This repetitive reaction sequence has two steps: abstraction of a hydrogen atom from the reacting hydrocarbon followed by the addition of acetylene molecule to the radical site formed. This sequence is named HACA which is an acronym for *H*-abstraction and C_2H_2 addition and is shown as below:

$$A_\mathrm{i} + H \longleftrightarrow A_{\mathrm{i}-} + H_2 \qquad 2.5$$

$$A_{\mathrm{i}-} + C_2H_2 \longleftrightarrow A_\mathrm{i}C_2H_2 \qquad 2.6$$

$$A_\mathrm{i}C_2H_2 + C_2H_2 \longrightarrow A_{\mathrm{i}+1} + H \qquad 2.7$$

Here A_i is the aromatic molecule with *i* being number of rings and $A_{i\text{-}}$ and $A_iC_2H_2$ are the aromatic radicals. In the end, the aromatic molecule gains an additional ring. The aromatic radicals may also react with species other than acetylene forming different products than PAH, differing in their carbon and hydrogen content. Overall, the main constituent of the soot is mostly carbon, but other elements such as hydrogen and oxygen are usually present in small amounts. Depending on the composition of surrounding gas, other species may also get absorbed on the soot surface.

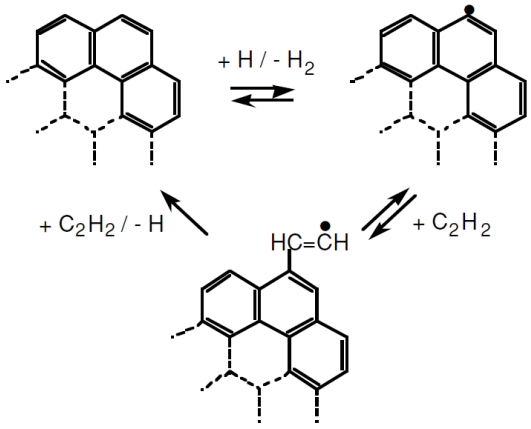

Figure 2.2: Ring growth by radicalic acetylene addition (Warnatz et al. [1])

Soot production is a chemically controlled phenomenon. The higher temperatures favour the formation of the radicalic precursors. Experimental studies also indicate that soot formation increases with increasing pressure, increasing the ratio of *C/O* [1]. But at even higher temperatures the soot precursors are oxidised and pyrolyzed so that the soot formation is limited to a temperature range between 1000 K to 2000 K.

2.2 Mass growth

The continued growth of the PAH will lead to the smallest distinguishable particles with diameters of 1 nm [10]. Physically they appear as a grape-like cluster of small spherical particles as shown in Figure 2.3. Typically, a single sphere reaches a size of 20-50 nm in diameter depending on combustion conditions. But roughly more than 95% of the mass of soot is formed by a mechanism other than inception [1].

Once formed these particles will grow by three mechanisms: condensation, coagulation and surface growth [10]. In condensation, the two-dimensional PAHs merge into one three-dimensional particle. And in coagulation, a larger spheroid is formed due to coalescence between the particles. Both of these processes are physical in nature. Surface growth occurs in parallel to physical processes. The soot particle reacts further with the gas phase species, on the active sites of the particle surface. It is generally agreed here as well that acetylene is mainly responsible for the growth of soot particles.

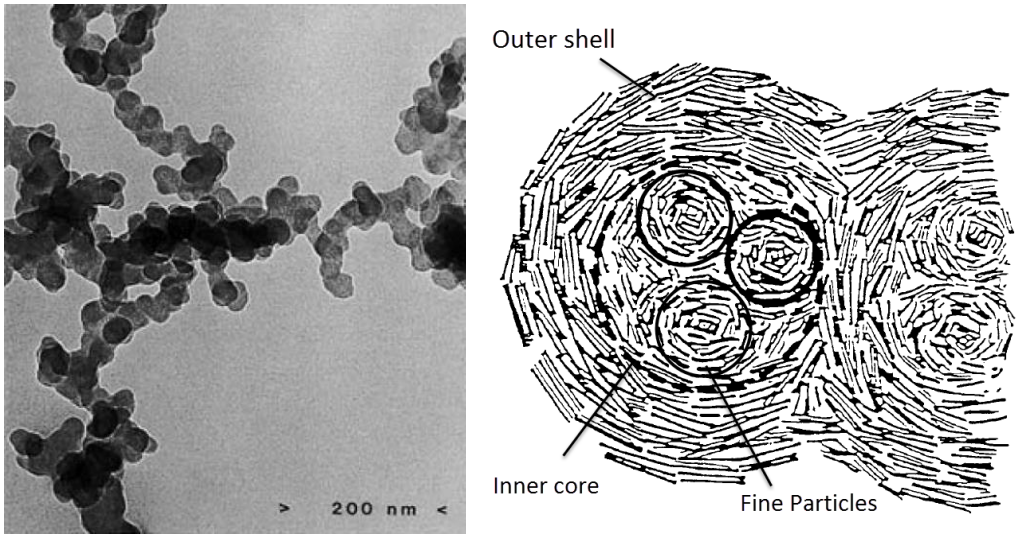

Figure 2.3: Photograph of a soot particle and a schematic of soot particle coagulation [1]

The rate of coagulation can be determined by the frequency of collisions, which is directly dependent on the Knudsen number, which is the ratio of the mean free path to the particle radius [12]. If the Knudsen number is large (particle radius is much smaller than the mean free path), the coagulation is in the free-molecular regime and the collision frequency is governed by kinetic theory[e]. When the Knudsen number is low, the coagulation is in continuum regime and the collision frequency is dependent on particle diffusion. To determine the coagulation rate, it is usually assumed that all soot particles are spherical, small in comparison of the mean free path and each collision of two particles result in coagulation.

When larger particles collide, they form chain-like structures and grow into larger soot aggregates. Many experimental results verify this behaviour but this transition to aggregation growth mechanism is not clear. The smaller particles grow quickly and their surface is also smoothened to spherical shapes. But for the larger particles the growth is slower and hence the shape is not smooth so they grow into agglomerates.

2.3 Soot oxidation

Apart from contributing to soot growth the gas phase species also oxidise soot as shown in Figure 2.1. Oxidation occurs primarily as a result of an attack by *O* atoms, molecular O_2 and the *OH* radicals which contribute to the reduction of the particle sizes. The oxidation on the soot surface produces intermediates which may then be desorbed and converted back to gas phase [10]. The HACA sequence used to explain the soot mass growth can be applied to explain this heterogeneous oxidation reaction as well [12].

$$C^i_{soot-H} + H \longleftrightarrow C^i_{soot-} + H_2 \quad (2.8)$$

$$C^i_{soot-} + C_2H_2 \longrightarrow C^{i+2}_{soot-H} + H \quad (2.9)$$

$$C^i_{soot-} + O_2 \longrightarrow oxidation\ products \quad (2.10)$$

$$C^i_{soot-} + OH \longrightarrow oxidation\ products \quad (2.11)$$

Here $C^i_{soot\text{-}H}$ is an active site on the soot particle surface and $C^i_{soot\text{-}}$ is a corresponding radical. In short, the HACA sequence can provide simplified kinetics for soot formation as well as soot oxidation.

Temperature plays an important role in soot oxidation. In a substantial amount, soot is considered to be a much stronger absorber as well as an emitter of radiation [10]. The total representative hemispherical emissivity[f] for soot is reported to be 0.95, which is highest among the non-metals [8]. Excessive radiation allows soot to cool down and the cooler combustion products prevent further oxidation of soot and it appears in the exhaust.

The oxidation of soot is primarily carried out by *OH* and O_2, because of lower concertation of free *O* in sooting flames. In the initial stages, the unconsumed oxygen results in a larger increase of the hydrogen-radical pool favouring the formation of precursor species and hence a much-enhanced soot growth is observed. This is followed by a gradual increase in the soot oxidation rates, progressively reducing the soot yield. For example, in the case of compartment fires, the product gases of combustion and soot will fill the room and rise to the ceiling [8]. As the fire grows the buoyant outflow of the hot combustion products will reduce the pressure inside the room and the fresh air with oxygen flows in through the doorway near the bottom. This will provide the new oxygen essential for the continuation of soot oxidation. This is discussed further in one of the validation cases, see chapter 4.4.

2.4 Effect of parent fuel

In an actual fire, soot production is normally dependent upon the breakdown path of the parent fuel. Knowledge of the chemical composition, structure and burning mechanism of this parent fuel is important in understanding the formation of soot [10].

- Certain fuels such as formaldehyde, formic acid, and methyl alcohol burn with non-luminous flames and are thus smokeless.
- The oxygenated fuels such as ethyl alcohol and acetone burn with considerable less smoke than the hydrocarbons.
- In contrast, hydrocarbon fuels have a tendency to produce smoke by the introduction of branching, unsaturation, and aromatic character.
- Similarly, hydrocarbon polymers such as polyethylene and polystyrene tend to yield far more substantial smoke
- Under the same free burning conditions less soot is generated by, oxygenated fuels such as wood and polymethylmethacrylate

The knowledge of combustion chemistry of these parent fuels will help in building practical models. For example, the aromatic hydrocarbons containing only a few rings will generate soot particles, whereas if they are large or cross-linked the residue will be in a form of stable protective char layer [8].

3 Soot modelling

As described in the earlier section, the physical mechanisms and chemical kinetics of soot formation is complex. When the intention is to know the amount of soot generated by simulating a sooting flame all these mechanisms have to be modelled into a generic soot model. The model also has to work in conjunction with all the other phenomena which can influence flames such as turbulence, reaction kinetics, radiation, convection and others. This can make the overall numerical code complex to run and often lead to long computation times. So, due to inadequate knowledge of combustion chemistry or to find a compromise between modelling simplicity and computational accuracy practical models are required. So, it is necessary to have a simplified soot model, which has an experimental basis and also has physical grounding. This is a challenging problem.

3.1 Soot models for field modelling

Practical models based on single-step and semi-empirical approaches are commonly applied in field modelling to determine the soot particle concentration. The degree of complexity for these models comes from the intricacies of soot formation and oxidation. The task is to formulate the appropriate reaction rates for the given problem so that they mimic the many important physical processes such as

a) Nucleation – particle inception
b) Coagulation
c) Surface growth and aggregation
d) Particle oxidation

The main drawback of this approach is that the pre-exponential constants and activation energies that appear in reaction rates, which have to be determined from experimental data. Some models make direct use of the experimental results or use experimental measurements only for calibration to adjust the parameters until agreements between predictions and experiment are obtained. Frequently, these models are appropriate only for specific fuel type, oxidant, pressure or even burner type. An extensive amount of experimental and theoretical work on this is reported in the literature from last few decades. Several models for soot formation already exist, and many have provided an excellent review of this work [1, 10, 12, 15, 16]. Highlights from their work are presented here.

The models can be grouped in categories like empirical correlations, semi-empirical approaches or detailed models. There is inevitably overlap between these categories, however, the classification is useful in bringing order to a large amount of material.

3.2 Single-step empirical rate

This is a simple approach where a single transport equation is required for the mean mass fraction of soot ($\tilde{Y}_s$) and average density ($\bar{\rho}$)[10]. A Favre-averaged[g] conservation equation can be written as,

$$\frac{\partial}{\partial t}\left(\overline{\rho}\,\tilde{Y}_s\right) + \frac{\partial}{\partial x_j}\left(\overline{\rho}\;\tilde{u}_j\tilde{Y}_s\right) = D_s^{th} + \underbrace{\frac{\partial}{\partial x_j}\left[\frac{\mu_T}{Sc_T}\frac{\partial \tilde{Y}_s}{\partial x_j}\right]}_{diffusion\ term} + \overline{\omega}_{s,f} + \overline{\omega}_{s,ox} \qquad 3.1$$

Where $\overline{\omega}_{s,f}$ and $\overline{\omega}_{s,ox}$ are the mean reaction rates due to soot formation rates and oxidation respectively, for which many models are proposed. In laminar flow, the diffusion of soot D_s^{th} occurs exclusively by thermophoresis[h]. In turbulent flow, the turbulent diffusion term dominates over the diffusion term due to thermophoresis. So, the term D_s^{th} can be safely ignored for most practical purposes.

3.2.1 Formation model by Khan and Greeves

This model, proposed in 1974, is widely cited for soot emission from diesel engines [17]. It assumes that soot particle production in flames is inherently a chemically controlled phenomenon and governed by soot formation inception rate.

$$\overline{\omega}_{s,f} = C_f \bar{P}_{fu} \emptyset^{\alpha} \exp\left(-\frac{E_a}{R_u \tilde{T}}\right) \qquad 3.2$$

Where C_f is a constant, $\bar{P}_{fu}$ is the mean partial pressure of fuel, $\emptyset$ is the local unburnt equivalence ratio, E_a is the activation energy, R_u is the universal gas constant and α is the exponent ascertained through experiments. The lower and upper limit of equivalence ratio is 2 and 8 respectively. Where the upper limit is defined mostly by the upper flammability limit. This model has been applied to a wide range of fuel types and has shown suitability in field modelling.

3.2.2 Oxidation model by Magnussen and Hjertager

Here a simple model for soot oxidation is proposed similar to eddy dissipation concept[i], where it is assumed that the combustion is controlled by the rate of mixing of the particle stream with the adjacent oxygen streams [12]. The oxidation rate of soot is,

$$\overline{\omega}_{s,ox} = minimum\left\{-C_R\,\bar{\rho}\,\tilde{Y}_s\frac{\varepsilon}{k}, -C_R\bar{\rho}\left(\frac{\tilde{Y}_o}{\tilde{Y}_s r_s + \tilde{Y}_{fu} r_{fu}}\right)\tilde{Y}_s\frac{\varepsilon}{k}\right\} \qquad 3.3$$

Where C_R is a model constant, r_s and r_{fu} are the soot and fuel stoichiometric ratios. ε/k is the ratio of dissipation of turbulent kinetic energy to turbulent kinetic energy. In regions where oxygen concentration is low, the oxygen becomes the limiting species that control the rate of consumption of soot. Here soot also has to compete for oxygen with the unburnt fuel. For rich oxygen conditions, the mass fraction ratio becomes unity and the

lower value of reaction rate determined by these two assumptions provides the local soot oxidation rate.

3.2.3 The model proposed by Lautenberger et al.

It is a fairly recent approach to model the soot formation and oxidation in non-premixed hydrocarbon flame targeted towards simplifying CFD calculations. It is generalised to multiple fuels by estimating relative sooting tendency empirically [15]. The soot oxidation process is modelled as a surface area independent process. It is assumed to be controlled by diffusion of molecular oxygen into the zone of active soot oxidation rather than limited by the reaction of *OH*- radicals with the available soot surface area.

The model is appropriate for use with moderately to heavily sooty flames as it considers only homogeneous soot formation. The initial results are encouraging and further work and calibrations are undergoing. More details on the formulation of the rate and governing equations can be found in the paper and dissertation by Lautenberger [15, 18]

3.3 Semi-empirical approach

In this approach, the model incorporates the physics and chemistry of soot formation phenomenon leading to the development of rate equations of soot precursor particles with combustion chemistry and transport equations with particulate number density which are solved with a transport equation for soot particles.

3.3.1 Formation model for nuclei and soot by Tesner and Magnussen

In 1971 Tesner et al. examined the formation of soot from small amounts of acetylene in hydrogen diffusion flames at about 1800 K. They presented their model in terms of generation of radical nuclei which form new particles and also interact with the existing particles. For the radical nuclei (*n*), and soot (*s*) the two-step – formation (*f*) and oxidation (*ox*), model is described as below

$$\omega_{n/s} = \omega_{n/s,f} + \omega_{n/s,ox} \tag{3.4}$$

$$\omega_{n,f} = \frac{1}{\rho}\frac{dn}{dt} = \frac{n_0}{\rho} + (f - g)Y_n - \rho\frac{g_0}{m_p}Y_nY_s \tag{3.5}$$

Where n_0 is the temperature dependent rate of spontaneous generation of nuclei; f and g are linear branching and termination coefficients respectively; g_0 is the rate of destruction of nuclei on the soot particle surface, m_p is the mass of soot particle. No allowance is made for coagulation in this model and the model does not offer any insight into the physical processes occurring in soot formation.

Magnussen et al. made some changes in the model and included it in his Eddy Dissipation Concept (EDC) model for turbulent combustion. They also developed a model for soot oxidation, as shown by equation 3.3, together with Tesner's formation model [12].

$$n_0 = 1.08\, a_o f_c Y_{fu} e^{-E/RT} \quad (3.6)$$

$$\omega_{s,f} = \frac{m_p}{\rho}\frac{dS}{dt} = \left(m_p a - b\rho Y_s\right) Y_n \quad (3.7)$$

$$m_p = \frac{\pi}{6}\rho_s d_p^3 \quad (3.8)$$

The equation for n_0 is also modified by Magnussen, where Y_{fu} is the mean fuel concentration and f_c is the carbon mass fraction in the fuel. And a_o is the constant dependent on soot particle diameter. Soot is allowed to grow on the radical nuclei and the total rate of soot formation is given by equation 3.7, where *S* is the soot particle concentration, *a* and *b* are model constants and m_p is mass of soot particle. E/R is found to be 90000, for the values of other constants refer thesis by Kleiveland [12]. The combustion rate of the nuclei and soot is assumed to the proportional to the combustion rate of the fuel.

Magnussen et al. developed a generalised version of the model which can be used for other fuels as well. Correction to the model is made for limiting the maximum amount of soot formed by the amount of carbon available in the fuel present. This model is widely applied on commercial CFD codes.

3.3.2 Models for all soot production steps by Lindstedt and Moss

Here, two semi-empirical models are presented, one by Lindstedt et al. and other by Moss et al. This model incorporates the essential physical processes of soot nucleation, coagulation, and surface growth influencing the soot volume fraction and particulate number density. The model has two transport equations one for soot particle density (N) and one for soot mass fraction (s). The respective source terms for different mechanisms in the model can be written as follows:

$$\rho\omega_s = (soot\ nucleation) + (soot\ mass\ formation) - (soot\ oxidation) \quad (3.9)$$

$$\rho\omega_N = (particle\ nucleation) - (agglomeration) \quad (3.10)$$

All of the rate source terms for soot nucleation, nucleation for particles, oxidation and soot mass growth are calculated from chemical kinetics. For agglomeration, the source term is evaluated using the free-molecule kinetic theory. For more information on model refer dissertation by Kleiveland [12].

3.3.3 A model with acetylene proposed by Leung

The model proposed by Leung et al. differs from those mentioned earlier in the aspect of assuming acetylene as the precursor for soot nucleation and growth. Acetylene here is assumed to be the product of fuel breakdown process. So, the rates of soot nucleation and growth are directly proportional to the acetylene concentration rather than fuel concentration. Although it complicates model by having the requirement to find one more term – acetylene mass fraction, it is generally accepted to be more plausible as shown in

chapter 2.1. This does not prove to be a difficulty if the reaction mechanism of the parent fuel is known. The model solves for the particulate number density *n* and soot mass fraction *Ys*.

3.4 Population balance approach to soot formation

The population balance method is getting attention lately from academics as well as industries due to the way it can handle a wide variety of particulate processes. In most cases, it is employed to predict the evolution of the particle size distribution for example in crystallisation or polymerisation processes. This process has been well documented by Yeoh et al [10].

A population balance on any system is generally concerned with maintaining a record for a number of entities, which may be solid particles, gas bubbles, biological cells or liquid droplets or events whose occurrence will impact the behaviour of the system. This record of particle size distribution is usually obtained by writing equations that describe the conservation of mass of the entities. Such equations are usually referred to as population balance equations.

The variables that distinguish between particles are usually classified as external coordinates such as its physical location and internal coordinates, which describe the entity in terms of size, mass, temperature, composition etc. The collection of this coordinates is referred to as a state of the entity and represented in a form of finite dimensional vector. This establishes a concept of entities distributed in a state space, which may change with time because of its existing variable values and expected changes in them due to random changes. There is also a birth process which creates new entities and death processes that destroy the existing ones. Nucleation of particles, breakup, and aggregation are some typical examples of such processes which are very relevant to soot production.

The structure of the population balance equation, which are in integrodifferential form, is generally very complex and some techniques have been suggested for their solution without overburdening the computational requirement [10] mostly for idealised situations.

3.5 Selecting soot models in fire modelling

Fire models' ability to predict soot formation and oxidation have a profound influence on its estimation of mass burning, flame spread, and fire growth because these processes are driven by thermal radiation. However, there is no universal soot model available. And most of the advanced soot models are impractical for use in fire safety engineering due to their complexity, computational cost, or a large number of fuel-specific parameters that are not easily available.

A simplified guideline is provided by Yeoh and Yuen [10] for selecting the soot models in fire modelling. Any fire can be categorised to be having either lightly or moderately to heavily sooty flames. For moderately to heavy sooty flames of complex fuels, the soot concentration can be estimated with single-step empirical rate models with the minimal computational

expense and it also predicts the radiation contribution due to soot particles. These models since governed by gas phases mechanisms are only applicable for homogeneous soot formation.

For lightly sooty flames heterogeneous soot formation process, as well as homogeneous soot formation, are important. Models which can offer flexibility in modelling of the essential formation steps like nucleation, coagulation, surface growth, aggregation and particle oxidation, in order to include the heterogeneous soot formation and not significantly overburden the computational load. Knowledge of combustion chemistry for the given fuel type governs the application of these models. A semi-empirical model is suitable in such a scenario.

Models proposed by Tesner et al. and Moss et al. do not include a detailed reaction mechanism of practical flames and hence prove to be beneficial to predict the soot nucleation and growth using parent fuel concentrations.

Conditions where acetylene is the only relevant precursor, even if it complicates the modelling, the reaction mechanism to determine its concentration can be included in the combustion model. One such alternative with minimal computational effort is provided by Leung et al.

Attempts to use the detailed model have been made to solve the rate equations for elementary reactions producing soot to predict the soot particle size distribution and its evolution. Such models are complicated and require substantial computational resources. And they do tend to provide better soot concentration predictions if the detailed chemistry of the parent fuel is fully realised [10].

3.6 Soot modelling in FLACS

As discussed earlier, the formation and growth of soot are proven to be a difficult phenomenon to understand. And despite the availability of different models in the literature, in practice, their application may not be practical. As a compromise between modelling simplicity and computational accuracy, models based on single-step and semi-empirical approaches are applied to find the concentration of soot particles.

For FLACS, the mixture fraction, the fuel composition and the local equivalence ratio (ER) are the parameters which can be used to determine the soot level. Hence, the models based on some intermediate species in combustion are not used. Apart from that, the use of memory and speed of code also govern the choice of model.

An internal memo at Gexcon by Melheim J. [19] indicates that three different soot models were investigated, of which two models are used in FLACS code. The Conversion Factor Model (CFM) and the Formation-Oxidation model (FOX). Details about these model approaches follow. The CFM contains only one adjustable parameter while the FOX model contains three.

3.6.1 Conversion factor model

A soot conversion factor model (CFM) is a simple model indicating how much of the fuel is soot on the product side independent of ER, temperature, time, etc. The only input to CFM is the soot conversion factor, which is given by the fraction of the fuel mass. To avoid soot production in lean mixtures and mixtures around the stoichiometric ratio, soot is only produced when the ER is above 1.5.

The values for the fixed conversion factor for typical fuel species are taken from the FLACS user manual [9] and from a compilation by Kent, J.A. [20]. A shorter version of these values is provided in Appendix A.

3.6.2 Formation oxidation model

The formation-oxidation model (FOX) has two source terms in the transport equation for soot, one for the formation and the other term for oxidation, similar to equation 3.4. Soot formation is a slow process, especially the formation of the nucleus which requires a rich mixture, certain flame temperature and residence time. Once the nucleus is formed, the formation of soot is comparatively quick. However, the formation of the nucleus will require its own transport equation, therefore it is not considered for FLACS. Also, it is to be noted here that only this model has a dependency on time and temperature.

The transport equation for soot mass fraction, which is similar to equation 3.1. The source term is transport equation is the sum of formation term and oxidation term,

$$\widetilde{\omega}_s = \widetilde{\omega}_{s,f} + \widetilde{\omega}_{s,ox} \tag{3.11}$$

The model for formation is taken from Khan and Greeves as shown in equation 3.2

$$\widetilde{\omega}_{s,f} = C_f p X_{fu} (\emptyset)^3 \exp\left(\frac{E_f}{RT}\right) \tag{3.12}$$

Where C_f = 1.5 and E_f/R = 20000 K for most hydrocarbons [9]. The value of equivalence ratio $\emptyset$ is between 1.67 to 3, otherwise, the soot formation rate is assumed to be zero. For soot oxidation, the model developed by Magnussen and Hjertager is used as shown in equation 3.3, which is similar to oxidation of fuel with EDC.

$$\widetilde{\omega}_{s,ox} = -\frac{\dot{m}\chi}{1-\gamma^*\chi}\tilde{Y}_{min} \tag{3.13}$$

$$\tilde{Y}_{min} = minimum\left(\tilde{Y}_s, \frac{1}{r_s}\tilde{Y}_{ox}\right) \tag{3.14}$$

Where $\dot{m}$ is mass rate, γ^* is a mass fraction of fine structures and it impacts the turbulence intermittency, the progress variable χ tells how much of the potential fuel that has burnt, r_s is the 8/3 the stoichiometric amount of oxidant required for soot combustion. The upper limit for the mass fraction of soot, when using the FOX model is given by the soot yield value, listed in Appendix A.

4 Validation

Although there are various definitions of model validation, most define it as the process of determining how well the mathematical model predicts the actual physical phenomena of interest [21]. A primary requirement of any modelling tool is to verify its ability to correctly captures the physics for the given problem. For any CFD code, it is important to populate a database with relevant validation cases that cover the entire range of applications. This database helps to organise the knowledge related to validation. Validation against available small and large-scale experiments in one way to approach this. This database helps to organise the knowledge related to validation.

Here an attempt is made to present a few validation cases to the validation matrix for soot modelling using several example cases. This validation matrix will help the way in which simulations are built and repeated efficiently to evaluate the effect of model changes during the development of the code. It is hoped that this resulting database will be useful for software testing, parameter optimisation, estimation of uncertainties in simulation results, training and documentation. Similar attempts for this have been made earlier as a topic for a master's dissertation for fire modelling [22, 23]. Several internal papers at Gexcon were referred to as a guide for conducting these validation cases [24, 25].

The focus of this thesis is to present the validation of FLACS fire predictions for soot in different fire conditions. The turbulence is modelled using the standard k-ε model, and combustion is modelled using the Eddy Dissipation Concept (EDC). For radiation discrete transfer radiation model (DTRM) is used with a weighted sum of grey gas[j] (WSGGM) for radiation property calculations.

Table 4.1: Validation cases

Author and reference	Experiment	Focussed parameters
Tessé L. et al. (2004) [4]	Turbulent ethylene air jet flame from 4 mm burner nozzle	Temperature, volume fractions of soot, CO_2, H_2O and radiative power
Wang CJ et al. (2018) [3]	Heptane pool fire on 0.8 m square hollow pan	Temperature, soot mass fraction
Chen Z et al. (2014) [6]	Heptane and toluene pool fire on 0.3 m circular pan	Temperature, soot volume fraction
Lock A. et al. (2008) [7]	Underventilated compartment fire in an ISO 9705 room (2.4 m x 3.6 m x 2.4 m)	Temperature, soot volume fraction, comparison with results from FDS

The soot is predicted using formation-oxidation model (FOX) as well as the conversion factor model (CFM). Comparisons are made between the experimental data and simulations. Four published papers with information on experimental data using different and well-understood

fuels are selected, based on their scale of experiments for this task. As Table 4.1 shows, these range from small scale to large scale, based on the dimensional scope of the test.

Apart from experiments, results from another CFD code Fire Dynamic Simulator (FDS), are used for comparison in a compartment fire case. FDS is an open-source software tools provided by the National Institute of Standards and Technology (NIST).

Each of the following sub-chapter is devoted to one of the papers mentioned above, The experimental and modelling setup is explained. A small section on sensitivity analysis is presented based on variations of different modelling parameters. In the end results from experiments and simulations are compared and discussed.

4.1 Turbulent ethylene sooty flame

The published paper by Tessé et al. [4] have considered an open diffusion flame as it has a simple geometry, turbulence intensity in the reactive zone is high. Pure gaseous ethylene is injected vertically upwards in atmospheric air at a velocity of 29.5 m/s leading to significantly high turbulence level. The injection duct diameter is 4 mm. Here measurements of volume fractions for soot, CO_2, H_2O and temperature are available.

Soot particles play an important role in radiative heat transfer and its impact on radiative heat loss is also under consideration. The turbulent flame will also impact the soot generation. Data on H_2O and CO_2 volume fraction are also available for comparison with soot.

4.1.1 Computational details

The centre of the burner duct is placed at (0,0,0) coordinate in the simulation environment. The computational domain is limited to 0.2 m x 0.2 m x 1 m with a uniform grid size of 0.01 m. Grid refinement is performed around the leak source as the nozzle diameter is very small.

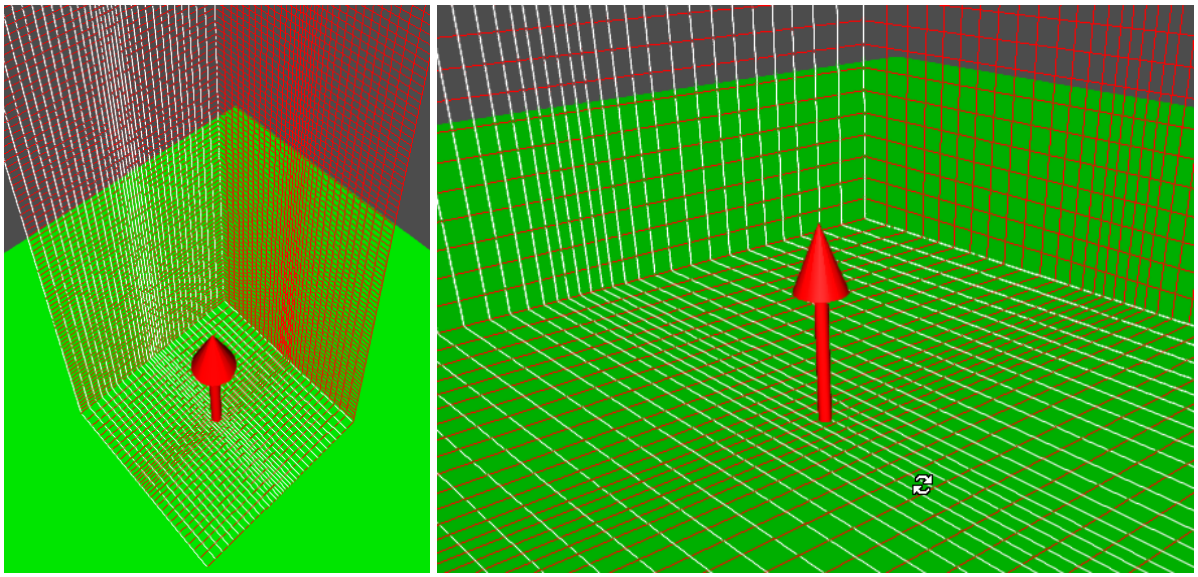

Figure 4.1: Calculation domain and grid distribution for turbulent ethylene sooty flame

Figure 4.1 shows the geometrical configuration, with grid and the location of jet leak. For radiation total number of rays used are varied between 108 and 300. Both the soot models are used as listed in Table 4.2.

Table 4.2: Model parameters for turbulent ethylene sooty flame case

Case tag	DTM Number of rays	Soot Model	Averaged Results Case tag
100000	108	FOX	900000
100100	300	CFM (0.12)	900100
100010	108	FOX	900010
100110	300	CFM (0.12)	900110

4.1.2 Sensitivity analysis for the variations

The only variation performed in this case is regarding a number of rays selected for radiation modelling with the Discrete Transfer Method (DTM). The DTM calculations take a significant part of the total computing time and increasing the number of rays will also increase overall calculation time [9].

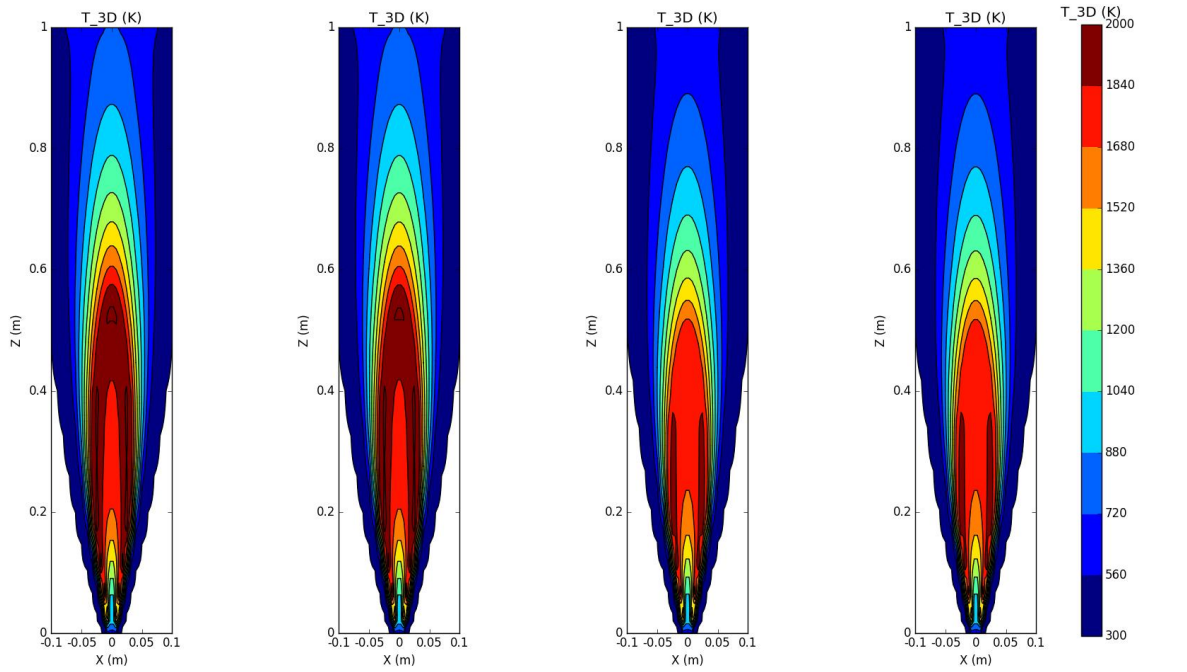

(a) 900000 FOX soot model, Radiation DTM 108 (b) 900100, FOX soot model, Radiation DTM 300 (c) 900010 CFM soot model, Radiation DTM 108 (d) 900110, CFM soot model, Radiation DTM 300

Figure 4.2: Impact of varying soot model and no. of radiation rays on temperature field

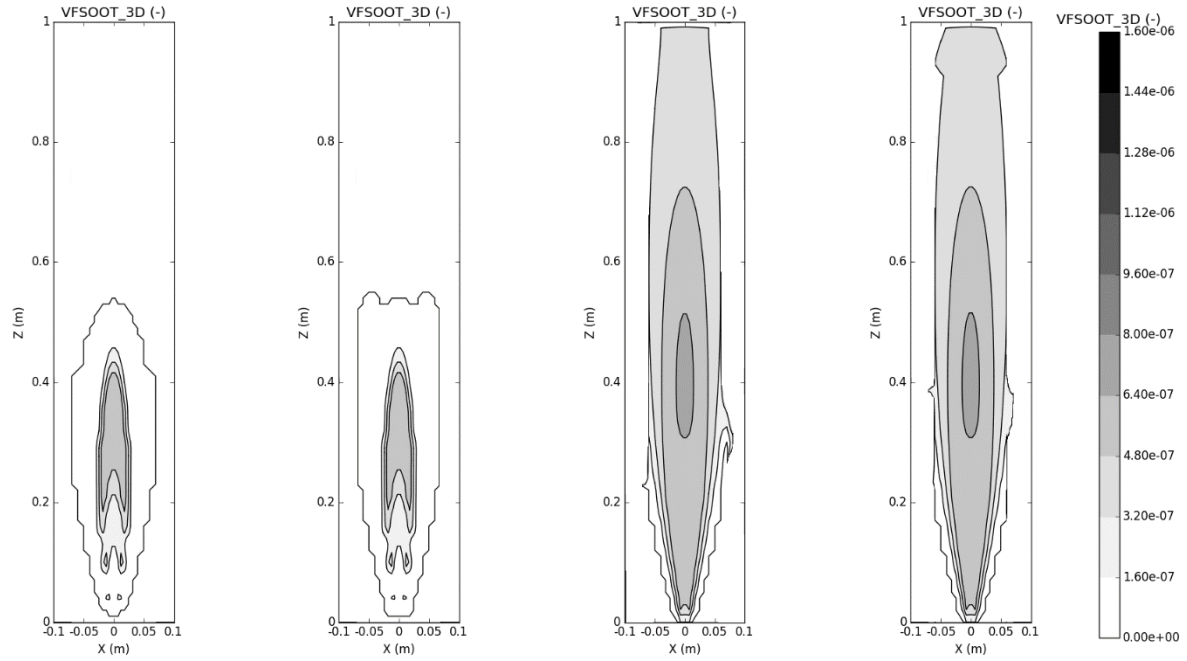

(a) 900000 FOX soot model, Radiation DTM 108 (b) 900100, FOX soot model, Radiation DTM 300 (c) 900010 CFM soot model, Radiation DTM 108 (d) 900110, CFM soot model, Radiation DTM 300

Figure 4.3: Impact of varying soot model and no. of radiation rays on soot vol. fraction field

Increasing the number of rays from 108 (default value) to 300 did not have any visible impact on temperature and field and soot mass fraction, compare results from case 900000 with 900100 and case 900010 with 900110 in Figure 4.2 and Figure 4.3. Using a finite number of rays will result in gaps between the ray, and may impact the quality of the result. The effect is stronger for the small or thin heat source and at a larger distance from source [9]. Since the focus of the analysis is not very far from the fuel source, the impact of a variation in a number of rays is insignificant.

On the other hand, varying soot model has a large impact, see Figure 4.3. The amount of soot generated with the FOX model is significantly low compared to CFM. In the CFM, it is assumed that 12% of the ethylene fuel carbon is converted to soot directly. In FOX model for soot two source terms in the transport equations are evaluated, which are for soot formation and soot oxidation. While using the FOX model the upper limit of mass fraction of soot is given by soot yield value also given in Appendix A and this value is also used in CFM.

4.1.3 Results and discussion

The simulation is run for 5 seconds with ignition starting at 1 second. The time average values over 1 to 5 seconds are used for presenting the results with tags starting with 9 instead of 1.

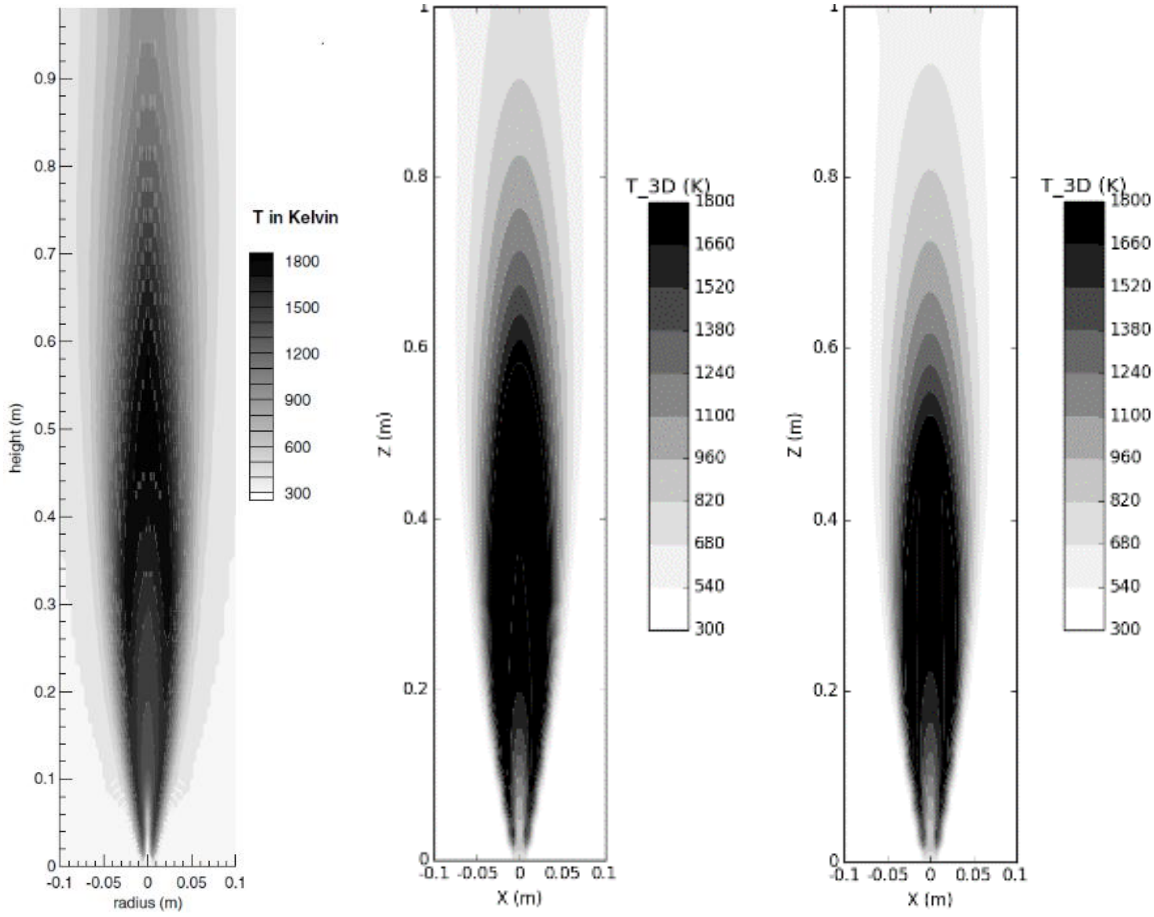

(a) from Tessé et al. (b) 900100 (FOX) (C) 900110 (CFM)

Figure 4.4: Time-averaged temperature field comparison for the ethylene flame

The comparison of the time-averaged temperature field from the ethylene flame is presented in Figure 4.4. The prediction of temperature shows good agreement with the data presented by Tessé et al. [4], especially with the case 900100 with FOX model. The flame expands downstream the of the leak, peak temperatures reaches quickly to higher than 1500 K. The trend while going upwards from the centre of the nozzle Is also similar. Due to turbulence, the higher temperature zone is shifted slightly upwards. The case with CFM predicts slightly less temperature but the overall trend and spread of temperature in the radial direction are similar.

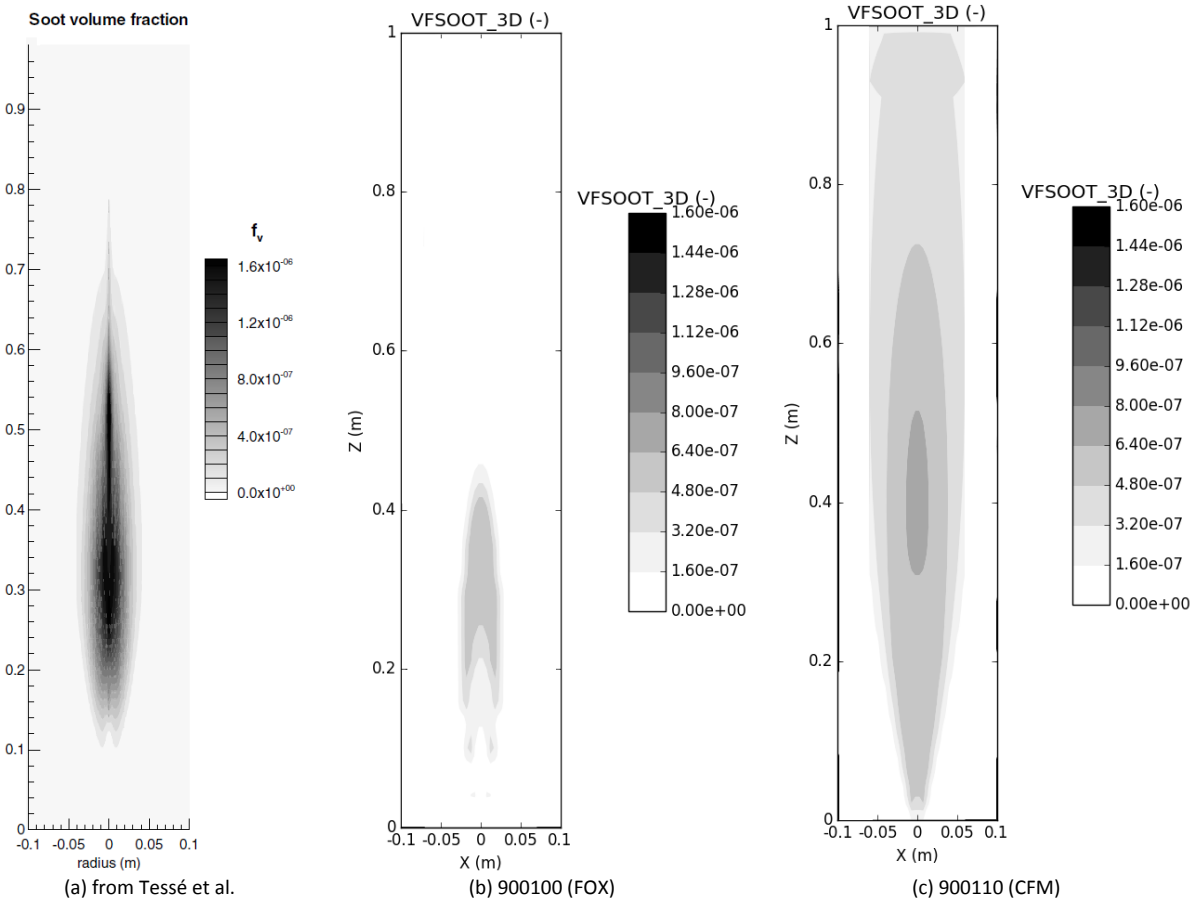

Figure 4.5: Soot volume fraction field comparison for the ethylene flame

Soot particles play an important role in radiative heat loss. Soot particles radiate the energy and in turn cools the combustion product. This impact of higher soot volume fraction of temperature is clearly visible in the field profile for temperature when Figure 4.5 is compared with Figure 4.4. The case with the FOX model (900100) predicts lower soot volume fraction and smaller sooting zone when compared with the case with CFM (900110). But in case of temperature, the higher temperatures of 1600 K range are visible even at Z = 0.6 m for the case with the FOX model, whereas this height for CFM is around 0.5 m. So, CFM generates a higher amount of soot which consequently radiates more energy and this heat loss brings the temperature of combustion products down.

Looking at Figure 4.5 it is clear that the soot formation zone is narrow, long and coincides with the high-temperature zone on the temperature field. There is a sharper drop in soot volume fraction outside this zone which may be due to oxidation of soot particles in the post-flame

high-temperature zone. Since FOX model predicts lower soot fraction, its spread in the soot formation zone is not as wide as that predicted by CFM. The maximum soot fraction zone is limited between 0.3 - 0.4 m for the FOX model, whereas the same for CFM is between 0.3 – 05 m. The formation of soot particles is limited in the small volume above the peak temperature level as the conditions of temperature and mixture ratio are suitable for soot there.

It is important to know the role of soot in radiative heat transfer; this can be done by comparing it with the role of other combustion species. Apart from soot other combustion species like CO_2 and H_2O also emit radiation, but they also tend to self-absorb the radiation. These combustion products are distributed everywhere and at other locations, the gaseous species emit radiation, while the soot particles are concentrated in the small volume and their contribution to radiation in that region is much higher.

Figure 4.6 compares the temperature profile, and volume fractions of soot, CO_2 and H_2O at 50 cm above burner height. As discussed earlier the amount of soot volume fraction found at this level by using CFM is lesser but wider in radial scope than compared to same from data by Tessé et al. With FOX model there is hardly any presence of soot at 50 cm from the burner.

The volume fraction of CO_2 estimated by FLACS is higher than the data from Tessé et al. The probable reason for this is clearly carbon balance. The amount of carbon not converted to soot is converted to CO_2. By the same reason at this height, the CO_2 generated by the FOX model is slightly higher than that by CFM. The CO_2 volume fraction field comparison is provided in Figure 4.8.

For volume fraction of H_2O estimated by FLACS is almost equal to the data from Tessé et al. In the case of FOX and CFM also these values are almost the same, see Figure 4.9. Overall the amount of H_2O generated probably has the same impact on radiative heat loss for all considered cases, and for FOX and CFM it can be assumed that the amount of CO_2 generated has the same impact on radiative heat loss.

When we focus on the radiative power emitted by the ethylene flame in Figure 4.7 we see that its quite the mirror image of soot volume fraction from Figure 4.6. The turbulence in the centreline can also possibly be the cause for increases in the radiative transfer in the flame. The minimum value of the radiative source term predicted with CFM is – 3500 kW/m^3 which is roughly 130% lower than that predicted with FOX soot model around -1500 kW/m^3, whereas the same reported by Tessé et al. is -12900 kW/m^3. The field profile for radiative power highlights this at different heights in Figure 4.10.

So, there is a huge impact on radiative heat transfer with respect to soot formation. In this case, the CFM predicted higher values soot volume fractions than the FOX model. But in terms of the impact of that soot on radiative power the values estimated by FLACS were much lower.

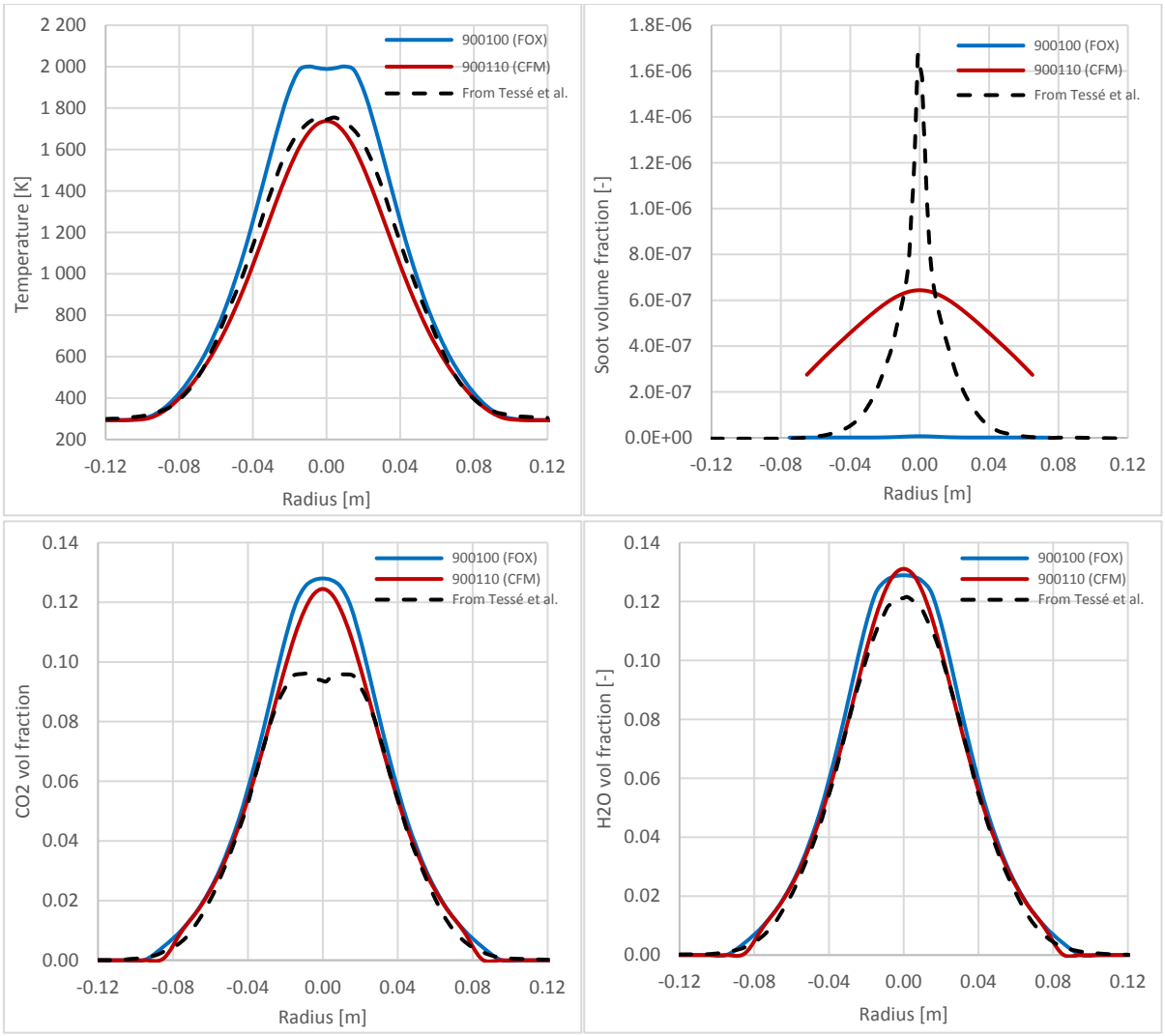

Figure 4.6: Comparison of temperature, soot volume fraction profiles, CO_2 volume fraction and H_2O volume fraction profiles for the ethylene flame 50 cm above ethylene inlet

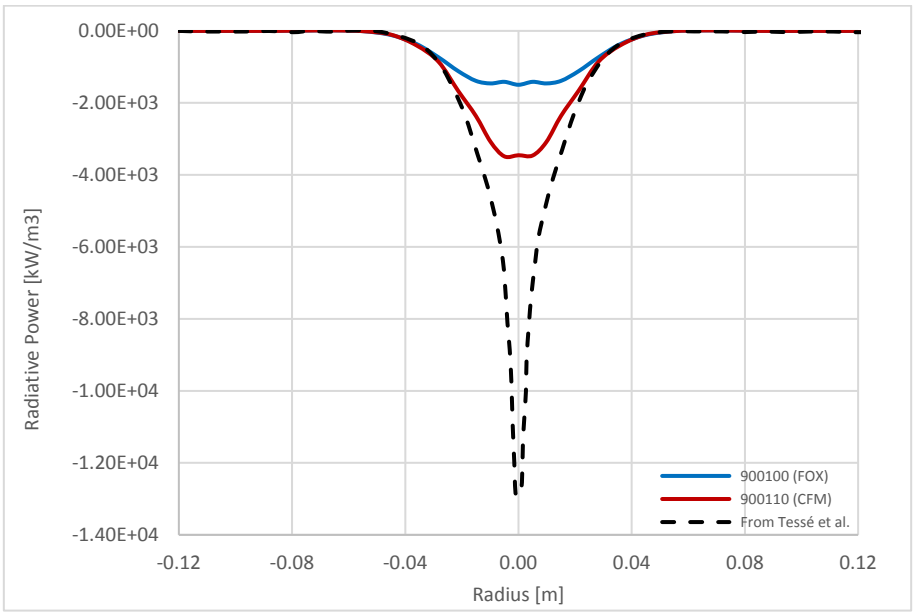

Figure 4.7: Comparison of radiative power profiles for the ethylene flame 50 cm above ethylene inlet

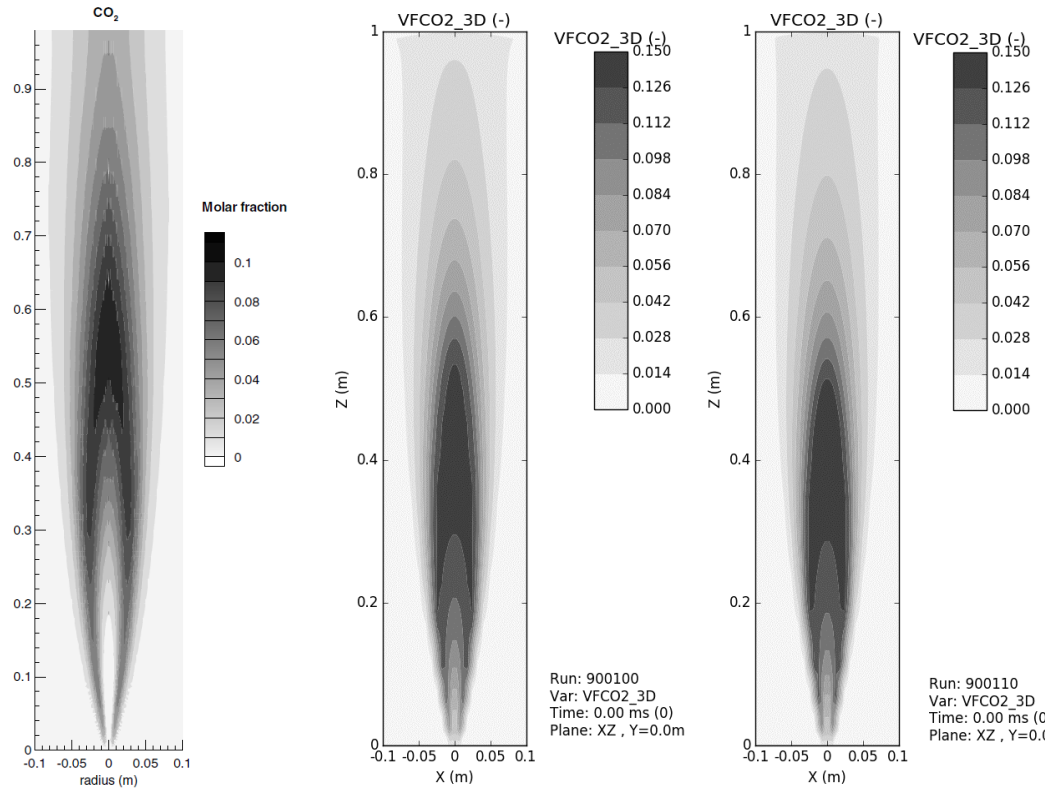

(a) from Tessé et al. (b) 900100 (FOX) (c) 910110 (CMF)

Figure 4.8: Time-averaged CO_2 volume fraction field comparison for the ethylene flame

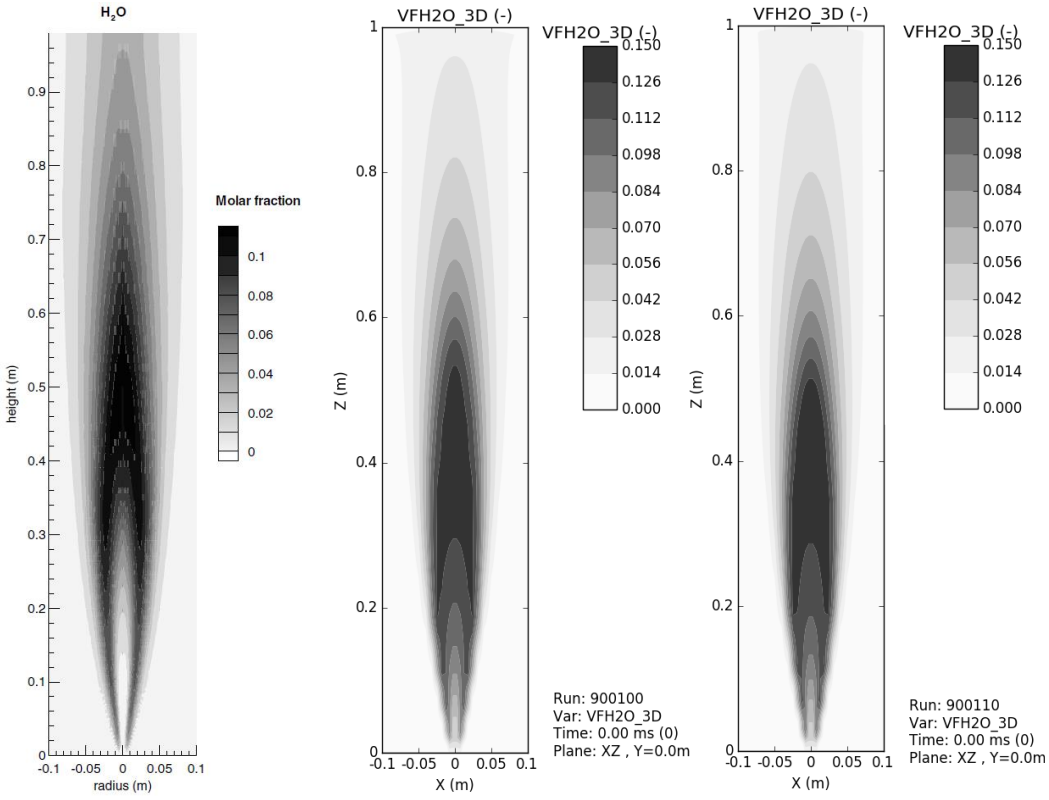

(a) from Tessé et al. (b) 900100 (FOX) (c) 910110 (CMF)

Figure 4.9: Time-averaged H_2O volume fraction comparison ethylene flame

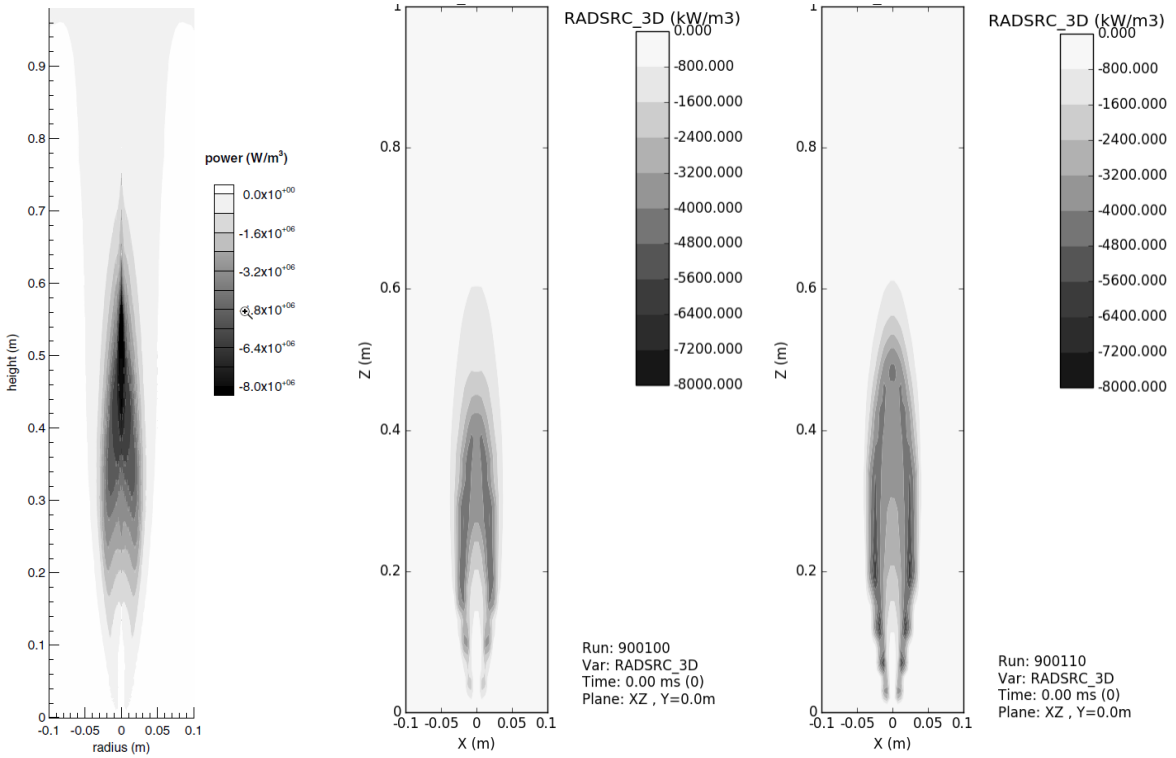

(a) from Tessé et al. (b) 900100 (FOX) (c) 910110 (CMF)

Figure 4.10: Time-averaged radiative power field comparison for ethylene flame (note the difference in units)

4.2 Heptane pool fire on a hollow square pan

Heptane pool fires with different mass burning rates on a hollow square pan, which has no fuel in the core region, were studied experimentally as well as numerically by Wang et al. [3, 5]. The observations made during the experiments motivated them to present a numerical study using a customised version of the FireFOAM code. The heptane fire was carried out on a 0.8 m x 0.8 m hollow square channel with a channel thickness of 0.1 m, as shown in Figure 4.11. During the experiment, it was found that after the fire was fully developed with constant burning rate, the radiation feedback resulted in fuel boiling in the pan. This led to the merging of fire which was originally sitting on the perimeter of the hollow square.

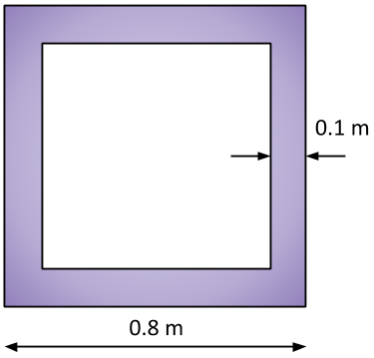

Figure 4.11: Hollow square pan for heptane pool fire [3]

These scenarios are modelled using the FLACS fire with different soot models. The burning rates chosen for this validation is 0.0247 kg/s. Different cases were generated based on variation soot model and modelling parameters. Dependency between key parameters is studied for such as centreline temperatures soot distributions with respect to soot models.

4.2.1 Computational details

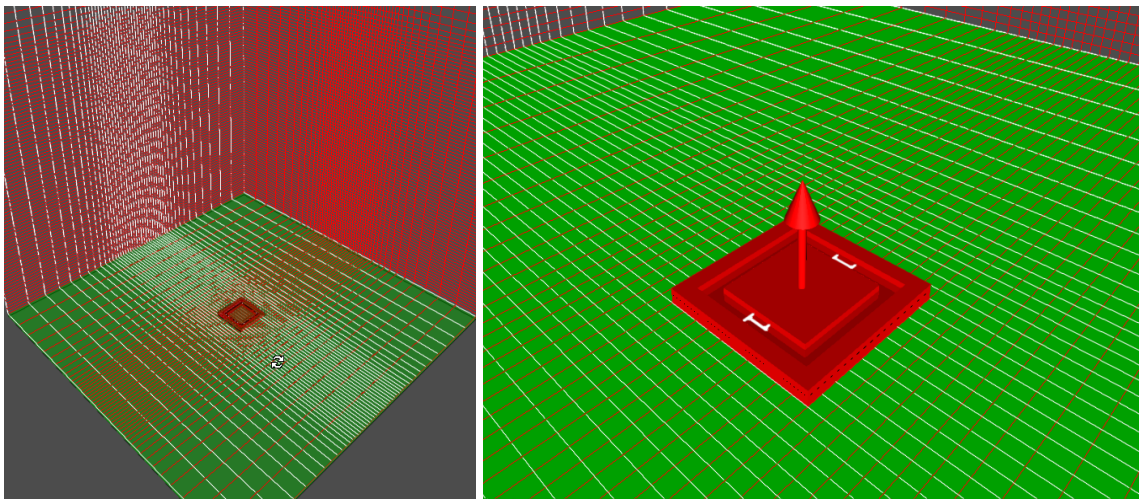

Figure 4.12: Calculation domain and grid distribution for heptane pool fire

The centre of the pan coincides with the centre of the model geometry. The computational domain is limited to 2 m x 2 m x 8 m with a uniform grid size of 0.1 m. Figure 4.12 shows the geometrical configuration, with grid, for the hollow square pan used in the pool fire. For radiation total number of rays used are 300. The leak is modelled as diffused leak with the burning rate of 0.0247 kg/s.

From the base case model, different variations are tested with respect to Fireswitch which changes the behaviour in combustion model [9]. Another variation is performed in the form of changing relative turbulence intensity (RTI) from 0.1 to 0.4. This impacts the value of turbulent kinetic energy (*k*). Two of the available soot models are also tested. Table 4.3 presents the list of variations performed for this case.

Table 4.3: Model parameters for heptane pool fire (square pan)

Case tag	Burning rate [kg/s]	RTI	Fire switch	Soot Model	Averaged Results Case tag
011100/10/20	0.0247	0.1 / 0.25 /0.4	2	FOX	911100/10/20
011200/10/20	0.0247	0.1 / 0.25 /0.4	0	FOX	911200/10/20
011121	0.0247	0.4	2	CFM (0.12)	911121

The simulation is run for 20 seconds with ignition starting at 5 seconds. The average values over 5 to 20 seconds are used for presenting the results. The averaged case tags start with 9 instead of 0.

4.2.2 Sensitivity analysis for the variations

Relative Turbulence Intensity (RTI) is the ratio between the isotropic fluctuating velocity and the mean flow velocity. Usually, 0.1 is suitable or recommended value. As seen in the figure, the variation in RTI does not have any visible impact on the estimation of temperature or soot mass fraction as shown in Figure 4.13.

Fireswitch changes the behaviour of the combustion model in FLACS Fire. There are three options: 0 - EDC only (default), 1 - Pre-mixed and EDC (selected automatically) and 2 - EDC for pool fires and extinction disabled.

Fireswitch = 0 is recommended when immediate ignition of jet fire is expected and for fires where consequences of the explosion are expected to be low. The second option of Fireswitch = 1 has not been completely validated and suggested to be used with caution, hence it is ignored. The third option of Fireswitch = 2 is recommended for pool fire simulations [9]. The overall impact of Fireswitch is not well understood here, however, the temperature predictions using Fireswitch value of 0, are very low. The peak values are around 600 K whereas the peak values estimated using Fireswitch value 2 are closer to 1600 K. See Figure 4.13 for details.

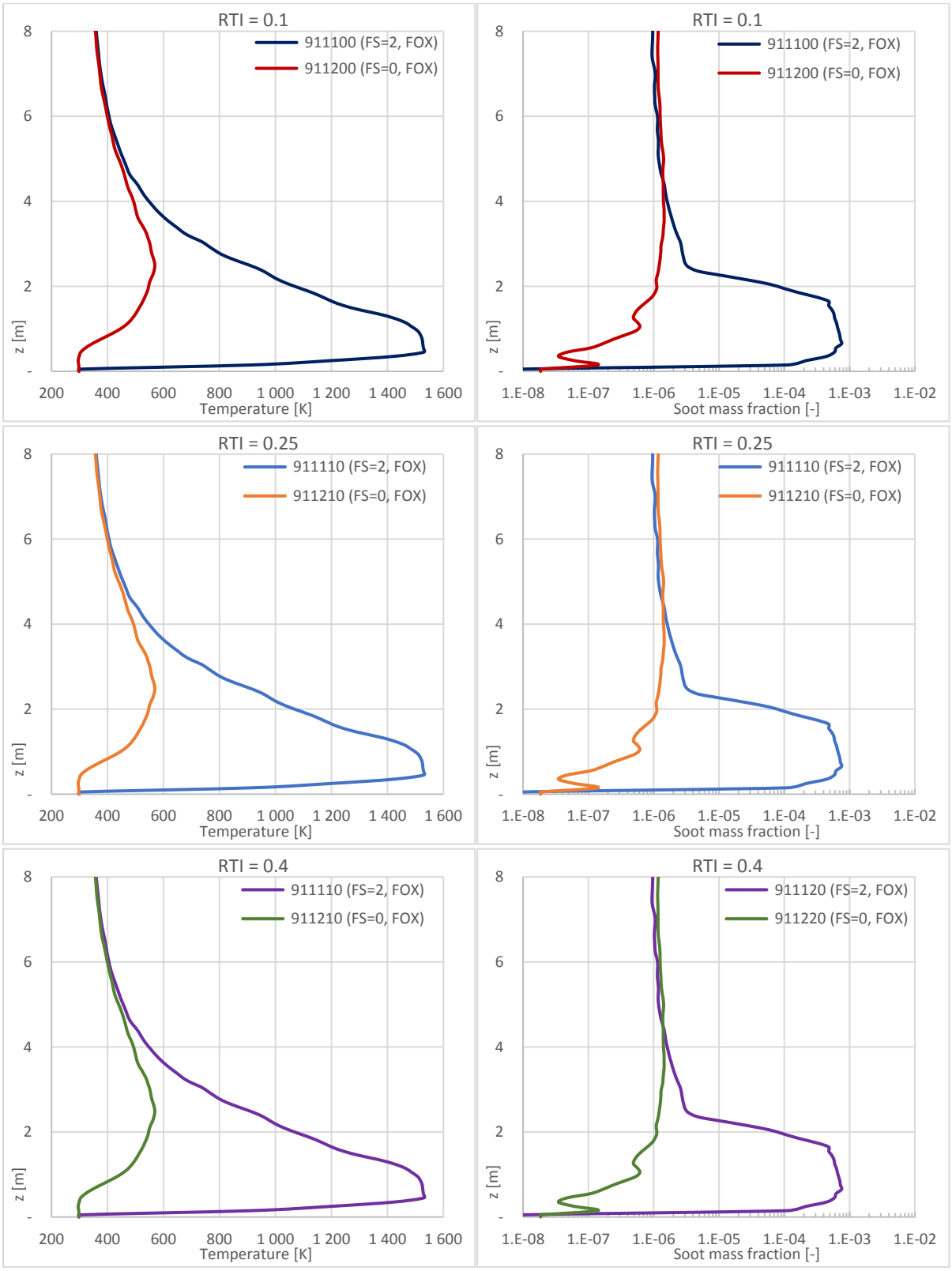

Figure 4.13: Impact of varying Relative Turbulence Intensity (RTI) and Fireswitch value on temperature profile and soot mass fraction along the height

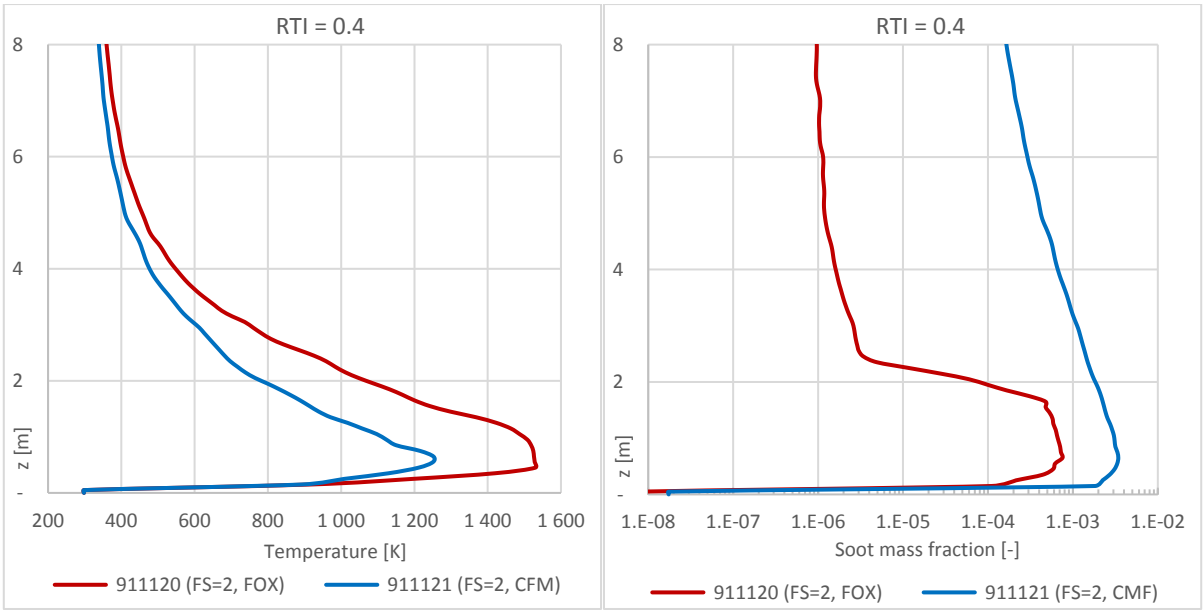

Figure 4.14: Impact of varying soot model on temperature profile and soot mass fraction along the height

As it can be seen from Figure 4.13 that there is hardly any impact of varying RTI, so only results with RTI of 0.4 are considered. The results using Fireswitch value 0 seem very unlikely, and hence for further calculation Fireswitch value 2, which is recommended for pool fire, is used.

On the other hand, varying soot model has a considerable impact on the temperature as well as soot mass fraction. The amount of soot generated with the FOX model is lower compared to the CFM. In the CFM, it is assumed that 12% of the heptane fuel carbon is converted to soot directly. Both of these models are considered and compared for further study.

4.2.3 Results and discussion

The time-averaged temperature contours are produced and compared with the fire which is in quasi-steady state[k]. These time-averaged temperature contours for the burning rate of 0.0247 kg/s are compared side by side with the ones provided by Wang et al. [3] in Figure 4.15 and Figure 4.16. It shows that the flame heights increase with the increase of the mass burning rate.

Even though the exact mean flame height is not available from the experiment, the overall heights of temperature contours are comparable. The temperature scale is colour calibrated to the available plot from the paper [3]. The flame merging can be seen here from Figure 4.15, which probably occurs as the fuel begins to diffuse to the centre and to consume the available oxygen. The temperature predicted from the FOX model is much higher than the same predicted by CFM. This can also be verified in Figure 4.16 with average centreline temperature variation along with the height.

The time-averaged centreline temperature prediction along the height seem reasonably closer. The centreline temperature firstly increases until it reaches the maximum value and then decays. The highest temperature prediction using CFM around 1250 K is very close to the temperature noted through experiments which is closer to 1210 K. On the other hand,

temperature prediction using FOX model is quite high, but it matches the overall spread of high-temperature zone along with the height better than CMF model.

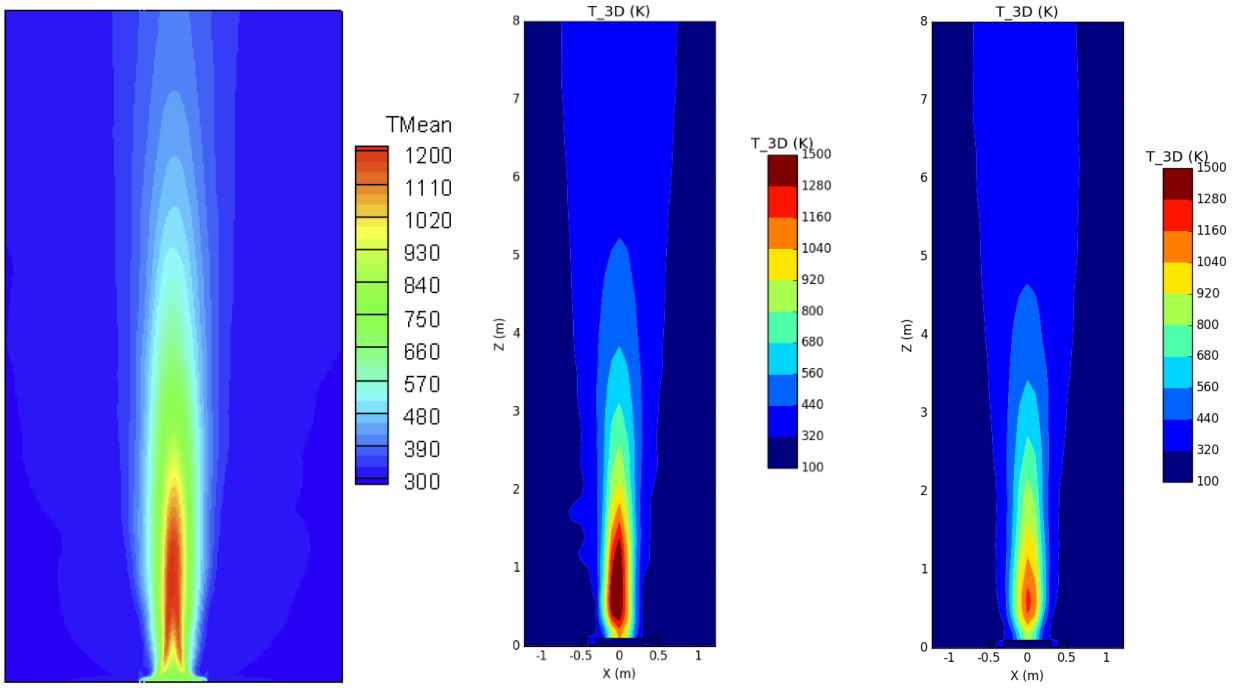

(a) from Wang et al. [3]

(b) 911120 (FOX) Scale is colour calibrated

© 911121 (CFM) Scale is colour calibrated

Figure 4.15: Time-averaged temperature contour comparison for the burning rate of 0.0247 kg/s (scales are colour calibrated)

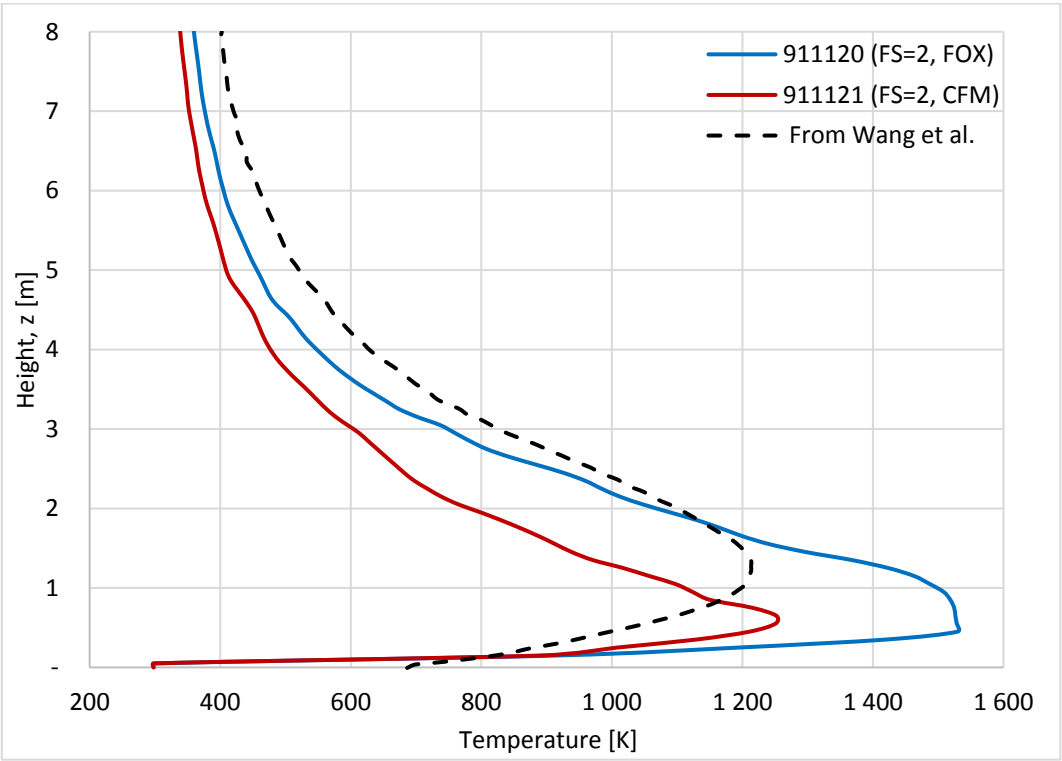

Figure 4.16: Centreline average temperature comparison for burning rate 0.0247 kg/s along the height

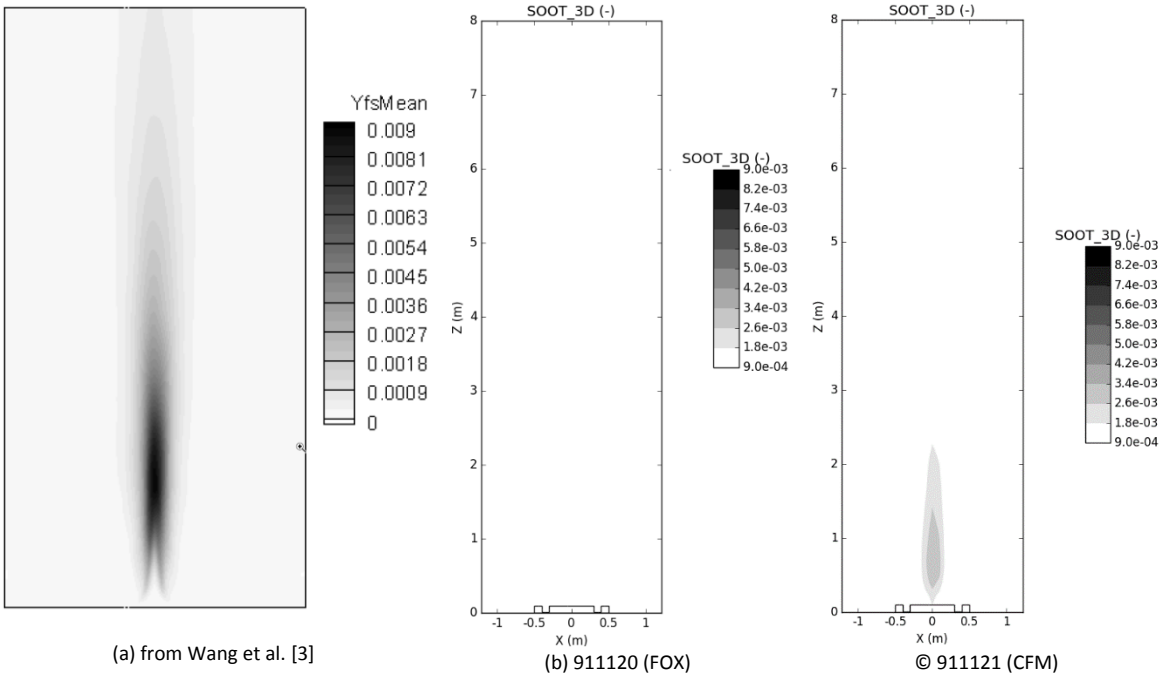

(a) from Wang et al. [3] (b) 911120 (FOX) © 911121 (CFM)

Figure 4.17: Time-averaged soot mass fraction contour comparison for the burning rate of 0.0247 kg/s

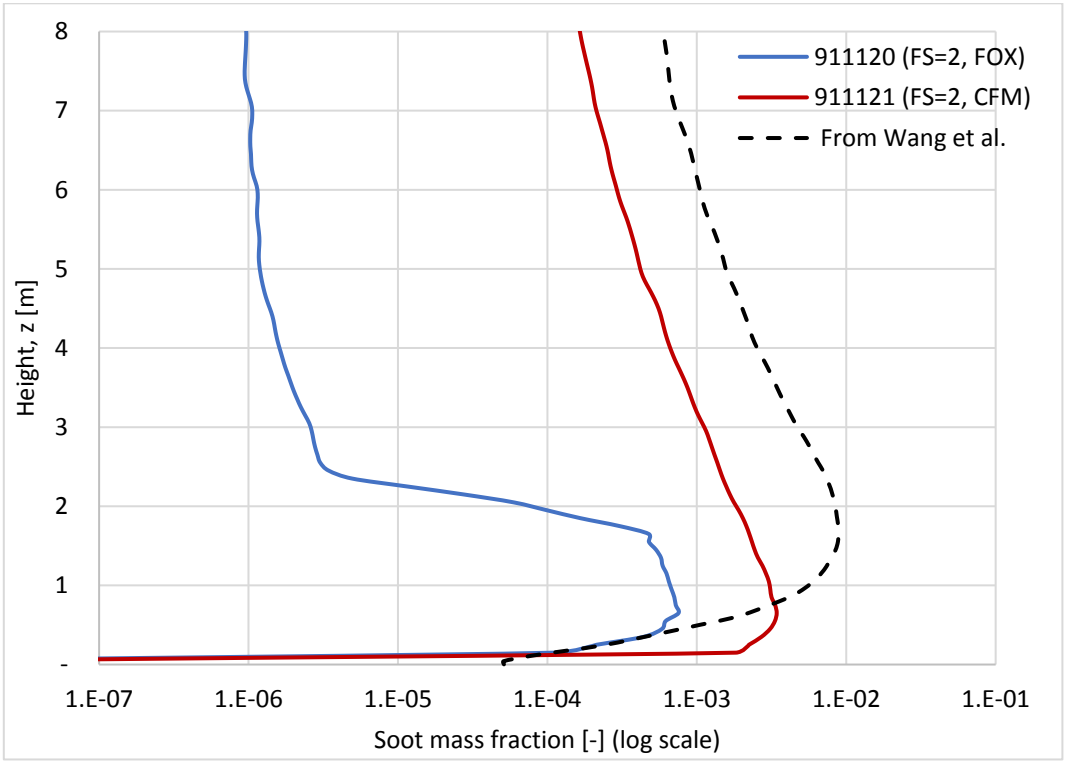

Figure 4.18: Centreline average soot mass fraction comparison for the burning rate of 0.0247 kg/s

The trend of change in soot mass fraction along the height is similar to that of temperature. In the experiments, the location of peak soot mass fraction zone is slightly away from the pool surface. Which also means that the maximum amount of soot is produced after the fire starts to merge.

The soot mass fraction predicted by FLACS using CFM soot model are lower but closer to the data obtained from experiments than the data using the FOX model. It is clear by comparing Figure 4.17 and Figure 4.18 side by side that the amount of soot produced by the FOX model is very low compared to the experimental data. Another reason for almost no soot seen in the Figure 4.17(b) is that the profile scale used from experiments ($9x10^{-4}$ to $9x10^{-3}$) is larger compared to the maximum amount of soot mass fraction predicted by FOX model which is $7.5x10^{-4}$.

On comparing soot predicted by CFM the trend along the height is quite similar to the experiment. The peak soot formation zone coincides with the peak temperature zone observed in the earlier temperature plots. Also, the reduction along the height is similar to that seen in experiments, which is probably due to slower soot oxidation along the height. For FOX model the drop in soot mass fraction after the peak zone is quick, this can be attributed to quicker oxidation of the soot particles post peak soot region.

Overall the predictions of temperature and soot mass fraction using FLACS with CFM gives arguably accurate predictions.

4.3 Heptane and toluene pool fire

In the paper published by Chen et al. [6], they have extended the cascade of eddy dissipation concept (EDC) to large eddy simulation (LES) framework and tested their model in open source FireFOAM solver with two medium-scale heptane and toluene pool fires in 2014. The original experiments were performed by Klassen and Gore [26] for NIST (National Institute of Standards and Technology) in 1994.

In this experiment, the pool fires for heptane and toluene were carried out in 30 cm diameter burners. The feeding rate was estimated by Chen et al. [6] to be 2.56 g/s and 3.05 g/s for heptane and toluene respectively. The inlet temperature was set to be 372 K for heptane and 384 K for toluene, which are also their boiling point temperature.

4.3.1 Computational details

The centre of the 30 cm burner pan is placed at (0,0,0) coordinate in the simulation environment. This problem is approached in two different ways wherein the first case the scenario is built with a jet leak with the feeding rate described earlier. And in the second case, the scenario is built with pre-existing fuel in the pan at the time of ignition as described in the NIST report by Klassen and Gore [26]. The computational domain in both this situation is limited to 1 m x 1 m x 3 m with a uniform grid size of 0.04 m.

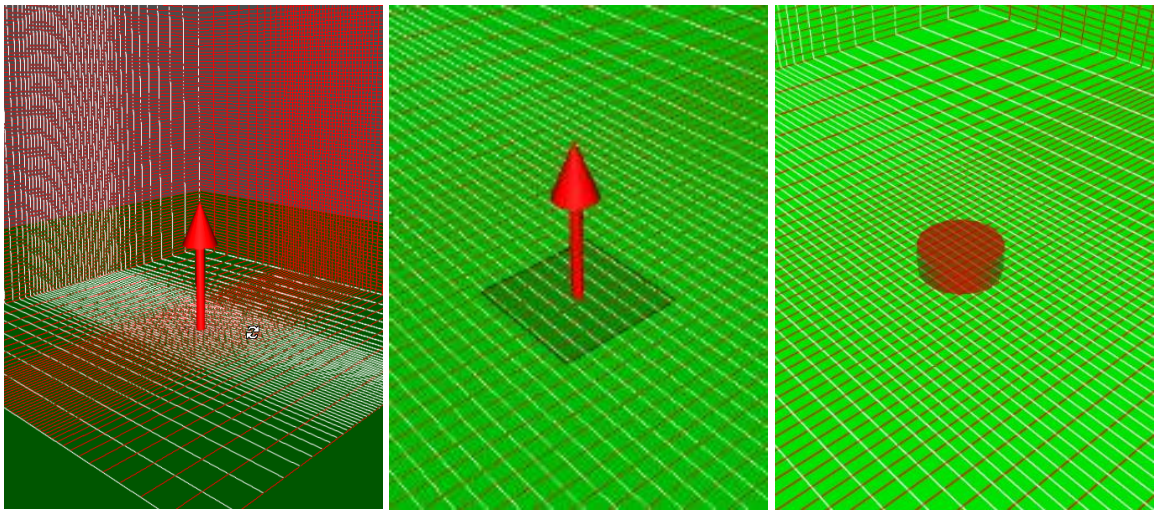

Figure 4.19: Calculation domain and grid distribution for heptane and toluene fire case, (jet leak and pool)

The simulation is carried out for 10 seconds and ignition is started at 1 second. A number of rays were kept at 300 for all variations. The fire-switch value is kept at 2 as pool fire is simulated. For pool fire, static circular pool model is selected, with an outer radius of 0.15 m. Solar radiation is neglected and ground surface type is selected to be a plate with a thickness of 1.6 mm, similar to the original experiments performed by Klassen and Gore [26].

FLACS provides a variety of option for fuels but toluene is not included in that database. It is simulated as a user-defined species and the required property database is generated and

used. This information and its comparison with other available species in the FLACS database are provided in Appendix B.

The variation cases for this task are listed in Table 4.4. Apart from the jet leak and pool fire, both the available soot models were tried for both the fuels. For toluene an addition case is performed with a constant conversion factor of 0.38, this information is obtained from the paper published by Kent [20] and provided in Appendix A.

Table 4.4: Model parameters for heptane and toluene pool fire case

Case tag	Fuel	Leak model	Soot Model	Averaged Results Case tag
100000	Heptane	Jet leak	FOX	900000
100010	Heptane	Jet leak	CFM (0.12)	900010
100100	Toluene	Jet leak	FOX	900100
100110	Toluene	Jet leak	CFM (0.12)	900110
100111	Toluene	Jet leak	CFM (0.38)	900111
101000	Heptane	Pool fire	FOX	901000
101010	Heptane	Pool fire	CFM (0.12)	901010
101100	Toluene	Pool fire	FOX	-
101110	Toluene	Pool fire	CFM (0.12)	-

4.3.2 Sensitivity analysis for the variations

The variations performed in this case are not related directly to the simulation parameters. Optimum simulation parameters are selected from experience with earlier evaluations discussed in chapter 4.1 and 4.2. As the main objective of this thesis both the soot models available in FLACS are applied.

In addition to that jet fire and pool, model are also varied. The pool and jet fire case for heptane as a fuel provides for a good comparison opportunity, which is discussed in the next section. The pool model assumes that the initial mass of heptane available in the pan is around 6.4 kg, this is calculated based on the pan used by Klassen et al. [26]. It was 30 cm internal diameter, with a depth of 15.2 cm, made of stainless steel with a thickness of 1.6 mm. The density of heptane was calculated at the specified temperature of 384 K using the methods provided in Perry's Handbook [27].

Unfortunately, the cases simulated for toluene using a pool fire model could not be completed successfully by the time of documenting this analysis. A probable cause for this may be that toluene as fuel was added as a user-specified species in the simulation. However, the simulation of toluene as a fuel with a jet fire scenario is completed and results are presented in the next section.

For toluene, various values of soot yield are reported in the literature and discussed by Kent [20], suggesting that maximum soot yield predictions are sensitive to flame diameter and size. And best predictions are obtained in similar conditions. An additional case for toluene jet fire using CFM with a different soot yield factor of 38% is added for comparison with 12% yield.

4.3.3 Results and discussion

The predicted time-averaged temperature and soot volume fraction are presented in Figure 4.20 for heptane pool fire. The temperature prediction using all the four scenarios where pool and jet fire case is modelled using CFM and FOX soot model is very close to the experimental values provided by Chen et al.

Looking closely it reveals that the values of average temperature from the experiment at 0.26 m (H/D = 0.9) start with a higher value (around 1300K) towards the centre of the pan at 0 m (radial centre). At higher elevation, the peak temperature remains the same until it reaches the 1.02 m, where it drops around 800 K. This behaviour is replicated by the temperature curves predicted by jet fire scenarios. Whereas the temperature curves predicted by the pool fire model start low (around 700 K) and slowly increase in temperature reaching peak values at the 1.02 m.

It should be noted from experimental data that as we go away from the centre of the pan radially the temperature drops and this drop is reduced with increasing elevation. This is clear by comparing the temperature values from the experiment at 0.26 m and at 1.2 m, where it is comparatively flat. And this behaviour is very well reproduced by the temperature curves generated using Jet fire and to some lesser extent by values produced by pool fire.

In terms of the soot model, the values of temperature predicted by CFM is lower than the values predicted by their FOX counterparts from the jet as well as pool fire scenarios. This is probably controlled by the amount of soot produced, and heat loss in the form of soot radiation.

While comparing the values of soot volume fraction from experiments, it is observed that its trend along the height and in the radial direction is similar to the experimental values of temperature. However, the prediction of soot volume fraction using different soot models is not as close as the prediction of temperature values.

Similar to earlier evaluations from chapter 4.1 and 4.2, the soot volume fraction values predicted by CFM values are lower but much closer to the experimental values i.e. in the same order of magnitude than the values predicted by FOX model. The FOX model predicted peak soot volume fraction values are very low and with a difference of 1-2 in terms of the order of magnitude.

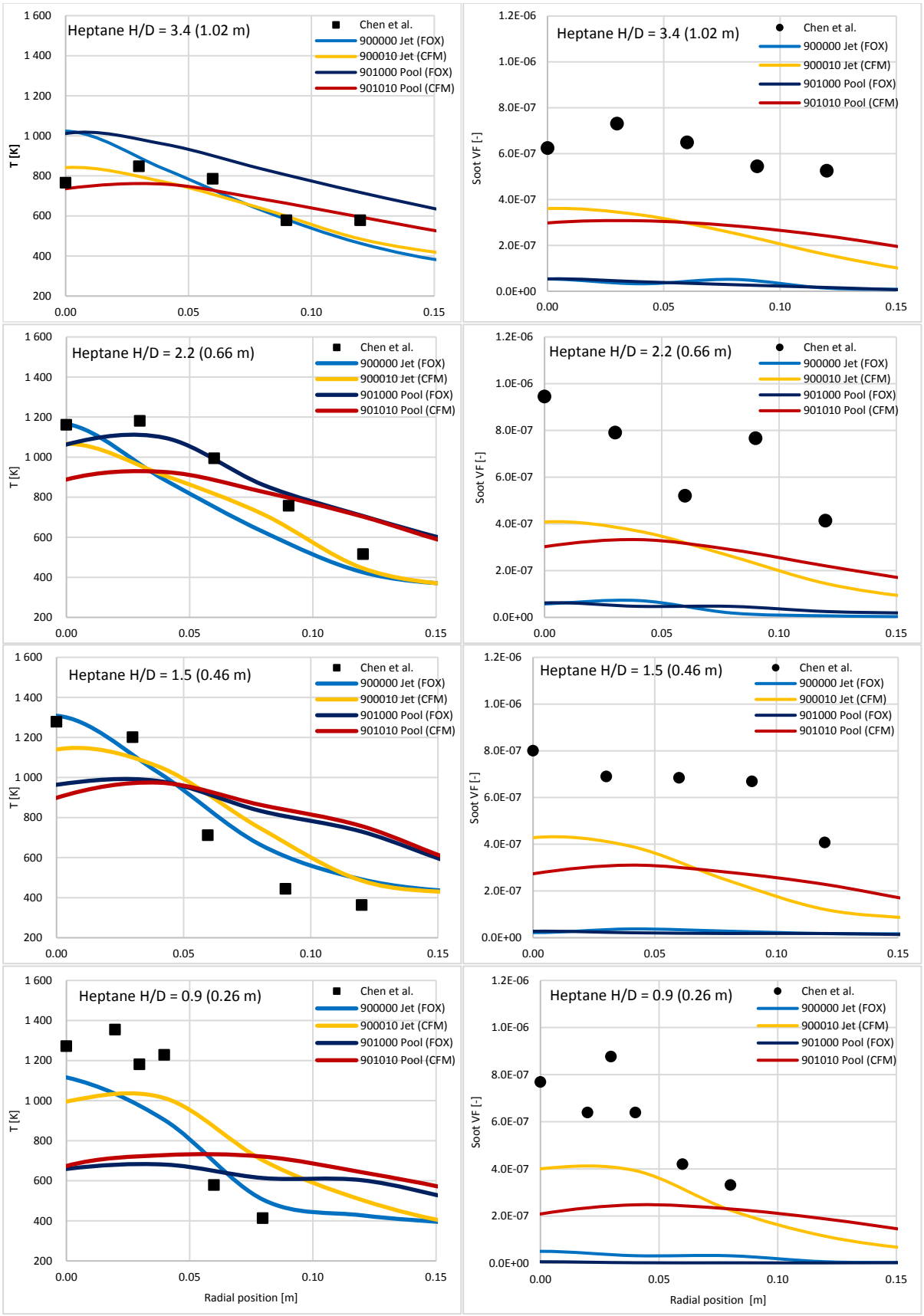

Figure 4.20: Comparison of temperature and soot volume fraction for heptane fire at different heights

In the case of toluene, shown in Figure 4.21, the trend for experimental values of temperature is quite similar to the same for heptane. The values of average temperature from the experiment at 0.22 m (H/D = 0.8) start with a higher value (close to 1190 K) towards the centre of the pan at 0 m (radial centre). But with an increase in elevation the peak temperature drops a little until it reaches the 1.02 m, where it drops below 500 K.

Again, this behaviour is replicated by the temperature curves predicted by jet fire scenarios, but this time it does not drop as rapidly as the experiment values. In that, the FOX model starts and ends with higher predicted temperature when compared with those resulted using CFM. In the case of CFM, the values predicted with higher soot yield factor (0.38) being higher than with the lower yield factor (0.12). This confirms the conclusion from earlier sections and with heptane fuel, suggesting that the temperature of the gas field is inversely proportional to the amount of soot formed.

Reasonable agreement is achieved between the predicted and measured soot volume fraction across the elevation, except at 0.22 m, using the CFM soot model with 0.38 as yield factor. At 0.22 m the predicted soot volume fraction did not follow the trend of experiment values being parallel to the experiment temperature values. However, reasonable predictions at elevations around 1 to 1.3 m by CFM highlights the importance of selecting yield correct factor for the tested fuel.

As found earlier, the predictions of soot volume fraction from the FOX model are very low compared to experimental data and CFM.

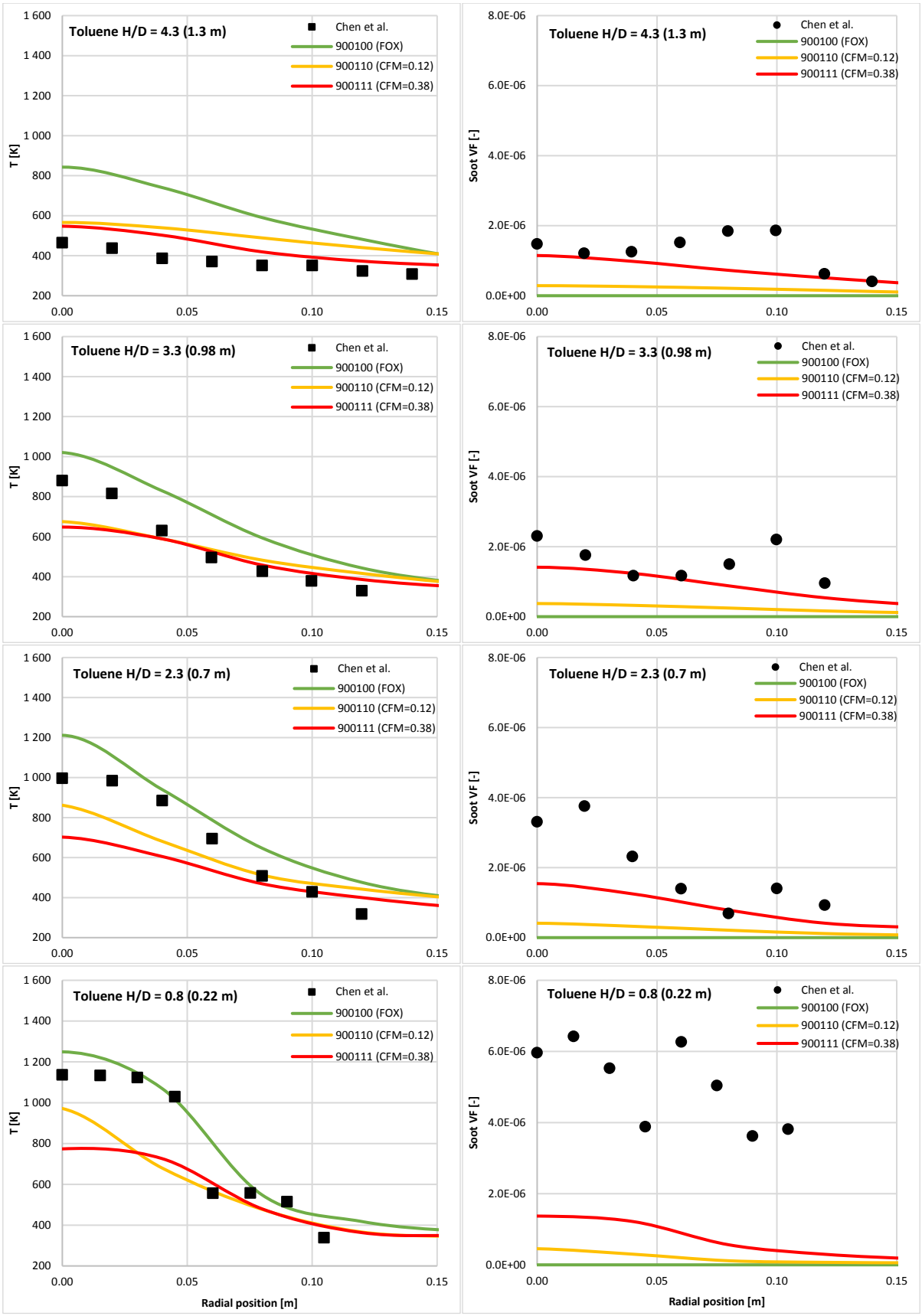

Figure 4.21: Comparison of temperature and soot volume fraction for toluene fire at different heights

4.4 Under-ventilated compartment fire

Full-scale compartment fire experiments were carried out by Lock et al. [7] in 2008. It was an experimental study of the effects of fuel type, fuel distribution, and vent size on full-scale under-ventilated compartment fires in an ISO 9705 room for NIST. The experiment results were also used to validate filed models, such as NIST Fire Dynamic Simulator (FDS). A wide range of fuel type was included in these experiments but for this study, the fuel is limited to heptane, as heptane is a well-understood fuel in fire-related studies. It produces a moderate level of soot and has a heat of combustion similar to gasoline. The full-scale enclosure (FSE) where the experiments were carried out is defined in ISO 9705 as a full- scale room for a test of surface products. Multiple sizes of burners were used and the ventilation was varied by modifying the door opening.

The full-scale enclosure illustrated in Figure 4.22, has standard internal dimensions of 2.4 m x 3.6 m x 2.4 m with a doorway of 80 cm x 200 cm. Only the width of the door was varied to reduce the ventilation area. The experiments included local measurements of temperature, heat flux and species composition, and global measurements of heat release rate and mass burning rate. Soot samples were extracted from within the enclosure and measured gravimetrically[l]. Optical soot measurements[m] were also performed.

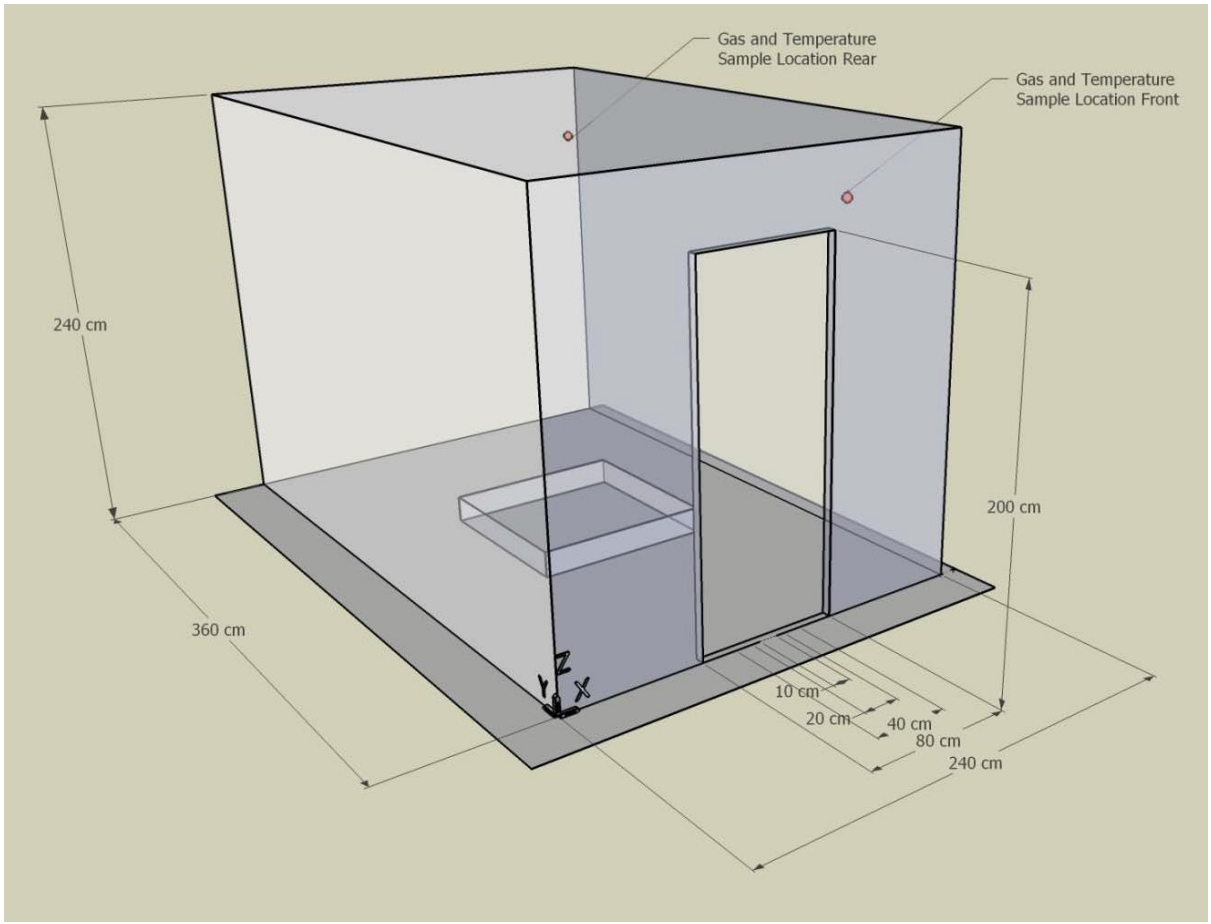

Figure 4.22: Internal dimensions of ISO 9705 enclosure for the test with a single burner (Lock et al. [7])

For validation purposes only fires with heptane as fuel is considered. The full-scale enclosure is modelled to be of same size and coordinates as shown in Figure 4.25. Two primary types of square burners were constructed with welded steel of size 0.5 m x 0.5 m with area 0.25 m^2 and 0.71 m x 0.71 m with an approximate area of 0.5 m^2 and with a 10 cm lip, were considered for the validation case. The burner is positioned in the geometrical centre of the room floor (position 1). In cases where 2 burners were used the second burner were placed along the centreline of the room next to the rear wall (position 2) as shown in Figure 4.23.

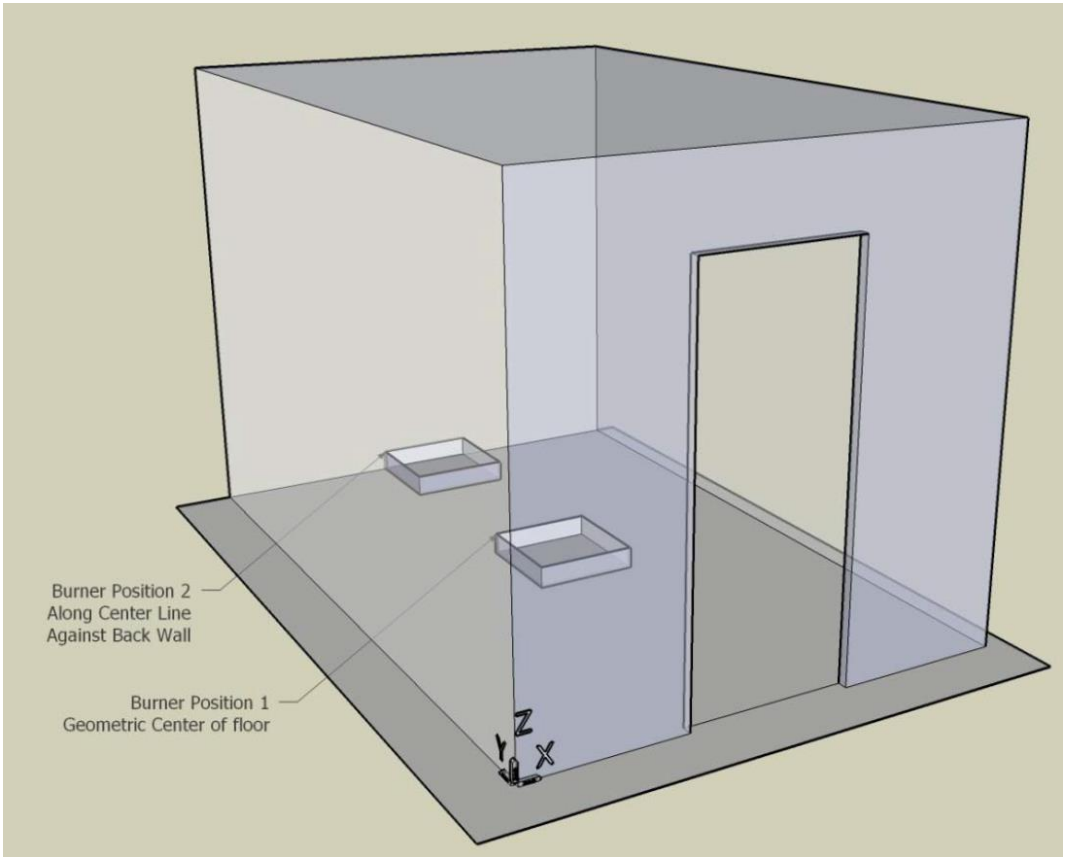

Figure 4.23: Positions of the pan burners (Lock et al. [7])

4.4.1 Computational details

There were thirty-two different experiments carried out by Lock et al. in their report, out of these experiments three unique conditions were considered for this study. Heptane fire with 10 kg fuel in a single burner, 20 kg fuel in a single burner and 20 kg fuel distributed in two identical burners. The details of the cases considered and model parameters are listed in Table 4.5. Only, 20 cm doorway ($1/4^{th}$ of the ISO 9705 standard) is used for the selected experiments.

For the simulation model, the location of the burner pans is kept identical as described earlier and shown in Figure 4.23. The computational domain is limited to 2.4 m x 5.4 m x 2.4 m with a uniform grid size of 0.1 m. The extra 2 m, in the negative Y direction, is included to study the flashover. The dynamic (PM3) pool model is applied, with an outer radius of 0.35 m for larger pans with area 0.5 m^2 and 0.25 m for a smaller pan with area 0.25 m^2. The ground temperature is kept at 283 K, and no solar radiation is assumed. The ground type is assumed

to be plate and thickness is considered to be 1 cm as described in the experiments. The simulation time is set to 30 seconds with ignition starting at 2 seconds. A number of rays for radiation were fixed to 300 for all cases fire switch value 2 is used as the scenario is pool fire.

Table 4.5: Model parameters for NIST compartment fire case

Case tag	Referred Test case ID § [7]	Total Fuel mass [kg]	Number of burners	Burner area [m^2]	Soot Model
000000	8	10	1	0.5	No soot model
100000	8	10	1	0.5	FOX
100010	8	10	1	0.5	CFM (0.12)
000001	9 (19)	20	1	0.5	No soot model
100000	9 (19)	20	1	0.5	FOX
100010	9 (19)	20	1	0.5	CFM (0.12)
000000	D12 (D13)	10 x 2	2	0.25	No soot model
100000	D12 (D13)	10 x 2	2	0.25	FOX
100010	D12 (D13)	10 x 2	2	0.25	CFM (0.12)

§ All the test case ID are prefixed with ISOHept- in the report [7]. The test cases in the bracket are different tests with the same initial conditions, so experiment results might differ.

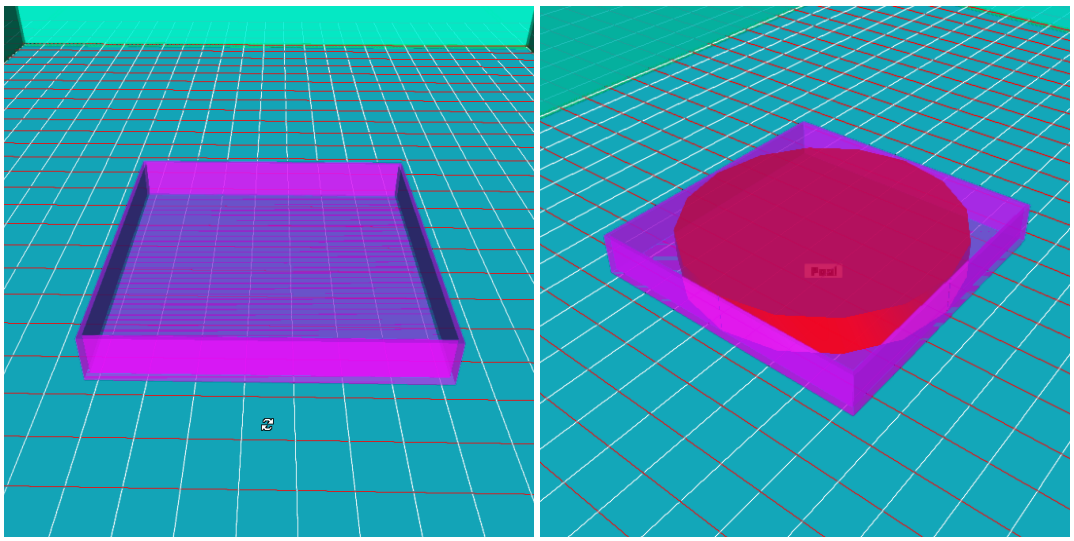

Figure 4.24: Single square burner with pool setup for NIST compartment fire case

In the case of placing 2 burners, a narrow trench between the two burners was assumed as indicated in Figure 4.26. This assumption had to be made as it was not possible to specify two different dynamic pool models at different locations. So the two burners were connected by a narrow trench and the dynamic pool was located in the burner at the geometrical centre of the room (position A) as shown in Figure 4.23.

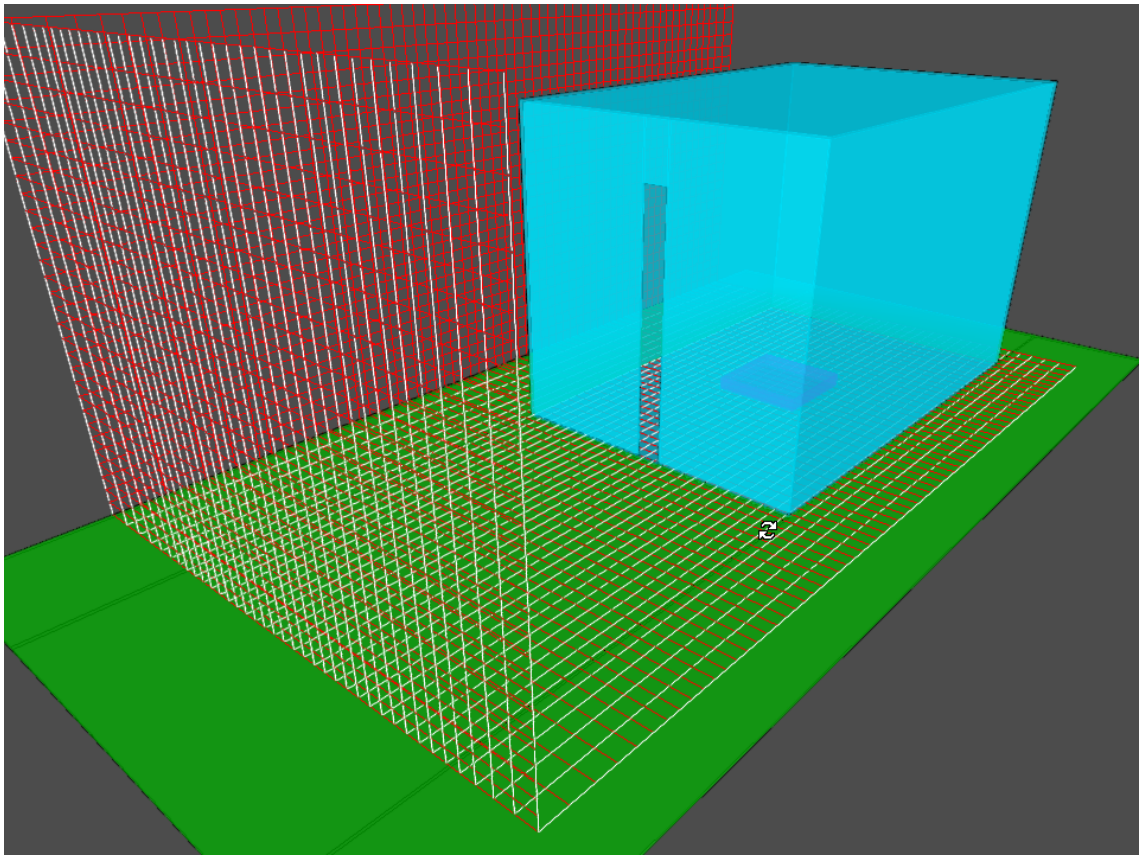

Figure 4.25: Calculation domain and grid distribution for NIST compartment fire case

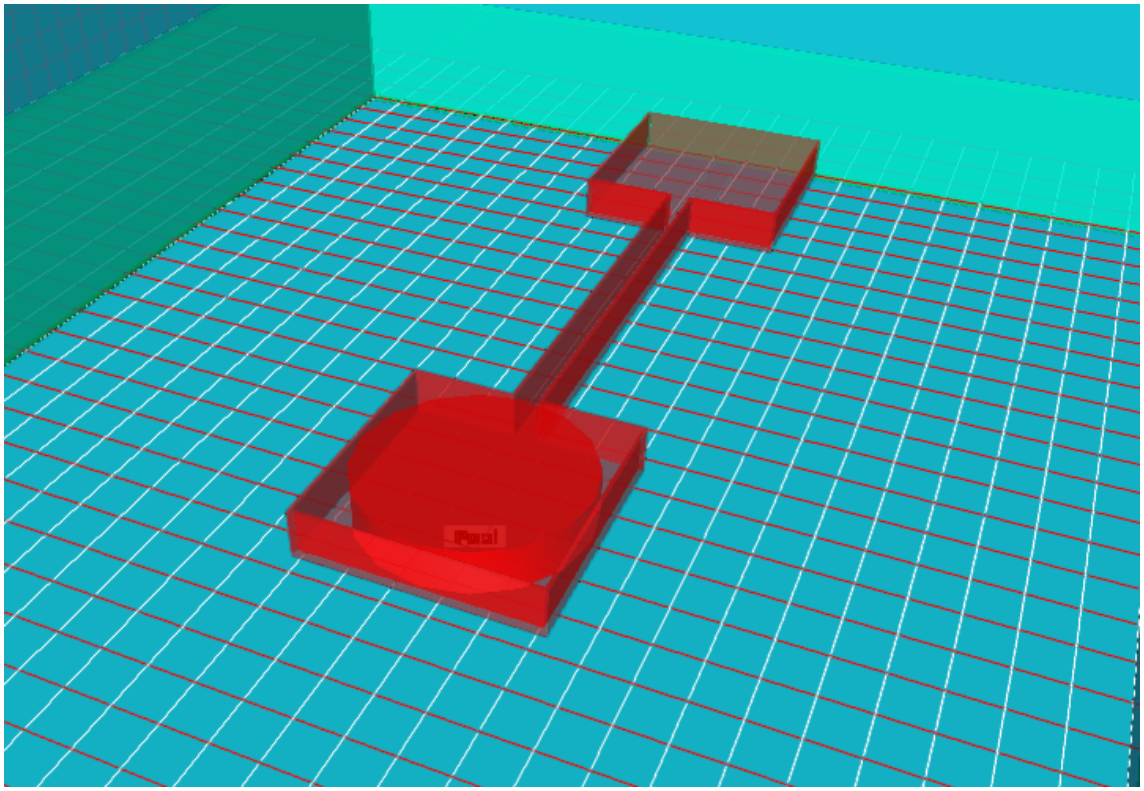

Figure 4.26: Two square burner with pool setup for NIST compartment fire case

4.4.2 Sensitivity analysis for the variations

The only variations performed for the three different tests is in term of soot models. All the other simulations parameters are kept identical so that comparison between results from the same tests using different soot model and among the tests themselves by varying fuel quantity can be made. These results are compared and discussed in the next section. Results from another simulation code, FDS are also compared.

4.4.3 Results and discussion

The test carried out by Lock et al. at NIST uses the full-scale enclosure for the underventilated compartment fire as per the ISO 9705, as described earlier. The experiments were designed to study the effects of fuel type, fuel distribution, and vent size on under-ventilated compartment fires. Three specific tests which had the same fuel - heptane, same door opening of 20 cm (25% of the original) but the different quantity of fuel and different placement of burner were selected as listed in Table 4.5.

The experimental results for temperature and soot mass fraction were available at noted monitoring point location for all the selected test cases except temperature measurement for test 8. Wherever results from identical test runs are available, they are used for the comparison, for example, D12 and D13. These tests are also used for validation of FDS, so results from these validation test are also compared.

The results from test D12 are presented from Figure 4.28 to Figure 4.32. The experimental data for temperature measurement are available for test D12 with D13 and the comparison to result from FDS is also made. As shown in Figure 4.28, for the front side where the ventilation door is situated and Figure 4.32 for the rear side, the temperature prediction differs from the experimental values. In general, the difference is as high as 200 degrees in some cases. The trend is similar to the temperature increases with elevation. And a consistently high temperature is obtained near the elevation of 0.8-1 m for front and 0.5 m for the rear.

This may be the result of the distinguishing feature of a common compartment fire where the hot layer and cold layer are separated. The hot gases are accumulated in the upper region, fresh air from the outside enters the from the ventilation doorway to supply the fresh oxygen for a fire at a lower level. Hot upper gas layers are composed of strongly participating media such as carbon dioxide, water vapour, and soot particles [8]. The height of this thermal interface between the hot and cold layer is usually the characterising dimension of compartment fires. As the volume of hot gases exceeds the volume of the enclosure, the hot gases spill off into the surroundings. These two counter flows create a rapid change of velocity at the doorway, see Figure 4.27.

As the flame gets larger, it will no longer be able to entrain sufficient oxygen, and products of incomplete combustion such as carbon monoxide and soot will be produced, increasing the radiative component of heat transfer. Due to the dominance of hot layer, the oxygen in the enclosure can drop below the certain level where a large amount of fuel in gas phase goes unburnt, this hot unburnt fuel spills off through the doorway and comes in contact with the

oxygen-rich outside air. This results in rapid combustion outside the enclosure, this is known as flashover. The key to fire safety design is to adopt practical preventive measures of not allowing the fire to grow to flashover, which can inflict severe damage to the building structure and the contents within [10].

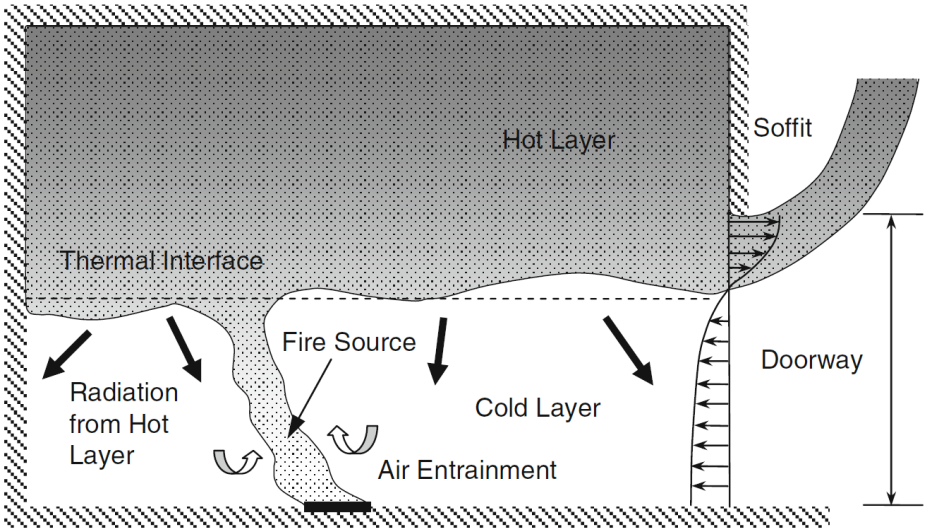

Figure 4.27: Schematic representation of a fire source in a single-compartment enclosure from Yeoh et al. [10]

The temperature predicted here might indicate the onset of flashover condition, this can be seen in Figure 4.31.

The temperature predicted by FDS, on the other hand, is much higher than the experiments. For FLACS, the temperature prediction using CFM is higher than that predicted by the FOX model. The influence of cold incoming gas layer can be seen for the prediction of temperature in the front area.

The comparison of soot mass fraction is done on a log scale. The predictions using CFM are within the same power of magnitude as the results from test D12 front and rear. The trend of soot mass fraction along the elevation is consistent with the temperature. The peak value is attained at an elevation around 0.6 m and almost consistent up to the ceiling height of 2.4 m. One probable reason for this consistency might be the absence of fresh oxygen to reduce the fuel or soot particles.

The soot prediction from FDS is even lower than the predictions using the FOX model. While comparing to the FDS it should be noted that for combustion in FDS by default, 2/3rd of the carbon in the fuel is converted to *CO* in the first combustion step and the remaining 1/3rd is converted to soot [21]. Also, note that the visualisation of the soot from FDS may potentially exaggerate the extent of the smoke compared to actual experiments as no scale information is available to compare the threshold values.

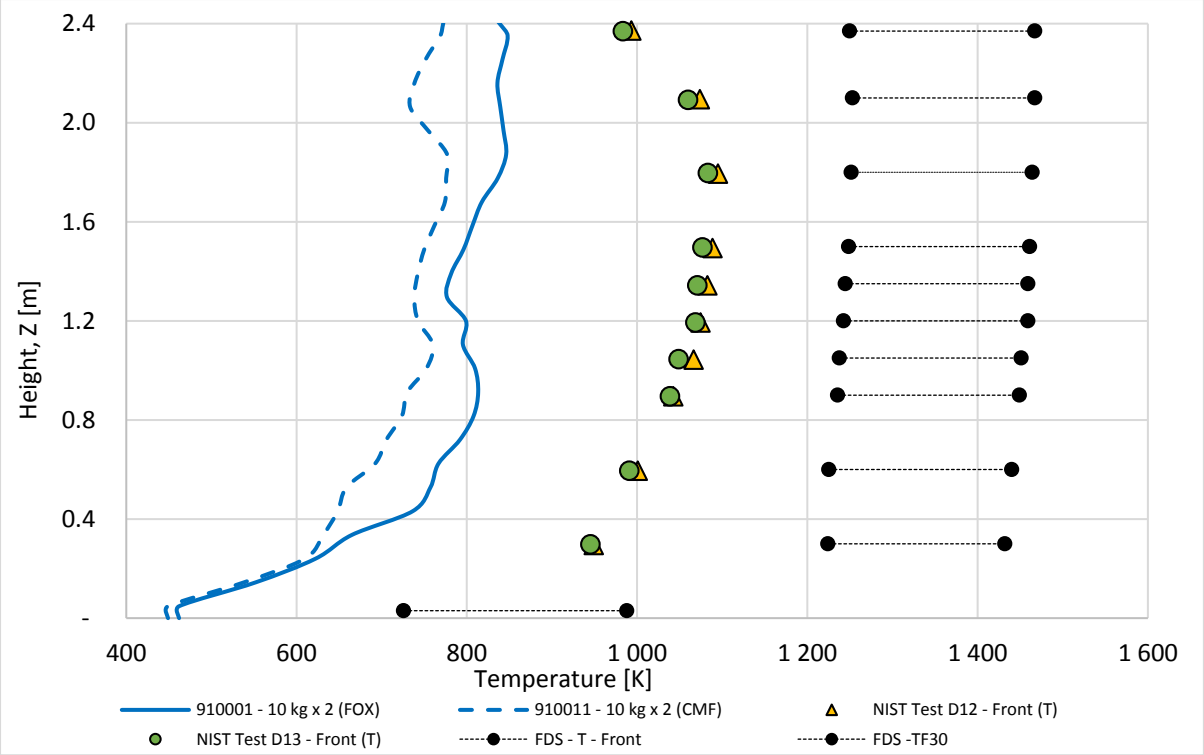

Figure 4.28: Comparison of temperature at front for Test D12, FLACS FOX and CMF model with experimental values (D12 and D13) and results from FDS

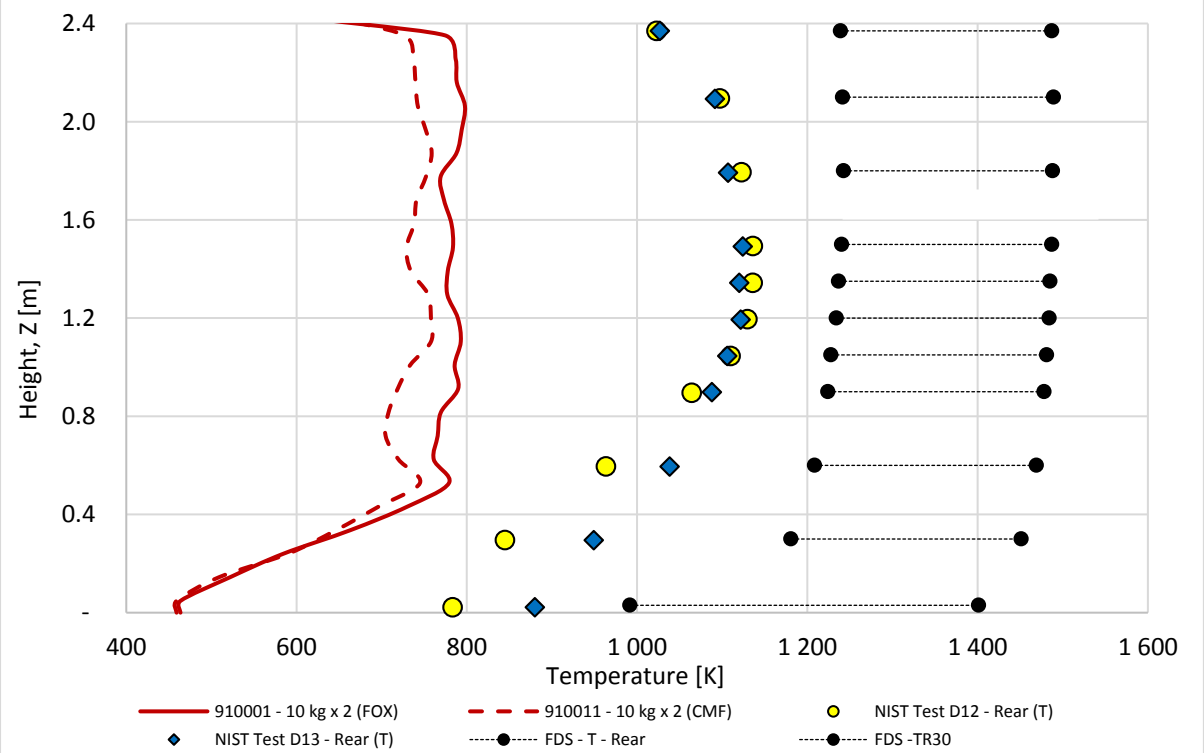

Figure 4.29: Comparison of temperature at rear for Test D12, FLACS FOX and CMF model with experimental values (D12 and D13) and results from FDS

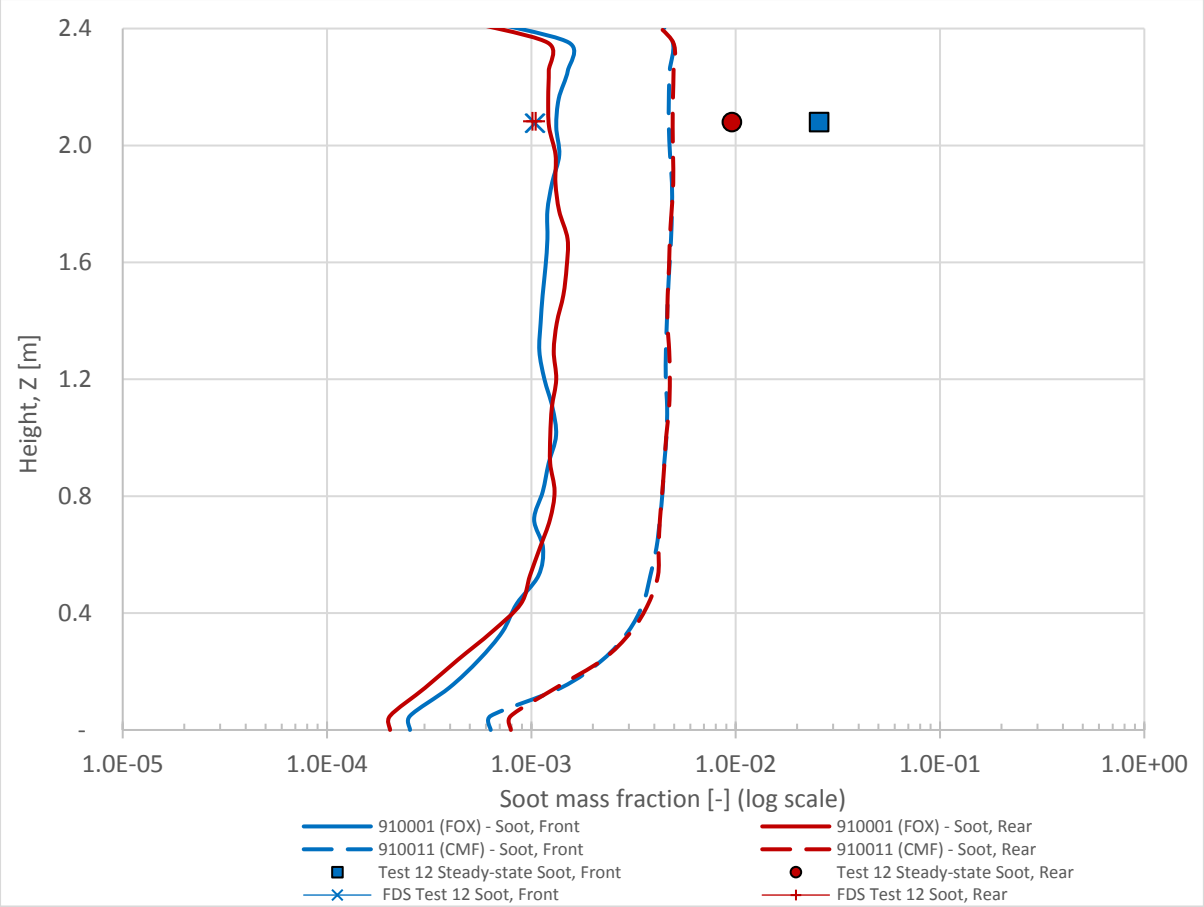

Figure 4.30: Comparison of soot mass fraction front and rear for Test D12, FLACS FOX and CMF model with experimental results and results from FDS

The effect of choosing different soot model options FLACS is seen in Figure 4.31. With no soot model, very high temperatures in combustion are seen as there is no soot present to radiate the combustion heat and reduce the temperature inside the enclosure. With the selection of FOX model and CFM, the soot generation is increases and the overall temperatures are seen decreasing.

The bottom of the temperature field figure shows that colder region compared to the rest of the enclosure. The amount of volume fraction of soot in that region is also low, clearly noticeable in the soot field figure for CFM case, probably because the soot formation temperature is not reached. The figure also demonstrates the occurrence of flashover, which also occurred during the experiments as confirmed by Lock et al [7].

FDS also predicts similar outcomes as shown in Figure 4.32. Note that the scale information for soot field plot is not available.

The results from test 9, are presented from Figure 4.33 to Figure 4.37. And the results from test 8, are presented from Figure 4.38 to Figure 4.42.

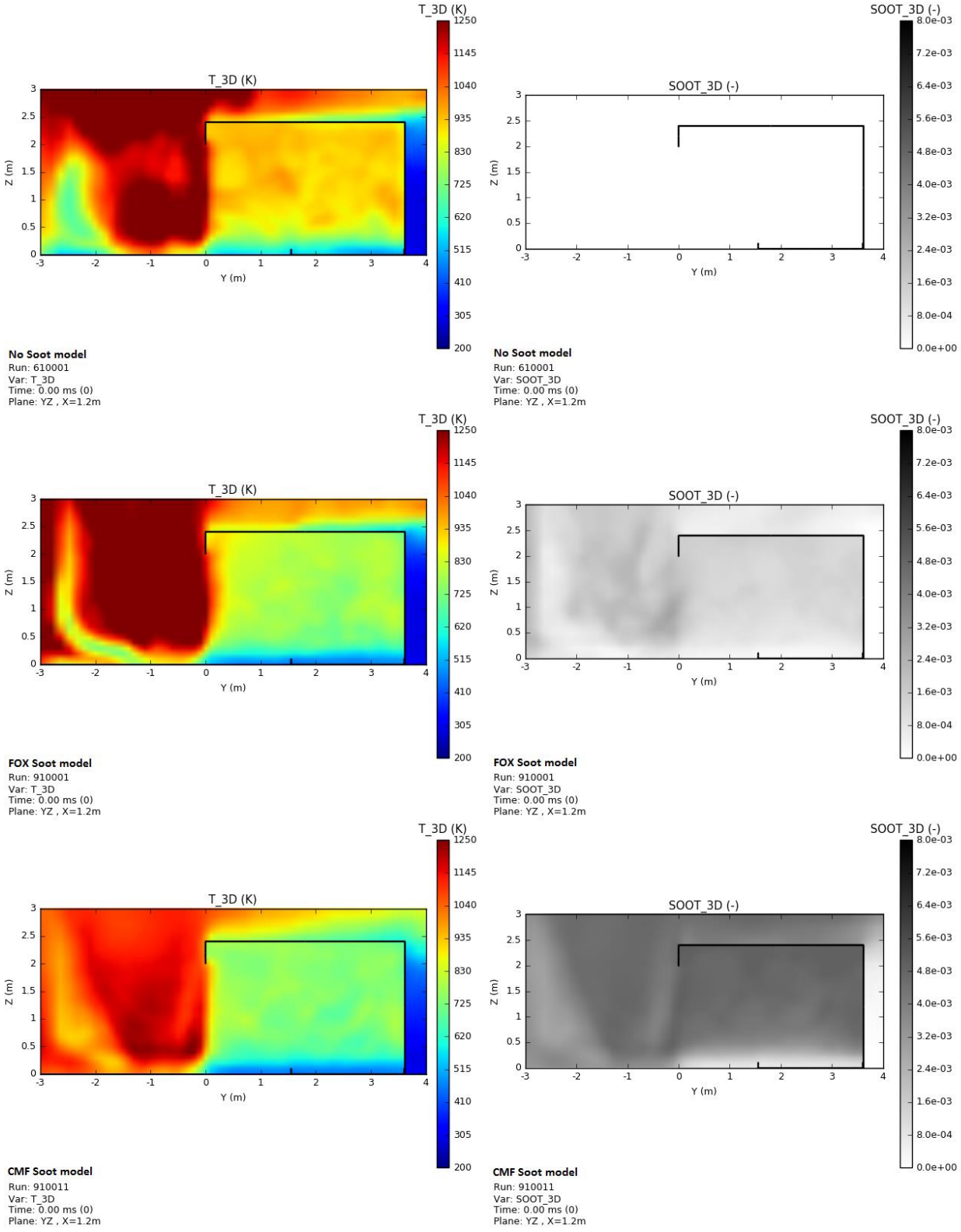

Figure 4.31: Time-averaged temperature and soot mass fraction contours predicted by FLACS, Test D12 (10 kg fuel x 2)

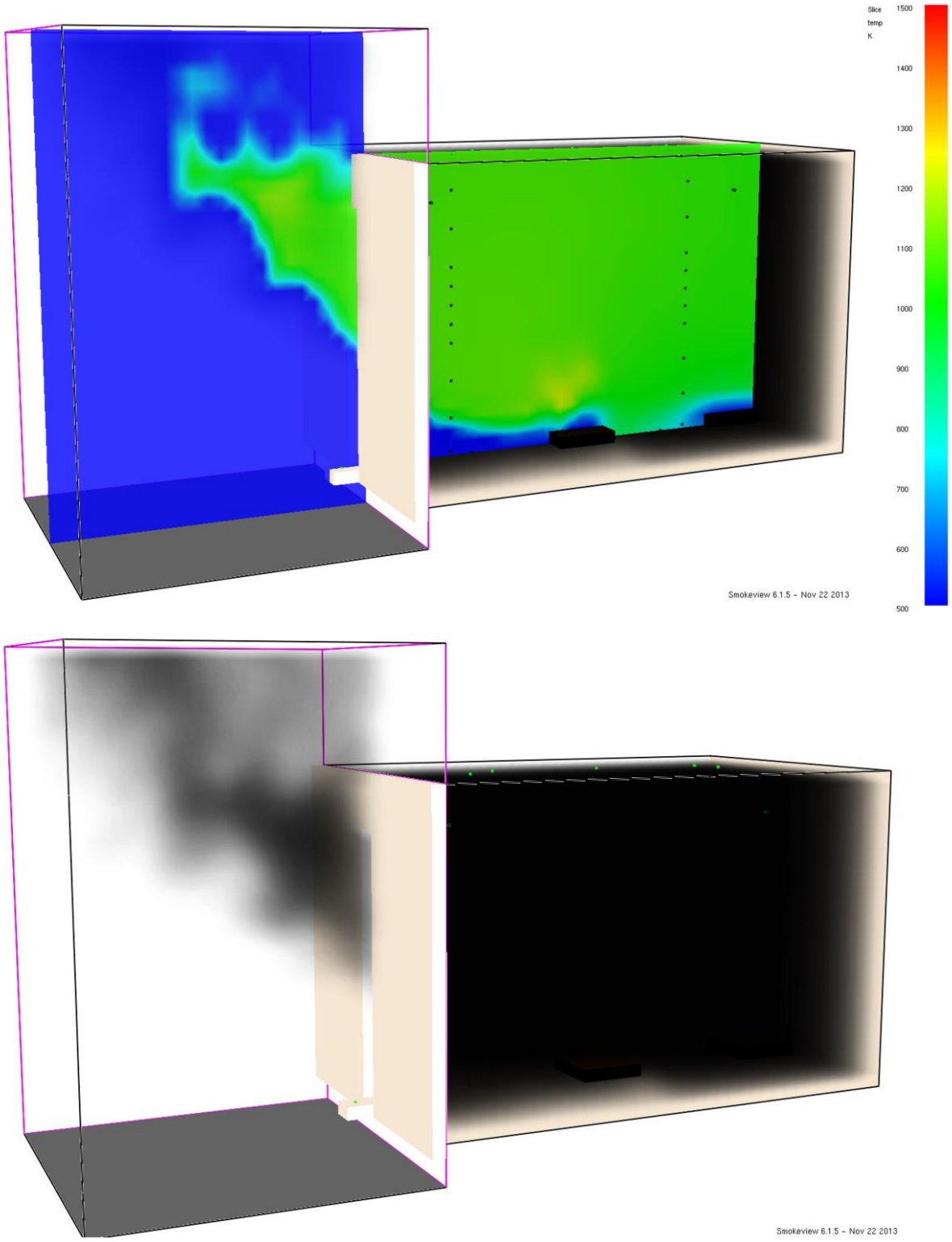

Figure 4.32: Temperature and soot mass fraction contours predicted by FDS, Test D12 (10 kg fuel x 2) at 250 s

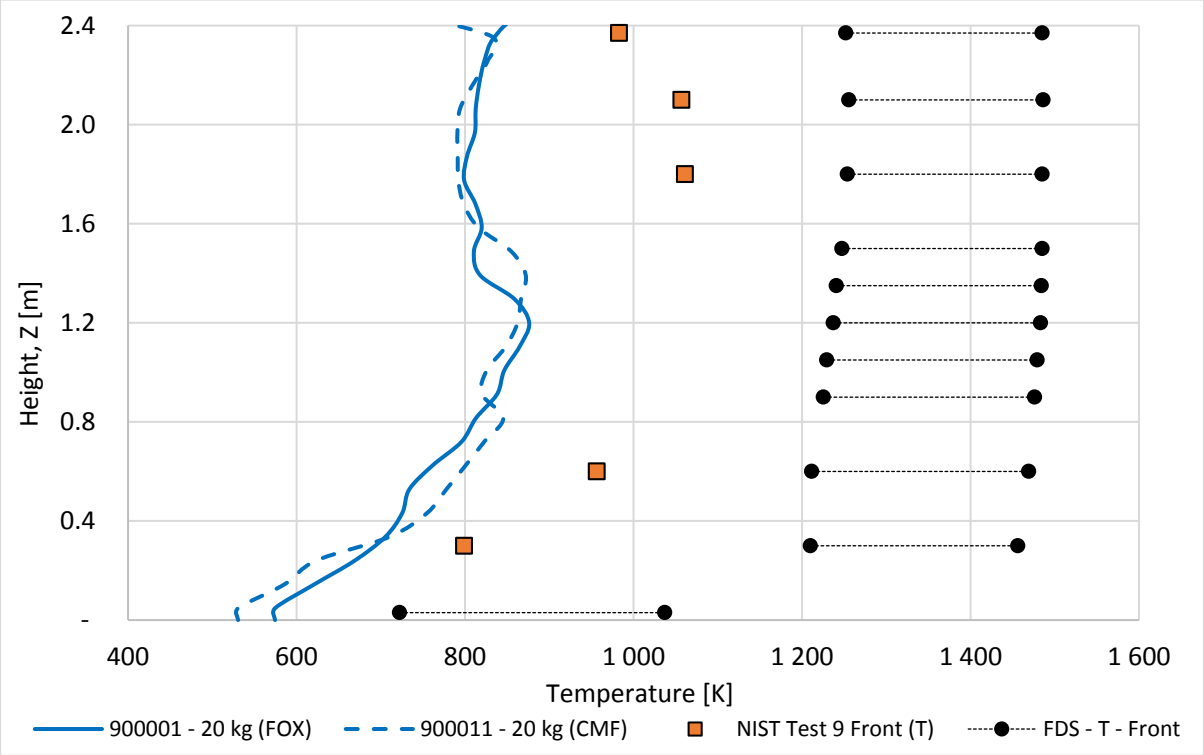

Figure 4.33: Comparison of temperature at front for Test 9, FLACS FOX and CMF model with experimental values and results from FDS

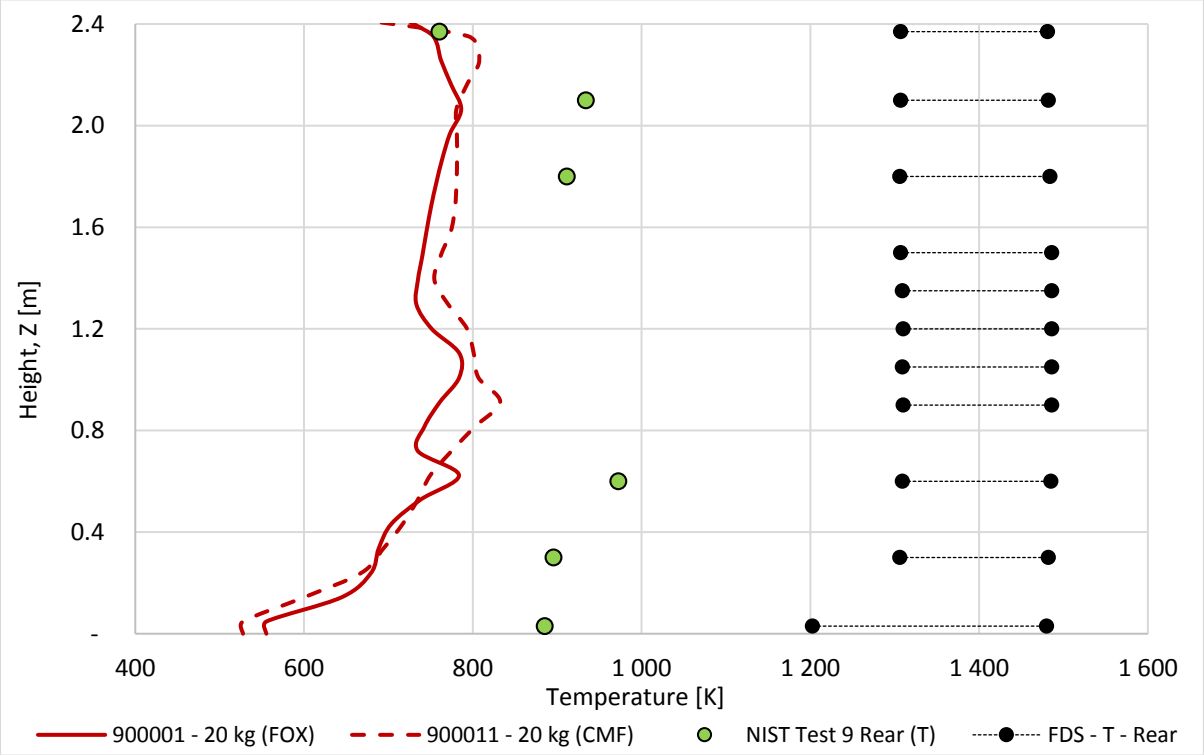

Figure 4.34: Comparison of temperature at rear for Test 9, FLACS FOX and CMF model with experimental values and results from FDS

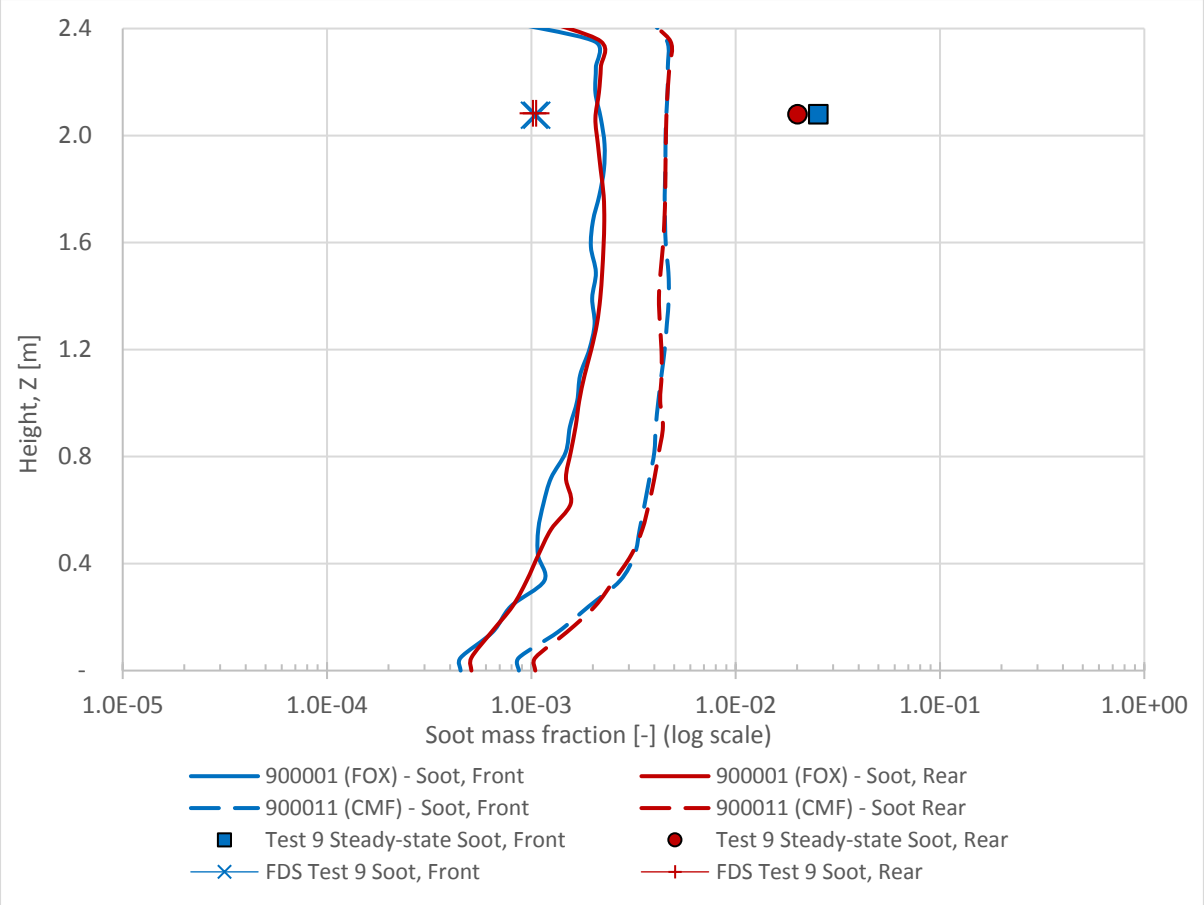

Figure 4.35: Comparison of soot mass fraction front and rear for Test 9, FLACS FOX and CMF model with experimental results and results from FDS

For test 9, the comparison outcomes for temperature and soot mass fraction are similar to the comparison outcomes for test D12. The temperature increases with the elevation for both front and rear location and the peak values are reached around 1.2 m for front and 0.6 m for the rear. The value of temperature predicted by FLACS is lower compared to experiments and values predicted by FDS are much higher than experiments.

The soot mass fraction prediction is also consistent with results from test D12. A consistent value is achieved at an elevation of 0.8 m and the predicted values are lesser than experiments but higher than those predicted by FDS.

The effect of higher soot concentration is evident from the temperature field diagram in Figure 4.36. The temperature plot for no soot model has considerably higher values when compared to FOX model or CFM.

The results from FDS in Figure 4.37 are also similar to the FOX soot model results from Figure 4.36, however, the impact of flashover is much clear in FLACS results. A probable reason for this may be that the FDS result is the screen-capture of transient result at 250 seconds which is roughly the midpoint of 500 seconds quasi-steady state simulation duration.

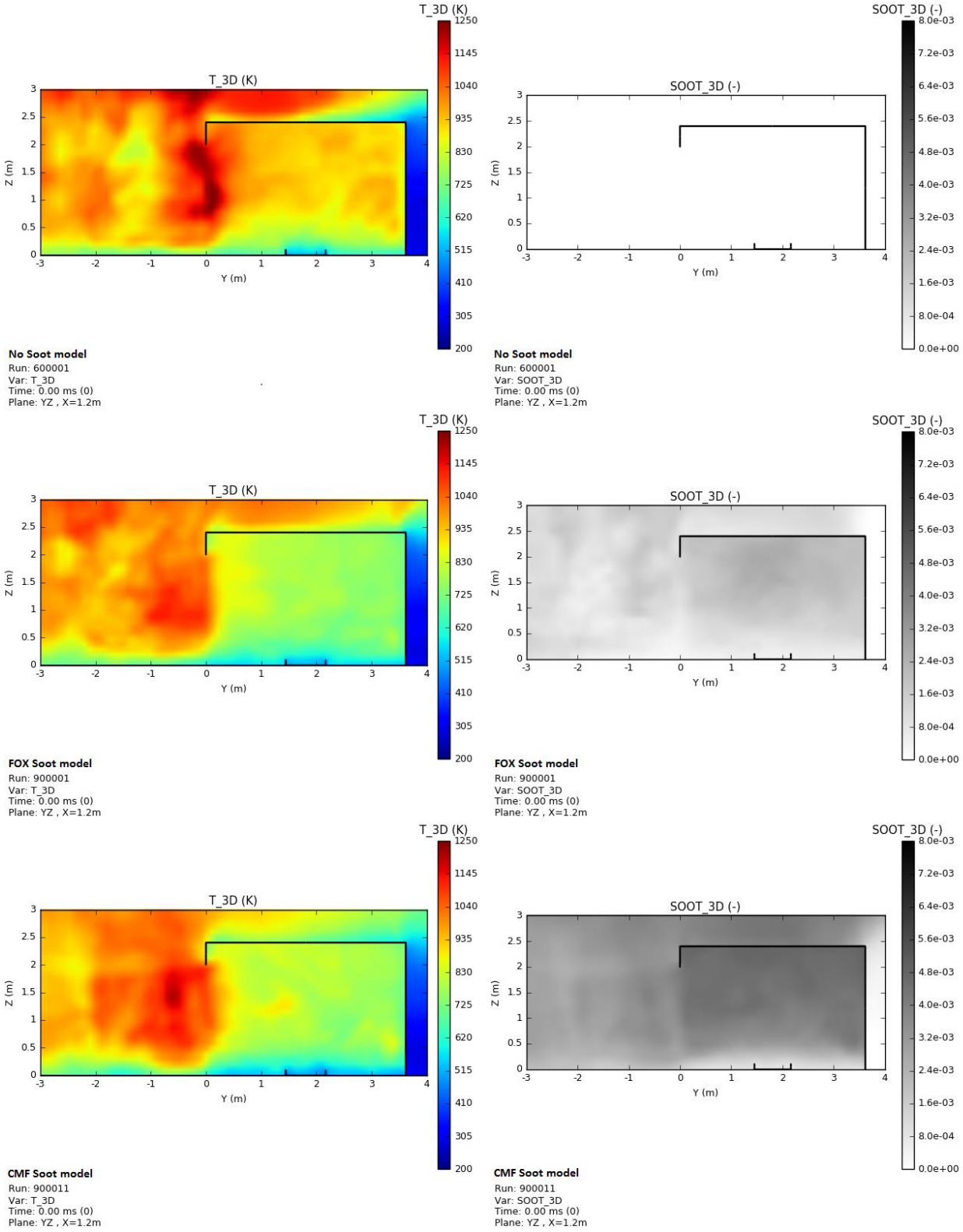

Figure 4.36: Time-averaged temperature and soot mass fraction contours predicted by FLACS for NIST Test 9 (20 kg fuel)

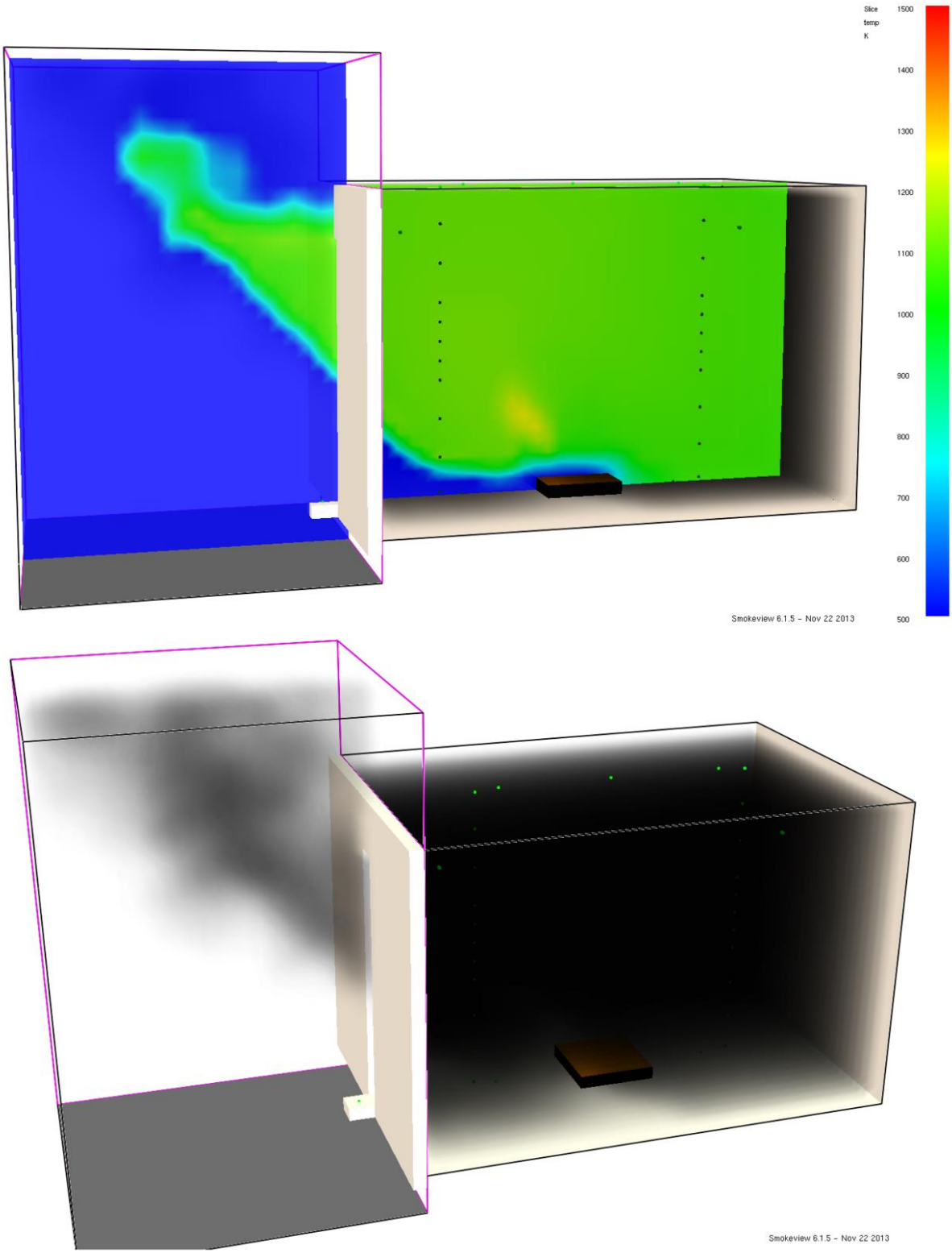

Figure 4.37: Temperature and Soot mass fraction contours predicted by FDS for NIST Test 9 (20 kg fuel) at 250s

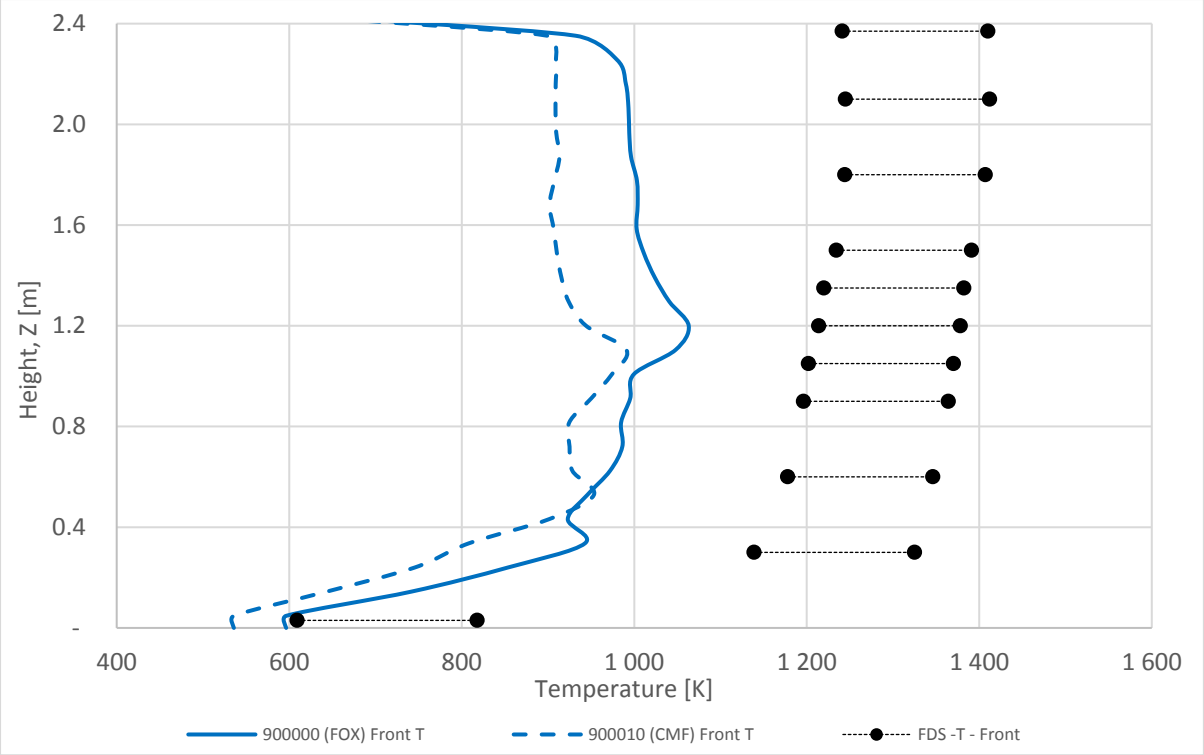

Figure 4.38: Comparison of temperature at front for Test 8, FLACS FOX and CMF model with results from FDS (No experimental results available for Temperature)

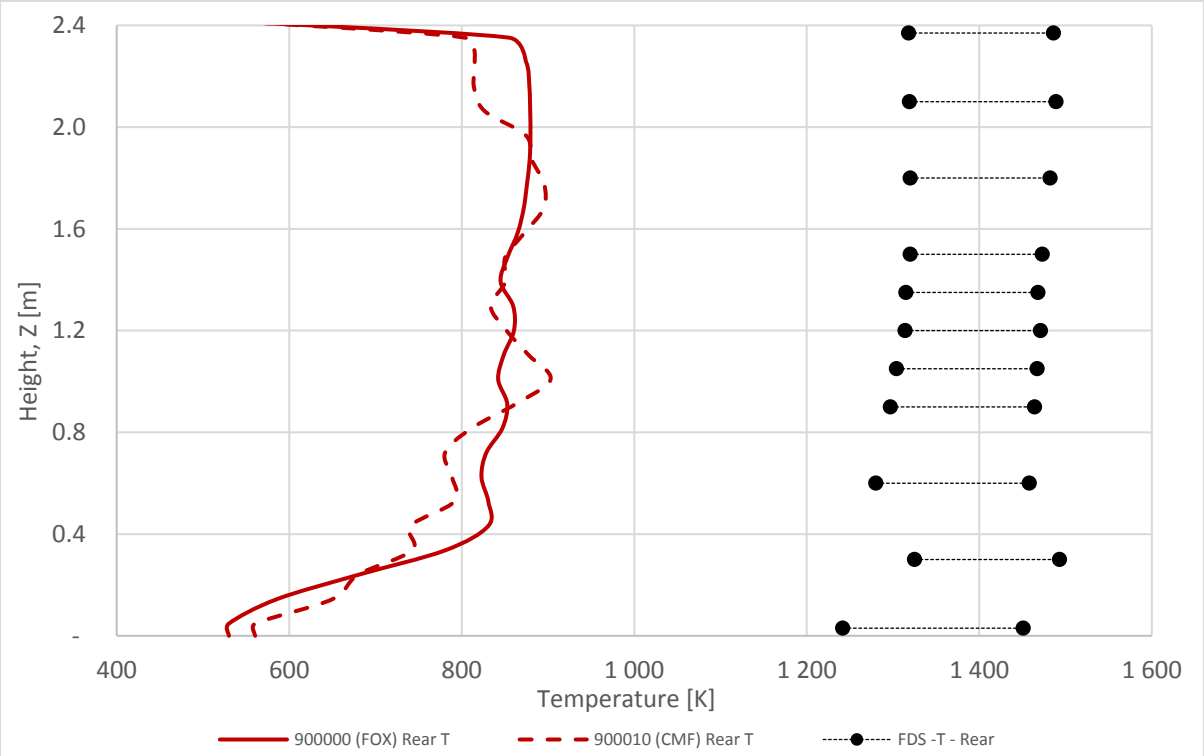

Figure 4.39: Comparison of temperature at rear for Test 8, FLACS FOX and CMF model with results from FDS (No experimental results available for Temperature)

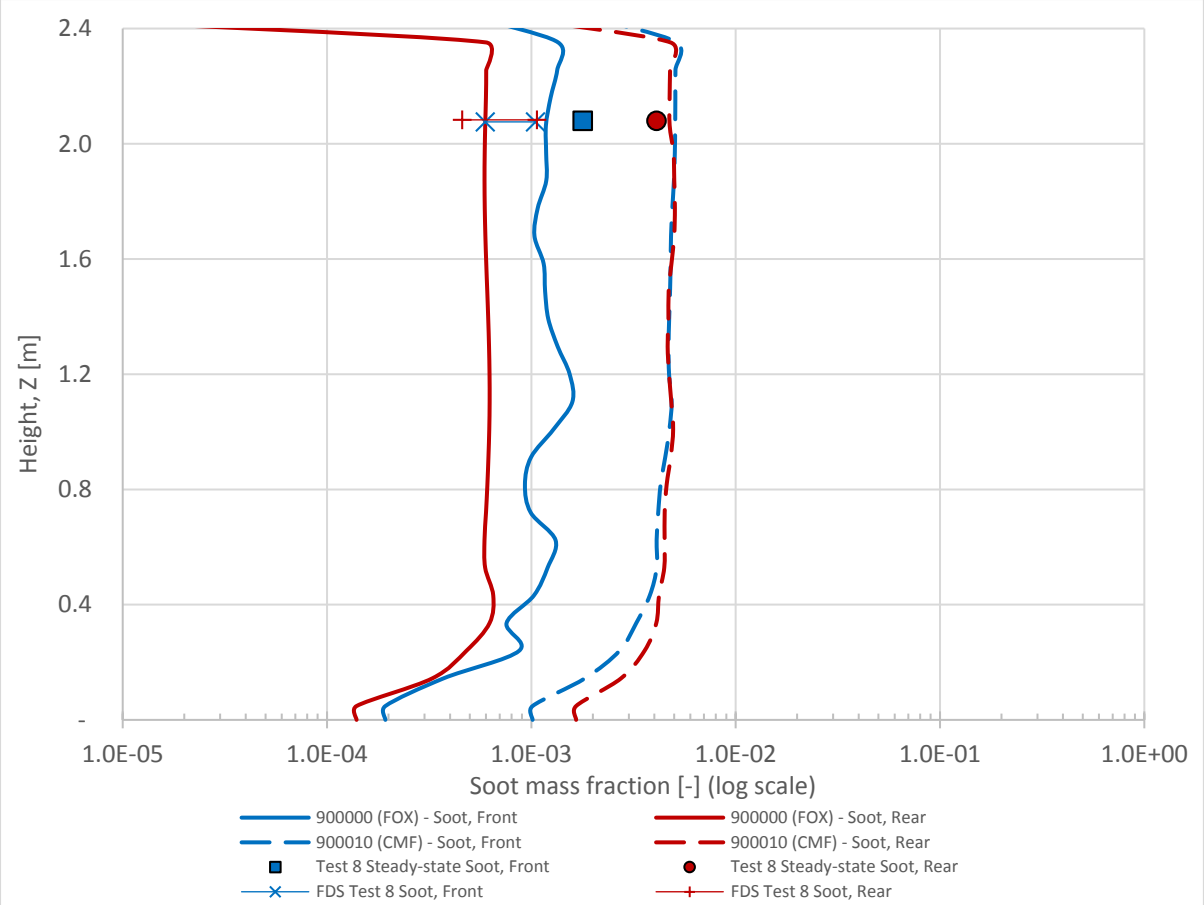

Figure 4.40: Comparison of soot mass fraction at front and rear for Test 8, FLACS FOX and CMF model with results from FDS (No experimental results available)

Though the experimental data for temperature measurement are not available for test 8, the comparison to FDS is made. As shown in the, Figure 4.38 for the front side where the ventilation door is situated and Figure 4.39 for the rear side, the temperature prediction differs from that predicted by FDS. In general, the difference is as high as 400 degrees in some cases. The trend is similar to the temperature increases with elevation. And a consistently high temperature is obtained near the elevation of 1 m for front and 0.4 m for the rear. This may be the result of the distinguishing feature of a common compartment fire where the hot layer and cold layer are separated, as described earlier with Figure 4.27.

The soot mass fraction prediction is different than the results from test 9 and test D12. A consistent value is achieved at an elevation of 0.6 m and the predicted values by the CFM are higher than experiments but those predicted by FDS and FOX model are still lower than the experiments.

Figure 4.41 shows that the flashover is about to happen, and the temperatures inside the enclosure for FOX and CFM is much higher than the same for test 9 and test D12.

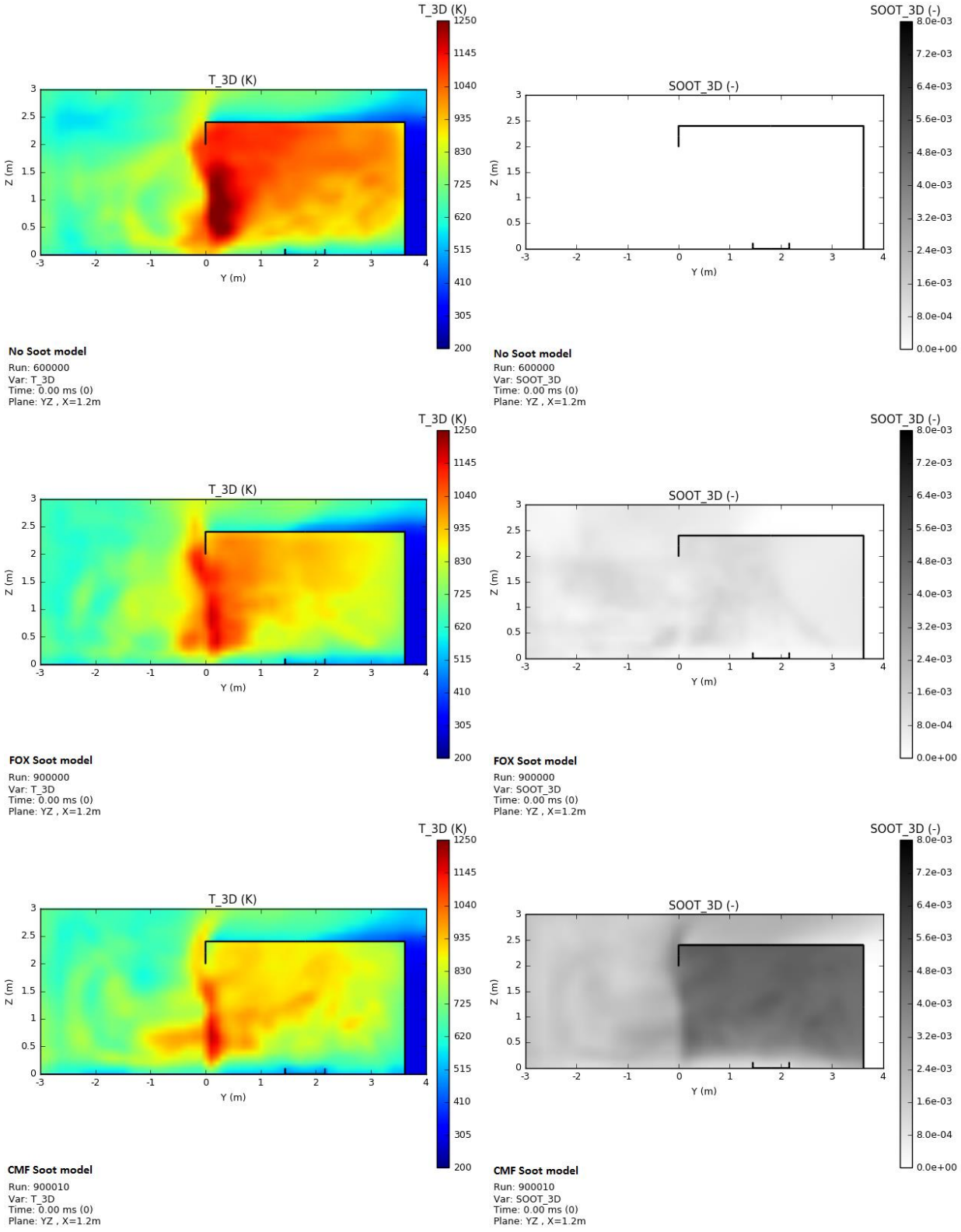

Figure 4.41: Time-averaged temperature and soot mass fraction contours predicted by FLACS for NIST Test 8 (10 kg fuel)

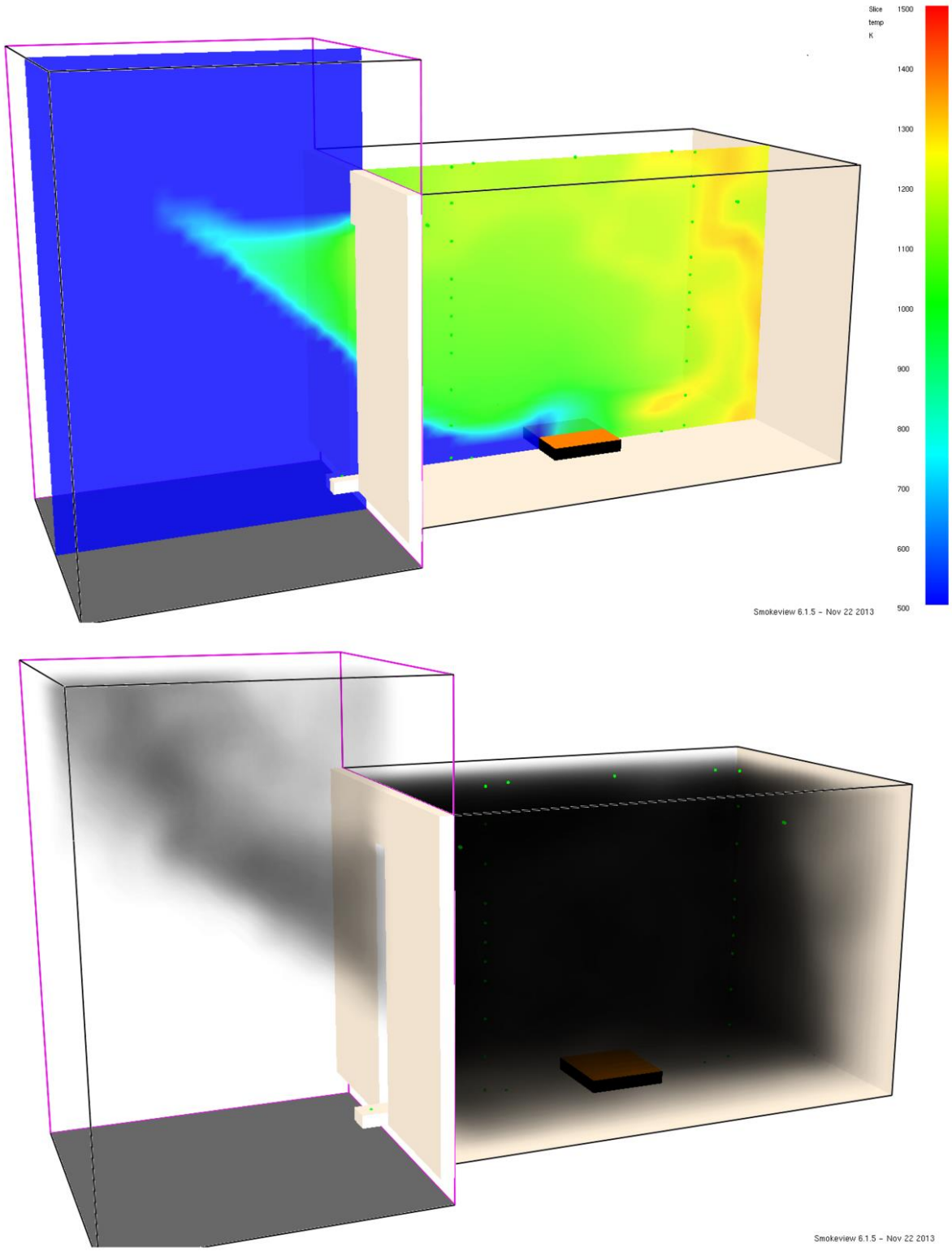

Figure 4.42: Temperature and Soot mass fraction contours predicted by FDS for NIST Test 8 (10 kg fuel) at 250s

Overall, we can compare Figure 4.31, Figure 4.36 and Figure 4.41 to gauge the effect of different quantity of initial fuel and number of burners. Test 8 had 10 kg of heptane in single burner whereas test 9 had 20 kg of heptane in the single burner (0.5 m^2) and test D12 20 kg of heptane distributed in two burners (0.25 m^2 each).

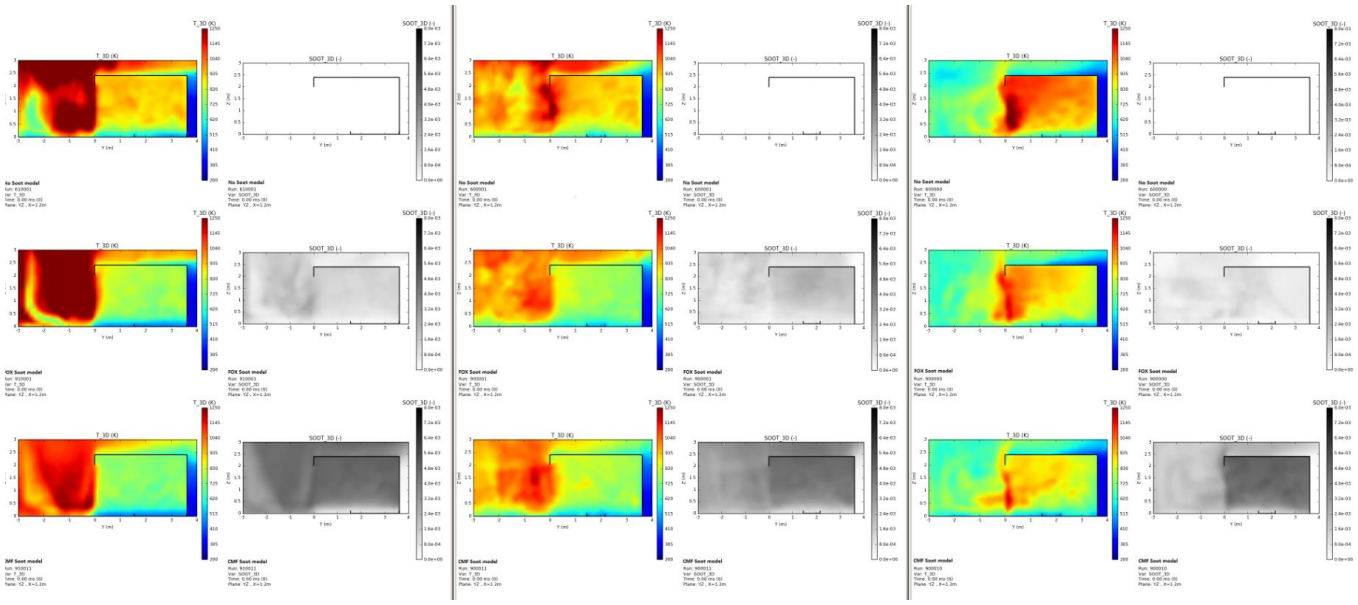

(a) Test D12, Fuel 10 kg x 2 (Figure 4.31) (b) Test 9, Fuel 20 kg (Figure 4.36) (C) Test 8, Fuel 10 kg (Figure 4.41)

Figure 4.43: Comparing the field map of temperature and soot volume fraction for all three NIST tests

A quick comparison is shown in Figure 4.43, going from left to right i.e. from a higher amount of fuel onwards some general conclusions can be made.

The higher amount of fuel generates a higher amount of soot and consequently contributes to lower temperature by radiating the energy. For test D12 and 9, despite having the same amount of fuel (total 20 kg) and same pan area (total 0.5 m^2) the amount soot generated is higher for test D12. This is possibly due to parallel combustion of fuel in two pans, hinting that in soot model soot formation is the rate controlling step and dependence on burning velocity.

Going for no soot model will probably predict very high values of temperatures, which may lead to over-design while designing a for flashover or under-design while evaluating the loss of visibility due to the presence of soot. Every fire results in some amount of soot formation which should not be ignored.

Overall soot prediction by FOX model is always lesser than that predicted by the CFM and often few powers of magnitude lesser or not comparable to the experimental values. The CFM predicts better results which are comparable to experimental values.

In the NIST report Lock, et al. [7] reported that the maximum soot fractions reach to 7% for the heptane and the toluene fires. There is a general agreement that toluene (C_7H_8, 38% soot yield) is a high soot-generating fuel when compared to heptane (C_7H_{16}, 12% soot yield) [20]. Based on that relationship if we assume that the maximum soot fraction for heptane was between 2-4%, the maximum soot mass fraction predicted by CFM was around 0.5%.

5 Conclusion

The objective of the present work has been the validation of soot model in FLACS Fire CFD code. Several fire scenarios of different scale were used to validate the available soot models. Overall the predictions of soot fractions and temperature achieved by using the Conversion factor model (CFM) were in reasonable agreement with the experimental observations. However, the estimates of soot fractions using Formation-Oxidation (FOX) model were very low when compared with the experiments.

Simulations done without soot model showed the importance of selecting a soot model as the temperature results were strongly overpredicted. Prediction of soot fractions is important for the accuracy of radiation-related predictions.

In summary, the important findings from the validation of the soot model for FLACS fire are as below:

- The CFM is a better alternative for predicting soot than FOX model when the fuel is generally known to produce at least some amount soot.
- However, CFM is governed by a single soot yield factor, which is a user input to the CFD code, which makes it independent of modelling parameters and a potential source of error.
- The amount of soot predicted by FOX model, which is time and temperature dependent, limited by the maximum yield factor used in CFM and independent of user input, needs to be improved so that it can accurately predict soot fractions.
- The temperature predictions using CFM were in better agreement with the experimental values than the predictions of the value using the FOX model.
- The amount of soot generated has a direct impact on radiative power emitted when compared to other combustion products such as CO_2 and H_2O. Higher soot fractions predicted by CFM can result in the radiative power to be 2 to 3 times the same predicted by using the FOX model.
- The prediction of temperature and the heat emission by radiation is directly linked to the amount of soot generated, which is again governed by the choice of the soot model.
- The choice of no soot model can only be justified when the parent fuel is generally known for not producing any soot, for example, hydrogen. But most fires with hydrocarbons results in some amount of soot formation which should not be ignored.
- The results from this validation might be helpful to select an appropriate soot model for a given scenario.

5.1 Further work

For any CFD code, it is important to populate a database with relevant validation cases that cover the entire range of applications. This database helps to organise the knowledge and useful for future development. Further changes and validation of soot model are necessary before it can be used with confidence to predict soot fraction and its contribution to the radiative heat loss. FOX model, which is the default choice for soot prediction in FLACS CFD code, should be capable of predicting the amount of soot comparable to experiments. More efforts should be devoted to improving this model as it is dependent on modelling results and independent of user-input.

Some suggestions for further work are listed below:

- Improvement in model constants for the FOX model is required so that it can be fine-tuned with respect to experimental results.
- CFM is suitable for fuel types for which the soot yield factor is known. This can be advantageous for users who only want to know the maximum soot to be produced in the given fire scenario, as an upper limit.
- Further research is required to elaborate database of soot yield values most commonly used fuel types. The present database is from 1986.
- Validation of the improved FOX model and CFM needs to be done with various experiments ranging from lab-scale to full-scale.
- For future validation, the study of the quantitative contribution of soot particles to radiative heat loss should be included.
- Validation with respect to different fuel types is strongly recommended, especially in order of their soot-generating capability.
- More species of fuel shall be available of by default, especially aromatic hydrocarbons.
- Simplifying the process for adding a user-defined species and including them into the combustion with jet and pool fire calculation will be extremely useful from a user perspective and also while performing validation with different fuels.

References

1. Warnatz, J., *Combustion: physical and chemical fundamentals, modeling and simulation, experiments, pollutant formation*. 4th ed. ed, ed. U. Maas and R.W. Dibble. 2006, Berlin: Springer.
2. *Shining a light on the darkness of soot in air pollution - by the University of Leeds*. https://phys.org/news/2017-02-darkness-soot-air-pollution.html, 2017.
3. Wang, C.J. and J. Wen, *Numerical Study of Heptane Pool Fires on a Hollow Square Pan.* Procedia Engineering, 2018. **211**: p. 689-698.
4. Tessé, L., F. Dupoirieux, and J. Taine, *Monte Carlo modeling of radiative transfer in a turbulent sooty flame.* International Journal of Heat and Mass Transfer, 2004. **47**(3): p. 555-572.
5. Wang, C., et al., *Burning rate of merged pool fire on the hollow square tray.* Journal of Hazardous Materials, 2015. **290**: p. 78-86.
6. Chen, Z., et al., *Extension of the eddy dissipation concept and smoke point soot model to the LES frame for fire simulations.* Fire Safety Journal, 2014. **64**(C): p. 12-26.
7. Lock, A.J., et al., *Experimental Study of the Effects of Fuel Type, Fuel Distribution, and Vent Size on Full-Scale Underventilated Compartment Fires in an ISO 9705 Room (NIST TN 1603)*, in *Technical Note (NIST TN) - 1603*. 2008.
8. Hurley, M.J. and E. Society of Fire Protection, *SFPE Handbook of Fire Protection Engineering*. Fifth edition. ed. 2016: Germany: Springer Verlag.
9. Gexcon, *FLACS v10.8 User Manual*. 2019: Gexcon AS.
10. Yeoh, G.H., *Computational fluid dynamics in fire engineering: theory, modelling and practice*, ed. K.K. Yuen. 2009, Amsterdam: Elsevier.
11. Venkataraman, C., et al., *Size distributions of polycyclic aromatic hydrocarbons in aerosol emissions from biofuel combustion.* Journal of Aerosol Science, 2002. **33**(3): p. 503-518.
12. Kleiveland, R.N., *Modelling of soot formation and oxidation in turbulent diffusion flames*. 2005, Norwegian University of Science and Technology, Department of Energy and Process Engineering: Trondheim.
13. Mehta, R., *Detailed modeling of soot formation and turbulence-radiation interactions in turbulent jet flames*, M.F. Modest and D.C. Haworth, Editors. 2008, ProQuest Dissertations Publishing.
14. Pugmire, R.J., et al., *Soot Formation Process*. 2003, University of Utah, Department of Chemical & Fuels Engineering.
15. Lautenberger, C.W., et al., *A simplified model for soot formation and oxidation in CFD simulation of non-premixed hydrocarbon flames.(Report).* Fire Safety Journal, 2005. **40**(2): p. 141.
16. Kennedy, I.M., *Models of soot formation and oxidation.* Progress in Energy and Combustion Science, 1997. **23**(2): p. 95-132.

17. Khan, I.a.G.G., *A method for calculating the formation and combustion of soot in diesel engines.* Heat Transfer Flame, 1974.
18. Lautenberger, C.W., *CFD simulation of soot formation and flame radiation*, in *Fire Protection Engineering*. 2002, Worcester Polytechnic Institute: Massachusetts.
19. Melheim, J.A., *Soot modelling in FLACS fire*. 2006, Gexcon AS. p. 1-8.
20. Kent, J.H., *A quantitative relationship between soot yield and smoke point measurements.* Combustion and Flame, 1986. **63**(3): p. 349-358.
21. McGrattan, K., et al., *Special Publication (NIST SP) - 1018 Fire Dynamics Simulator, Technical Reference Guide*, in *Special Publication (NIST SP) - 1018*. 2013, NIST.
22. Skarsbø, L.R., *An Experimental Study of Pool Fires and Validation of Different CFD Fire Models*. 2011, The University of Bergen.
23. Pedersen, N., *Modeling of jet and pool fires and validation of the fire model in the CFD code FLACS*. 2012, The University of Bergen.
24. Muthusamy, D. and K.v. Wingerden, *Numerical Simulation of Vapour Cloud Fires using FLACS-Fire*. GexCon AS: Bergen, Norway.
25. Muthusamy, D. and B. Lilleberg, *Validation of FLACS-Fire for Jet Fires under Ventilation-Controlled Conditions* GexCon AS: Bergen, Norway.
26. Klassen, M. and J.P. Gore, *Structure and radiation properties of pool fires*. 1994, Center for Fire Research of the Building and Fire Research Laboratory of the National Institutes of Standards and Technology.
27. Perry, R.H. and D.W. Green, *Perry's chemical engineers' handbook*. 8th ed. ed. 2008, New York: McGraw-Hill.
28. Meng, Z., K. Liang, and J. Fang, *Laminar burning velocities of iso-octane, toluene, 1-hexene, ethanol and their quaternary blends at elevated temperatures and pressures.* Fuel, 2019. **237**: p. 630-636.
29. Wang, G., et al., *Investigation on laminar burning velocities of benzene, toluene and ethylbenzene up to 20 atm.* Combustion and Flame, 2017. **184**: p. 312-323.
30. Sileghem, L., et al., *Laminar burning velocity of gasoline and the gasoline surrogate components iso-octane, n-heptane and toluene.* FUEL, 2013. **112**(C).

Appendix

Appendix A Soot yield values

Table A.1: Maximum soot volume fraction and maximum soot yield [9, 20]

Fuel		Maximum Soot Volume Fraction (x 10^6)	Maximum Soot Yield* (%)
Methane	CH_4	-	0.7
Ethane	C_2H_6	-	2
Acetylene	C_2H_2	15.3	23
Ethylene	C_2H_4	5.9	12
Propylene	C_3H_6	10	16
Propane	C_3H_8	3.7	9
Butane	C_4H_{10}	4.2	10
Pentane	C_5H_{12}	-	10
Cyclohexane	C_6H_{12}	7.8	19
Hexane	C_6H_{14}	-	10
n-Heptane	C_7H_{16}	4.6	12
Cyclooctane	C_6H_{16}	10.1	20
Octane	C_8H_{18}	-	12
Iso-octane	C_8H_{18}	9.9	27
Nonane	C_9H_{20}	-	12
Decalin	$C_{10}H_{18}$	15.4	31
Decane	$C_{10}H_{22}$	-	12
Dodecane	$C_{12}H_{26}$	-	12
Hendecane	$C_{11}H_{24}$	-	12
4-Methylcyclohexene	C_7H_{12}	13.3	22
1-Octene	C_8H_{16}	9.2	25
1-Decene	$C_{10}H_{20}$	9.9	27
1-Hexadecene	$C_{16}H_{32}$	9.2	22
1-Heptyne	C_7H_{12}	14.7	30
1-Decyne	$C_{10}H_{18}$	14.7	30
Toluene	C_7H_8	19.1	38
Styrene	C_8H_8	17.9	40
o-Xylene	C_8H_{10}	20	37
1-Phenyl-1-propyne	C_9H_8	24.8	42
Indene	C_9H_8	20.5	33
n-Butylbenzene	$C_{10}H_{14}$	14.5	29
1-Methylnaphthalene	$C_{11}H_{10}$	22.1	41

* soot yield = soot mass / fuel carbon mass

Appendix B Properties of the fuel

Fuels not defined in FLACS can be defined manually. And a number of parameters need to be defined depending on the type of scenario. For example for modelling dispersion the requires parameters are limited, but for modelling combustion parameters related to laminar burning velocity are required to be defined as indicated in FLACS user manual [9].

For defining user defined species, following laminar burning velocity, which is SL [m/s], related parameters are necessary to be defined:

SLR [-] SL dependency on flame radius

SLP [-] SL dependency on pressure:

$$SL_{\text{after}} = SL_{\text{before}} \times (P/P_0)^{\text{SLP}}$$

SLA [-] SL dependency on initial temperature T_0:

$$SL_{\text{after}} = SL_{\text{before}} \times \left(\frac{T_0}{298.15\text{K}}\right)^{\text{SLA}}$$

SLB [-]: SL dependency on initial pressure P_0:

$$SL_{\text{after}} = SL_{\text{before}} \times \left(\frac{P_0}{10^5\text{Pa}}\right)^{\text{SLB}}$$

A quick comparison of laminar burning velocity related parameters for various fuel compounds is presented in Figure A.1.

Here SL_{after} is the modified value of the laminar burning velocity (SL) after the dependency is taken into account. More details on defining other properties and on this subject can be found in FLACS user manual [9]

The required properties for toluene are predicted with the help from papers by Meng et al. [28], Wnag et al [29] and Sileghem et al. [30]

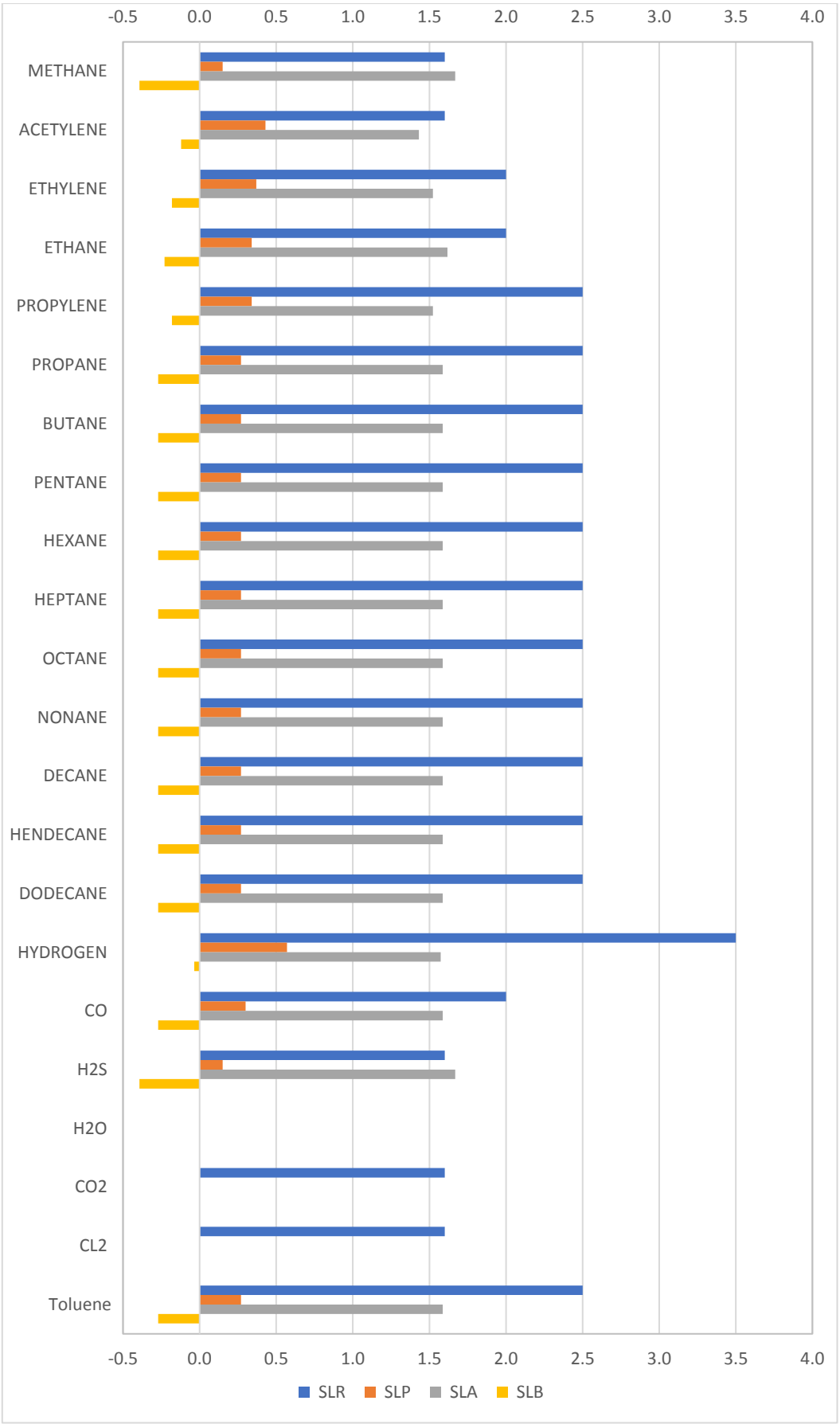

Figure A.1: Parameters related to laminar burning velocity (SL)

Appendix C FLACS – CFD Model

The Computational Fluid Dynamics (CFD) tool FLACS has been developed by Chr. Michelsen Institute (CMI), Christian Michelsen Research (CMR) and currently GexCon since 1980, primarily aimed at stimulating the dispersion of flammable gas in process areas, and subsequent explosions of gas-air mixtures. FLACS solves the compressible conservation equations for mass, momentum, enthalpy, and mass fraction of species on a 3-D Cartesian grid using a finite volume method. Hjertager (1985, 1986) describes the basic equations used in the FLACS model, and Hjertager, Bjørkhaug & Fuhre (1988a, b) present the results of explosion experiments to develop and validate FLACS initially. During the course of more than 25 years of development and evaluation of the FLACS software, the numerical methods have been steadily modified and revised.

The inherent capability of FLACS has been performing explosion and dispersion calculations to help in the improvement of oil and gas platform safety with initial focus on the North Sea. Significant experimental validation activity has contributed to the wide acceptance of FLACS as a reliable tool for prediction of natural gas explosions in real process areas offshore and onshore (Hansen, Storvik & van Wingerden, 1999). FLACS is also used as an accident investigation tool.

FLACS-Fire uses many of the same software components and underlying models that are already used in FLACS for dispersion and gas explosions, these include the pre/post processor, standard k-epsilon RANS model, the distributed porosity concept (Hjertager, 1982) and simple pressure correction scheme. To capture the specific physics in fires; additionally, a number of fire specific models have been implemented in FLACS-Fire to model the fire combustion and heat radiation, most notably the Eddy Dissipation Concept (EDC), Discrete Transfer Model (DTM), Weighted Sum of Grey Gas Model (WSGGM) and Oxidation-Formation soot model (FOX).

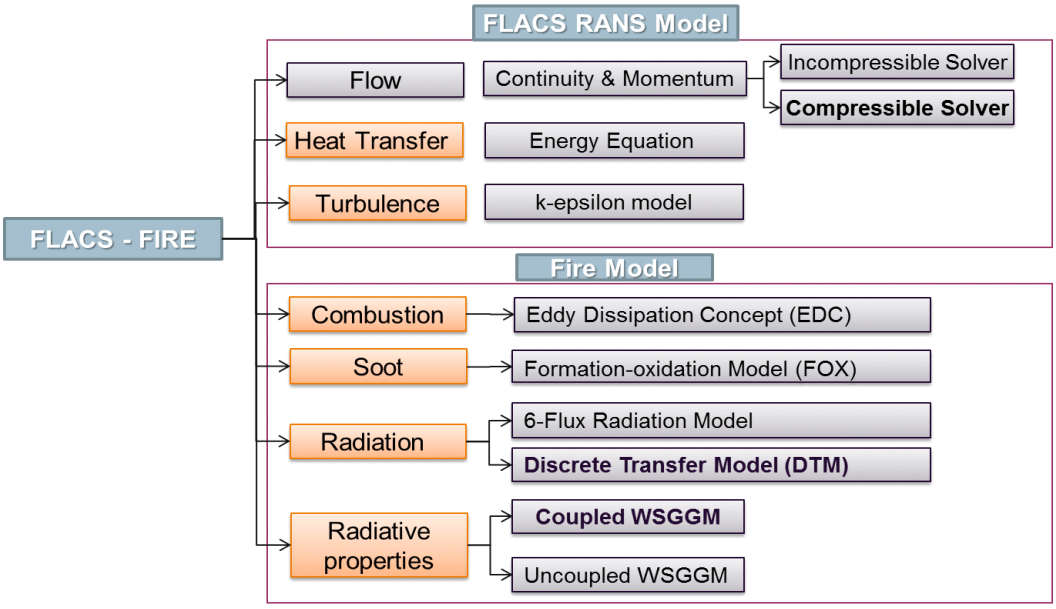

Figure A.2: Key building blocks of FLACS-Fire

FLACS-Fire has been validated for a wide range of test cases and has generally performed well. The validation cases include various free and impinging jet fires (Hydrogen, Methane, Propane, Ethylene), flash fires, the compartment fires (well and under ventilated) and various pool fires. For examples of validation cases refer to the following conference papers (Muthusamy & Lilleberg 2012) & (Muthusamy & van Wingerden, 2015). Additionally, a concise summary of validation cases can be found in (Muthusamy, 2014).

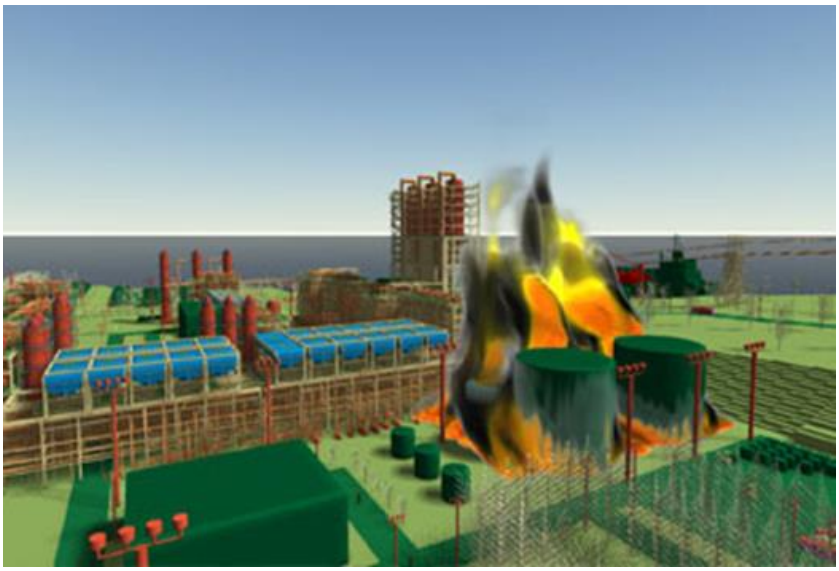

Figure A.3: Pool fire simulation using FLACS-Fire

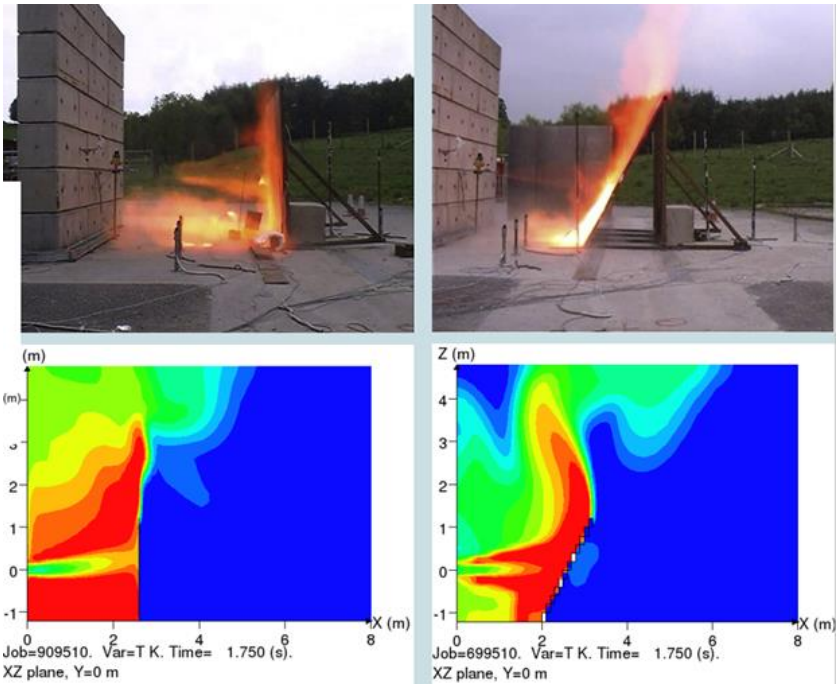

Figure A.4: FLACS-Fire simulation of Impinging hydrogen jet fires

C.1 Highlights of FLACS

- FLACS is a commercial CFD tool that is widely used in the process industry, and well recognized by major oil companies and authorities.
- FLACS is user-friendly and efficient compared to other CFD-tools.
- FLACS represents geometry on a structured Cartesian grid by the so-called distributed porosity concept. Large objects and walls are resolved on the grid, whereas flow resistance, turbulence generation and flame folding due to smaller objects are represented by sub-grid models.
- FLACS has been extensively validated for fire, explosion and dispersion studies in petrochemical facilities.
- FLACS users will be able to use the same geometry models for dispersion, explosion and fire simulations.
- FLACS-Fire is developed and optimized for fire simulations (typically offer a fire-engineer-friendly approach)

C.2 Capabilities of FLACS-Fire

- Compressible and incompressible flow solvers
- Turbulence: standard k-ε model
- Combustion: Eddy Dissipation Concept (EDC)
- Two Radiation Models: Discrete Transfer Model (DTM) and Six-Flux Model
- Three radiative properties models (uncoupled and coupled)
- Two soot models: Oxidation-Formation soot model (FOX) and Fixed Conversion rate
- Small-scale, medium-scale and large-scale complex geometries
- Point and area leaks
- Various gases fuel (More than 10 + user defined) and mixtures of these
- Wind boundary conditions with wind profiles
- Predicting fire growth and behaviour
- Heat transport from fire
- Flow rates of gas through openings
- Pollutant emissions
- Fire impact on structures and process equipment (Heat fluxes and heat dose)
- Impact of fire (temperature, radiation and smoke) on persons
- 2D and 3D field plots of various Variables for Fire Simulations variables
- Efficient and user-friendly pre-processor (CASD) and postprocessor (FLOWVIS-5)

C.3 Application area

- Both indoor and outdoor fires
- Simulation of jet and pool fires

- Offshore installations
- Fire in factory buildings
- Can be used to simulate:
    - Jet fires in the open
    - Jet fires in Cross-wind (flares)
    - Impinging Jet
    - Jet release with delayed ignition (dispersion and fire) – Flash fire
    - Confined jet fires
    - Compartment fires (over, under ventilated)
    - Different fuel mixtures

C.4 Publications related to FLACS-Fire

(i) Deiveegan Muthusamy & Franz Zdravistch (2016). Validation of the FLACS-Fire for Pool Fires in Trenches. Sixth International Symposium on Fire Investigation Science and Technology (ISFI 2016). Scottsdale Arizona, USA, September 12-14, 2016.

(ii) Deiveegan Muthusamy & Lilleberg. B. (2012). Validation of FLACS-Fire for jet fires under ventilation-controlled conditions. Fifth International Symposium on Fire Investigation Science and Technology (ISFI 2012). University of Maryland, USA, 15-17 October 2012: 485-494.

(iii) Deiveegan Muthusamy (2017). Validation of FLACS-Fire for Large Scale Fires of Natural Gas/Hydrogen Mixtures. 26th International Colloquium on the Dynamics of Explosions and Reactive Systems, July 30 - August 4, 2017 Boston, USA.

(iv) Deiveegan Muthusamy, & Kees van Wingerden (2012). Numerical Simulation of Vapour Cloud Fires using FLACS-Fire. IFireSS Symposium. University of Coimbra, Portugal, 20-22 April 2015.

(v) Deiveegan Muthusamy, FLACS Fire, Gexcon Internal report, 2012.

(vi) Deiveegan Muthusamy, Hansen, O.R., Royle, M. & Willoughby, D. (2011). Modeling of hydrogen jet fires using CFD. Fourth International Conference on Hydrogen Safety, San Francisco, California, 12-14 September 2011: 11 pp.

(vii) Deiveegan Muthusamy, Skjold, T. & Hansen, O.R. Validation of a radiative transfer model in FLACS-Fire, "Tenth International Symposium on Fire Safety Science, University of Maryland, 19-24 June 2011.

(viii) FLACS v10.8 user's manual. (2019).

(ix) Hansen, O.R., Storvik, I.E., van Wingerden, C.J.M., (1999). Validation of CFD-models for gas explosions, where FLACS is used as example; model description and experiences and recommendations for model evaluation. Proceedings European Meeting on Chemical Industry and Environment III, Krakow, Poland.

(x) Hjertager, B.H. (1985). Computer simulation of turbulent reactive gas dynamics. J. Model. Identification Control, 5, 211–236.

(xi) Hjertager, B.H., (1986). Three-dimensional modeling of flow, heat transfer, and combustion. Handbook of Heat and Mass Transfer. Gulf Publishing Company, P.O. Box 2608, Houston, Texas 770011, pp. 304–350 Chapter 41.

(xii) Hjertager, B.H., Bjørkhaug, M., Fuhre, K., (1988a). Gas explosion experiments in 1:33 scale and 1:5 scale; offshore separator and compressor modules using stoichiometric homogeneous fuel–air clouds. J. Loss. Prev. Process Ind. 1, 197–205.

(xiii) Lilleberg, B. & Deiveegan Muthusamy (2012). Modelling of fire under ventilation-controlled conditions. Scandinavian-Nordic Section of the Combustion Institute: Eight Topical Meeting on Fire and Explosion Safety. Hosted by University of Bergen and GexCon, 1-2 November 2012, Bergen, Norway: 2 pp.

(xiv) Malalasekera, W., Deiveegan Muthusamy, Sadasivuni, S.S. and Ibrahim, S.S., Evaluation of Turbulence/interaction effects using LES combustion simulation data, Proceedings of the Eurotherm Seminar 83: Computational Thermal Radiation in Participating Media III - 2009, Colelho, P., Lemonnier, D., Lybaert, P and Selcuk, N (editors), IST Press, Lisbon, ISBN 987-972-8469-83-2, pp. 221-233.

(xv) Melheim, J.A., Introduction to FLACS-Fire, GexCon Internal report, 2007.

(xvi) Sadasivuni, S., Deiveegan Muthusamy, Malalasekera, W., Ibrahim, S., Coupled Radiation Effects on Turbulence-Chemistry Tested on Bluff Body Stabilized Flames, The Fifth European Combustion Meeting, Cardiff University, 28th June - 1st July 2011.

Appendix D Concepts and definitions

[a] Smoke and Soot:

Smoke is a collection of tiny solid, liquid and gas particles. Although smoke can contain hundreds of different chemicals and fumes, visible smoke is mostly carbon (soot), tar, oils and ash. Smoke occurs when there is incomplete combustion (not enough oxygen to burn the fuel completely). In complete combustion, everything is burned, producing just water and carbon dioxide. When incomplete combustion occurs, not everything is burned. Smoke is a collection of these tiny unburned particles. Each particle is too small to see with your eyes, but when they come together, you see them as smoke. (https://www.sciencelearn.org.nz/resources/748-what-is-smoke)

[b] Smoke point:

The smoke point, also known as burning point of a hydrocarbon, is the temperature at which, under specific and defined conditions, it begins to produce a continuous bluish smoke that becomes clearly visible. Another definition (and more applicable to fire safety) is the heat release rate at which smoke just begins to be released from the flame tip [8].

[c] Poly-disperse characteristics:

The dispersity is a measure of the heterogeneity of sizes of molecules or particles in a mixture. A collection of objects is called mono-disperse or uniform if the objects have the same size, shape, or mass. A sample of objects that have an inconsistent size, shape and mass distribution is called poly-disperse or non-uniform.

[d] Atomic mass unit:

An atomic mass unit (symbolized AMU) is defined as precisely 1/12 the mass of an atom of carbon-12. In imprecise terms, one AMU is the average of the proton rest mass and the neutron rest mass which is approximately 1.6738 x 10-27 kg. The prime application of AMU is to express relative masses of various isotopes of the element so that they can be differentiated. For example, Uranium-235 has an AMU of approximately 235 whereas Uranium-238 is slightly heavy i.e. it has 3 more neutrons than U-235.

[e] Kinetic theory:

The body of theory which explains the physical properties of matter in terms of the motions of its constituent particles. For example, the kinetic theory of gases explains the macroscopic properties of gases, such as pressure, temperature, viscosity, thermal conductivity, and volume, by considering their molecular composition and motion. The theory posits that gas pressure results from particles' collisions with the walls of a container at different velocities.

[f] Emissivity:

It is the ratio of the actual amount of radiation emitted by a surface to the maximum possible amount of radiation that could be emitted by that surface if it was a blackbody. Since no surface can emit more thermal radiation than a blackbody, a logical tool for normalizing thermal emission from real surfaces is the blackbody [8].

[g] Favre averaged:

A density-weighted variant of Reynolds averaging (Favre averaging) is often necessary for the treatment of regions where density fluctuations have a significant effect [8].

[h] Thermophoresis:

Thermophoresis is a phenomenon observed in mixtures of mobile particles where the different particle types exhibit different responses to the force of a temperature gradient. An example that may be observed by the naked eye with good lighting is when the hot rod of an electric heater is surrounded by tobacco smoke: the smoke goes away from the immediate vicinity of the hot rod. As the small particles of air nearest the hot rod are heated, they create a fast flow away from the rod, down the temperature gradient. They have acquired higher kinetic energy with their higher temperature.

[i] Eddy dissipation concept:

The Eddy Dissipation Concept (EDC) of Magnussen is a general concept for treating the interaction between the turbulence and the chemistry in flames. It is based on the assumption that the chemical reactions occur in the regions where the dissipation of turbulence energy takes place.

[j] Weighted sum of grey gas:

Weighted Sum of Grey Gas model (WSGGM) models how much of the heat radiation is absorbed and emitted by the gas. It is a reasonable compromise between the oversimplified grey gas model and a complete model which takes into account particular absorption bands.

[k] Quasi-steady state:

A situation that is changing slowly enough that it can be considered to be constant. (http://glossary.ametsoc.org/wiki/Quasi_steady_state)

[l] Gravimetric measurements:

Gravimetric analysis is a technique through which the amount of an particles can be determined through the measurement of mass.

[m] Optical measurements

The optical measurements depends on photo-detectors which convert the parameter to be measured into some form of electrical signal. The probe continuously extracted a sample through an optical path; the measured attenuation of a laser passing through the sample was used to determine the soot mass concentration [7].